Université de Montréal

Abdominal aortic aneurysm follow-up after endovascular repair in a canine model with non-invasive vascular elastography

par
Elie Salloum

Institut de Génie Biomédical
Faculté de Médecine

Mémoire présenté à la Faculté de médecine
en vue de l'obtention du grade de Maîtrise
en Génie Biomédical
(option recherche)

Novembre, 2014

Université de Montréal
Faculté des études supérieures et postdoctorales

Ce mémoire intitulé :

Abdominal aortic aneurysm follow-up after endovascular repair in a canine model with non-invasive vascular elastography

Présenté par:
Elie Salloum

a été évalué par un jury composé des personnes suivantes :

Matthias Friedrich, président-rapporteur
Gilles Soulez, directeur de recherche
Guy Cloutier, co-directeur
Rosaire Mongrain, membre externe du jury

RÉSUMÉ

Le traitement chirurgical des anévrismes de l'aorte abdominale est de plus en plus remplacé par la réparation endovasculaire de l'anévrisme (« endovascular aneurysm repair », EVAR) en utilisant des endoprothèses (« stent-grafts », SGs). Cependant, l'efficacité de cette approche moins invasive est compromise par l'incidence de l'écoulement persistant dans l'anévrisme, appelé endofuites menant à une rupture d'anévrisme si elle n'est pas détectée. Par conséquent, une surveillance de longue durée par tomodensitométrie sur une base annuelle est nécessaire ce qui augmente le coût de la procédure EVAR, exposant le patient à un rayonnement ionisants et un agent de contraste néphrotoxique.

Le mécanisme de rupture d'anévrisme secondaire à l'endofuite est lié à une pression du sac de l'anévrisme proche de la pression systémique. Il existe une relation entre la contraction ou l'expansion du sac et la pressurisation du sac. La pressurisation résiduelle de l'anévrisme aortique abdominale va induire une pulsation et une circulation sanguine à l'intérieur du sac empêchant ainsi la thrombose du sac et la guérison de l'anévrisme.

L'élastographie vasculaire non-invasive (« non-invasive vascular elastography », NIVE) utilisant le « Lagrangian Speckle Model Estimator » (LSME) peut devenir une technique d'imagerie complémentaire pour le suivi des anévrismes après réparation endovasculaire. NIVE a la capacité de fournir des informations importantes sur l'organisation d'un thrombus dans le sac de l'anévrisme et sur la détection des endofuites.

La caractérisation de l'organisation d'un thrombus n'a pas été possible dans une étude NIVE précédente. Une limitation de cette étude était l'absence d'examen tomodensitométrique comme étalon-or pour le diagnostic d'endofuites. Nous avons cherché à appliquer et optimiser la technique NIVE pour le suivi des anévrismes de l'aorte abdominale (AAA) après EVAR avec endoprothèse dans un modèle canin dans le but de détecter et caractériser les endofuites et l'organisation du thrombus.

Des SGs ont été implantés dans un groupe de 18 chiens avec un anévrisme créé dans l'aorte abdominale. Des endofuites de type I ont été créés dans 4 anévrismes, de type II dans 13 anévrismes tandis qu'un anévrisme n'avait aucune endofuite. L'échographie Doppler (« Doppler ultrasound », DUS) et les examens NIVE ont été réalisés avant puis à 1 semaine, 1 mois, 3 mois et 6 mois après l'EVAR. Une angiographie, une tomodensitométrie et des coupes macroscopiques ont été réalisées au moment du sacrifice. Les valeurs de contrainte ont été calculées en utilisant l`algorithme LSME. Les régions d'endofuite, de thrombus frais (non organisé) et de thrombus solide (organisé) ont été identifiées et segmentées en comparant les résultats de la tomodensitométrie et de l'étude macroscopique. Les valeurs de contrainte dans les zones avec endofuite, thrombus frais et organisé ont été comparées.

Les valeurs de contrainte étaient significativement différentes entre les zones d'endofuites, les zones de thrombus frais ou organisé et entre les zones de thrombus frais et organisé. Toutes les endofuites ont été clairement caractérisées par les examens d'élastographie. Aucune corrélation n'a été trouvée entre les valeurs de

contrainte et le type d'endofuite, la pression de sac, la taille des endofuites et la taille de l'anévrisme.

Mots-clés : Aorte, anévrisme de l’aorte abdominal, réparation endovasculaire de l’anévrisme, élastographie non-invasive vasculaire, ultrasonographie, tomodensitométrie, endofuite, thrombus.

ABSTRACT

Surgical treatment of abdominal aortic aneurysms is increasingly being replaced by EVAR using SGs. However, the efficacy of this less invasive approach is jeopardized by the incidence of persistent flow within the aneurysm, called endoleaks leading to aneurysm rupture if not properly detected. Hence, a life-long surveillance by computed tomography (CT) angiography on an annual basis is increasing the cost of EVAR, exposing the patient to ionizing radiation and nephrotoxic contrast agent.

The mechanism of aneurysm rupture secondary to endoleak is related to a pressurization of the aneurysm sac close to the systemic pressure. There is a relation between sac shrinkage or expansion and sac pressurization. The residual pressurization of AAA will induce sac pulsatility and blood circulation in the sac thus preventing sac thrombosis and aneurysm healing.

NIVE using the LSME may become a complementary follow-up imaging technique for EVAR. NIVE has the capability of providing important information on the thrombus organization within the aneurysm sac and on the detection of endoleaks.

The characterization of the thrombus organization was not possible in a previous NIVE study. A limitation was the absence of CT examinations as gold standard for endoleak diagnosis. In the current study, we aimed to apply and

optimize NIVE of AAA after EVAR with SG in a canine model to detect endoleaks and characterize thrombus organization.

SGs were implanted in a group of 18 dogs with an aneurysm created in the abdominal aorta. Type I endoleak was created in 4 aneurysms, type II in 13 aneurysms and no endoleak in 1 aneurysm. DUS and NIVE examinations were performed at baseline, 1-week, 1-month, 3-month and 6-month follow-up after EVAR. Angiography, CT-scan and macroscopic tissue slides were performed at sacrifice. Strain values were computed using the LSME. Areas of endoleak, solid thrombus (organized) and fresh thrombus (non-organized) were identified and segmented by comparing the results of CT scan and macroscopic tissue slides. Strain values in areas with endoleak, organized and fresh thrombi were compared.

Strain values were significantly different between endoleak and organized or fresh thrombus areas and between organized and fresh thrombus areas. All endoleaks were clearly characterized on elastography examinations. No correlation was found between strain values and type of endoleak, sac pressure, endoleak size and aneurysm size.

Keywords : Aorta, abdominal aortic aneurysm, endovascular repair, non-invasive vascular elastography, ultrasound, computed tomography, endoleak, thrombus.

TABLE OF CONTENTS

RÉSUMÉ i

ABSTRACT iv

TABLE OF CONTENTS vi

LIST OF TABLES ix

LIST OF FIGURES ix

LIST OF ABBREVIATIONS xiv

DEDICATION xv

AKNOWLEDGEMENTS xvi

Section I: Clinical Perspectives of Abdominal Aortic Aneurysm 1

Chapter I: Abdominal Aortic Aneurysm, a chronic degenerative disorder 3

1. Abdominal Aortic Aneurysm, a chronic degenerative disorder 4

1.1. Background 4

1.2. Anatomy and Physiology 5

1.2.1. Abdominal Aorta 10

1.2.2. Abdominal arteries and pelvic arteries 12

1.3. Pathophysiology of abdominal Aortic Aneurysm 14

1.3.1. Elastin and Collagen 15

1.3.1.1. Elastin 15

1.3.1.2. Collagen 17

1.3.2. Smoking 17

1.3.3. Other factors increasing the pressure on the aortic wall 18

1.4. Epidemiology 19

1.4.1. Age and sex 19

1.5. Abdominal Aortic Aneury 21

1.5.1. Rupture 21

1.5.2. Imaging techniques 22

1.5.2.1. Surveillance 24

1.5.2.2 Screening and diagnosis 25

1.5.3. Intervention 25

1.5.3.1. Open Surgical Repair 27

1.5.3.2. Endovascular aneurysm repair 28

1.5.3.3. Comparison between Open Surgical Repair and EVAR 30

1.5.3.4. Thrombus 31

Chapter II: Endoleak 33
2. Endoleak 34
2.1. Endoleak Types 34
2.2. Imaging detection techniques 38
2.2.1. CT Scan 38
2.2.2. Ultrasound 41
2.2.3. Angiography 43
2.2.4. Magnetic Resonance Imaging 45

Chapter III: Quasi-static elastography (QSE-LSME) 49
3. Elastography 50
3.2. Quasi-static elastography 53
3.3. Lagrangian speckle model estimator (LSME) 54

Section II: Abdominal aortic aneurysm follow-up after endovascular repair in a canine model with non-invasive vascular elastography 60

Chapter IV: Abdominal aortic aneurysm follow-up after endovascular repair in a canine model with non-invasive vascular elastography 62
4. Aortic aneurysm in a canine model 63
4.1. Abdominal aortic aneurysm follow-up after endovascular repair in a canine model with non-invasive vascular elastography 65
4.1.1. Introduction to Manuscript 65
4.1.2. Role of authors 66
4.1.3. Thesis format of submitted manuscript 70
4.2. Manuscript submitted to Radiology 70
- Abbreviated title page 71
- Introduction 76
- Methods 78
- Results 85
- Discussion 87
- Conclusion 90
- Tables 92
- Figure caption 96
- References 115

4.3. Further discussion and future perspectives 118
4.3.1. Study methodology 118
4.3.2. Limitations 122
4.3.3. Future work 123
4.3.4. Final Conclusion 124

Section III: Reference list ……...……. 125

List of Tables

Table 4.1: NIVE strain parameters in segmented regions.

Note: Max/MinAxStrain = maximum and minimum axial strains; MaxCumAxStrain = maximum cumulated axial strain; Max/MinStrainRate = maximum and minimum strain rates; E = Endoleak; OT = Organized Thrombus; FT = Fresh Thrombus; * = Wilcoxon rank sum test.

Table 4.2: Comparison as a function of endoleak type (aneurysms with type I vs type II endoleak).

Comparison of strain values in endoleak, organized thrombus and fresh thrombus regions as a function of endoleak type (aneurysms with Type I vs type II endoleak). No statistical significant difference was found for any of the parameters.

Table 4.3: Aneurysm and endoleak size measurements.

Note: Type of endoleak according to the Society of Vacular Surgery Classification (0= no endoelak). (ref). The % of difference in aneurysm diameter is measured between sacrifice and 1 week after implantation of the SG on DUS. A (+) sign indicates that the diameter has increased whether a (-) sign indicates a shrinkage in the aneurysm diameter. The dog number 15 had no endoleak detected through CT scan, DUS and macroscopic tissue slides.

LIST OF FIGURES

Figure 1.1: Cardio vascular system (CVS)

Figure 1.2: The three layers forming the arterial wall: The tunica intima, tunica media and tunica adventitia

Figure 1.3: The aorta is divided in 4 sections: The ascending aorta, the aortic arch, the descending aorta and the abdominal aorta

Figure 1.4: Posterior abdominal wall after removal of the peritoneum

Figure 1.5: Abdominal arteries and pelvic arteries

Figure 1.6: Abdominal Aortic Aneurysm pathogenesis

Figure 1.7: The architecture of the healthy human artery showing the elastin and collagen fibrils

Figure 1.8: Prevalence of AAA depending on age and sex from Sweden and Kansas City

Figure 1.9: A CT scan examination showing an AAA with a contained rupture

Figure 1.10: Ultrasound gray scale mode of an AAA

Figure 1.11: CT scan identifying the AAA lumen, wall, calcification, thrombus

Figure 1.12: Open surgical repair

Figure 1.13: EVAR where a SG is placed inside the aneurysm without exposure of the abdominal aorta

Figure 2.1: Visualization of the 4 types of endoleak. Type I: Blood flow coming from the proximal distal neck; Type II: Collateral flow coming from the collateral arteries; Type III: A gap in the SG leading to a blood flow inside the aneurysm sac; Type IV: graft porosity

Figure 2.2: Axial CT scan image of an 80 years old female showing a type I endoleak

Figure 2.3: Doppler ultrasound acquisition showing a blood flow outside the SG and inside the aneurysm sac (endoleak)

Figure 2.4: Angiography acquisition of a 80 years old female showing a type I endoleak on the left side (indicated with a white arrow)

Figure 2.5: Contrast enhanced MRI image showing a type II endoleak (white arrow)

Figure 3.1: Two different tissues: Soft and hard giving different reactions toward a compression

Force

Figure 3.2: Three elastography imaging approaches: (a) Quasi-static elastography where the mechanical source is either from outside or inside the organ of interest (*e.g.*, from inside in the case of the pulsation of an artery), (b) harmonic elastography, and (c) transient elastography

Figure 3.3: A stress/strain curve of a linear elastic material. Beyond a certain level of deformation, the material reaches an elastic limit and breaks

Figure 4.0: Representation of the AAA reconstruction

Figure 4.1: The macroscopic tissue slide is first analyzed to detect the presence of an endoleak through a defect/gap in the aneurysm sac. If the presence of the defect correlates with CT scan contrast enhancement in the same region, presence of an endoleak is confirmed. The rest of the tissue in the aneurysmal sac is characterized as organized or fresh thrombus according to its appearance on macroscopic cuts.
Note: C+ means contrast on CT scanner.

Figure 4.2: Example of macroscopic tissue slide (a) with endoleak (1), fresh thrombus (2) and organized thrombus (3). Corresponding histology with Movat staining (b) and immunostaining of alpha smooth muscle actin (αSMA, in brown)) (c and d). The brown region corresponds to the dense fibrous connective tissues (organized thrombus). The blue region corresponds to the fresh thrombus (c and d) which confirms the areas of fresh thrombus (loose thrombus with black brown coloration and absence of fibrous organization) and organized thrombus (dense fibrous organization with a yellowish appearance) on the macroscopic tissue slides

Figure 4.3a: LSME was applied to compute time varying strain curves for 3 or more consecutive cardiac cycles. This figure shows the instantaneous axial strain curve on 90 frames (7 cycles). MaxAxStrain and MinAxStrain represent the mean value, over acquired cardiac cycles, of positive and negative peaks of the time varying instantaneous axial strain curve, respectively.

Figure 4.3b. A cumulated axial strain curve over the same 90 frames (7 cycles). MaxCumAxialStrain is the average, over acquired cardiac cycles, of maximum positive values of the cumulated axial strain curve, corresponding to peak dilatation.

Figure 4.4a. CT scan image of dog 1 (A Stena Labrador female, 6 years old and weights 30.5 Kg) taken before sacrifice and showing a large type I endoleak at the proximal neck. CT scan is used as a reference for endoleak segmentation and registration on elastogram.

Figure 4.4b. Transverse acquisition of Doppler Ultrasound at the same level than CT scan (Figure 4.4a).

Figure 4.4c. A macroscopic tissue slide at the same level shown in figure 4.4a and 4.4b. The endoleak area is well visible (dashed arrow). A small area of fresh thrombus seen as a soft black brown area is depicted (white arrow). The organized thrombus is seen at the upper portion (thin arrow with an oval head) of the macroscopic cut. These 3 regions of interest located on the macroscopic tissue slide are segmented and registered on the elastogram for computation of strain parameters.

Figure 4.4d**:** Cumulated axial strain elastogram of the entire aneurysm sac at the same level that Figure 4.4,a,b,c The region of accumulation of very high and low strain values on the middle left of the elastogram (white arrow) corresponds to the region of endoleak.

Figure 4.4e: Cumulated axial strain elastogram of the endoleak region of the same dog 1 at the same level segmented based on the CT scan and macroscopic results showed in figure 4.4a and 4.4c.

Figure 4.4f**:** Cumulated axial strain elastogram of the fresh thrombus region of the same dog 1 at the same level segmented based on the macroscopic results showed in figure 4.3c.

Figure 4.4g. Cumulated axial strain elastogram of the organized thrombus region of the same dog 1 at the same level segmented based on the macroscopic results showed in figure 4.3c.

Figure 4.5: Mean and SD Maximum Axial Strain values for the three regions of interest. A statistical significant difference was found when comparing the endoleak, organized and fresh thrombi.

Figure 4.6: No correlation has been found between the pressure measured inside the aneurysm sac and the maximum axial strain parameter results.

Figure 4.7: No correlation has been found between the aneurysm area measured on CT scan and the maximum axial strain parameter results.

Figure 4.8**:** No correlation has been found between the endoleak area measured on CT scan and the maximum axial strain parameter results.

Figure 4.9: Quasi-static compression elastography examination of a breast carcinoma. The color indicates the relative stiffness (red to blue)

Figure 4.10: The resolution and penetration of some imaging modalities

LIST OF ABBREVIATIONS

2D, two-dimensional

3D, three-dimensional

AAA, Abdominal aortic aneurysm

CEUS, contrast-enhanced ultrasound

CHUM, centre hospitalier de l'Université de Montréal

CRCHUM, centre de recherche du centre hospitalier de l'Université de Montréal

CT, computed tomography

CTA, computed tomography angiography

CVS, cardio vascular system

DUS, Doppler ultrasound

E, Young's elastic modulus

EVE, endovascular ultrasound elastography

EVAR, endovascular aneurysm repair

IVUS, intravascular ultrasound

LBUM, Laboratory of biorheology and medical ultrasonics

LCTI, clinical image processing Laboratory

LSME, lagrangian speckle model estimator

MRI, magnetic resonance imaging

n, number (as in number of subjects or number in sample population)

NIVE, non-invasive vascular elastography

QSE, quasi-static elastography

r, Pearson correlation coefecient

RF, radiofrequency

ROI, region of interest

SG, stent graft

US, ultrasound

Knowledge cultivates your seeds and does not sow in your seeds
Gibran Khalil Gibran

À ma mère, mon père. À ma femme

Acknowledgements

I would like first of all to thank Dr. Gilles Soulez for offering me the chance to be part of his team and work on this stimulating project. His patience and his professional advices showed me the way through to finish my research with success. He didn't stop encouraging me, believing in me and being concerned on the personal and academic levels. I will be thankful to him the rest of my life. I also would like to thank Dr. Guy Cloutier for accepting me in his lab, part of the quasi-static elastography team and guiding me with professional advices that will remain with me through my entire professional career.

Thank you to Dr. Marie-Hélène Roy-Cardinal, Jonathan Poré and Zhao Qin for their help in answering all my questions and optimizing the quality of my elastograms. Thank you to each member of the LBUM: Dr. Louise Allard, Boris Chayer, Dr. Zahra Kesha Mottamed, Dr. Shahrokh Shahriari, Emmanuel Montagnon, Daniel Posada, Dr. Damien Garcia, Abderrahmane Ouared and Julián Andrés García Duitama for their support and everyday smile, they were a family to me the past 2 years. I would also like to thank Andrée Cliche, Dr. Claude Kauffmann, Michel Gouin, Jocelyne Lavoie, Dr. Sophie Lerouge, Anthony Bertrand Grenier and the entire animal house team for their kindness, patience and help in obtaining the final results. It was really a pleasure working with all of you.

I am grateful for the CRCHUM and to the Biomedical Engineering Institute of the University of Montreal and for each association I have received a scholarship from.

A special acknowledgment for my parents who dedicated their life for my education, for raising me and leading me through each step till I was able to reach my dream. I know how difficult that job is in a third world country. Also a special acknowledgment for all the friends I met in Montreal who became my family, for their support and encouragement.

At the end I thank God for all the people he put on my road, all the happy and sad moments I experienced and for giving me the patience to perceive my dream till the end. Mostly for sending me the most wonderful person who has been my angel. A special acknowledgment to my wife.

Section I

Clinical Perspectives of Abdominal Aortic Aneurysm

This page is left intentionally blank

CHAPTER I

Abdominal Aortic Aneurysm, a chronic degenerative disorder

1. Abdominal Aortic Aneurysm (AAA), a chronic degenerative disorder

1.1 *Background*

The abnormal dilation involving the vascular wall three layers: the intima, the media and the adventitia defines an aneurysm. The word itself derives from the Greek word “aneurusma” that has the meaning of widening. A perivascular pulsatile hematoma secondary to a vessel injury is not limited by the three layers and is called false aneurysm [1]. Aneurysms can be designed as fusiform or “saccular” depending on whether the entire circumference of the aorta is affected or a part of it respectively [1]. The normal diameter of the abdominal aorta measures between 15 and 24 mm depending on the age, sex and bodyweight. It is considered an AAA when exceeding the 30 mm diameter and preventive treatment is needed when reaching 50 mm in diameter [2, 3].

This chapter will focus on understanding the clinical and pathological aspects of the abdominal aortic aneurysm. Other issues related to the AAA will be described and further explanation of the project will be presented.

1.2 *Anatomy and Physiology*

The arterial system is classified based on the specific vascular territories it supplies and it is divided in three classifications (figure 1.1):

- The large vessels as the aorta and iliac arteries characterized with an elasticity that helps in maintaining the diastolic blood pressure.
- The medium-sized vessels that distribute blood to capillary beds as visceral branches, brachial arteries, superficial femoral and muscular arteries.
- The small arterioles that play a role in blood pressure regulation, vascular tone modulation and oxygen and nutrients delivery to the different body tissues [4].

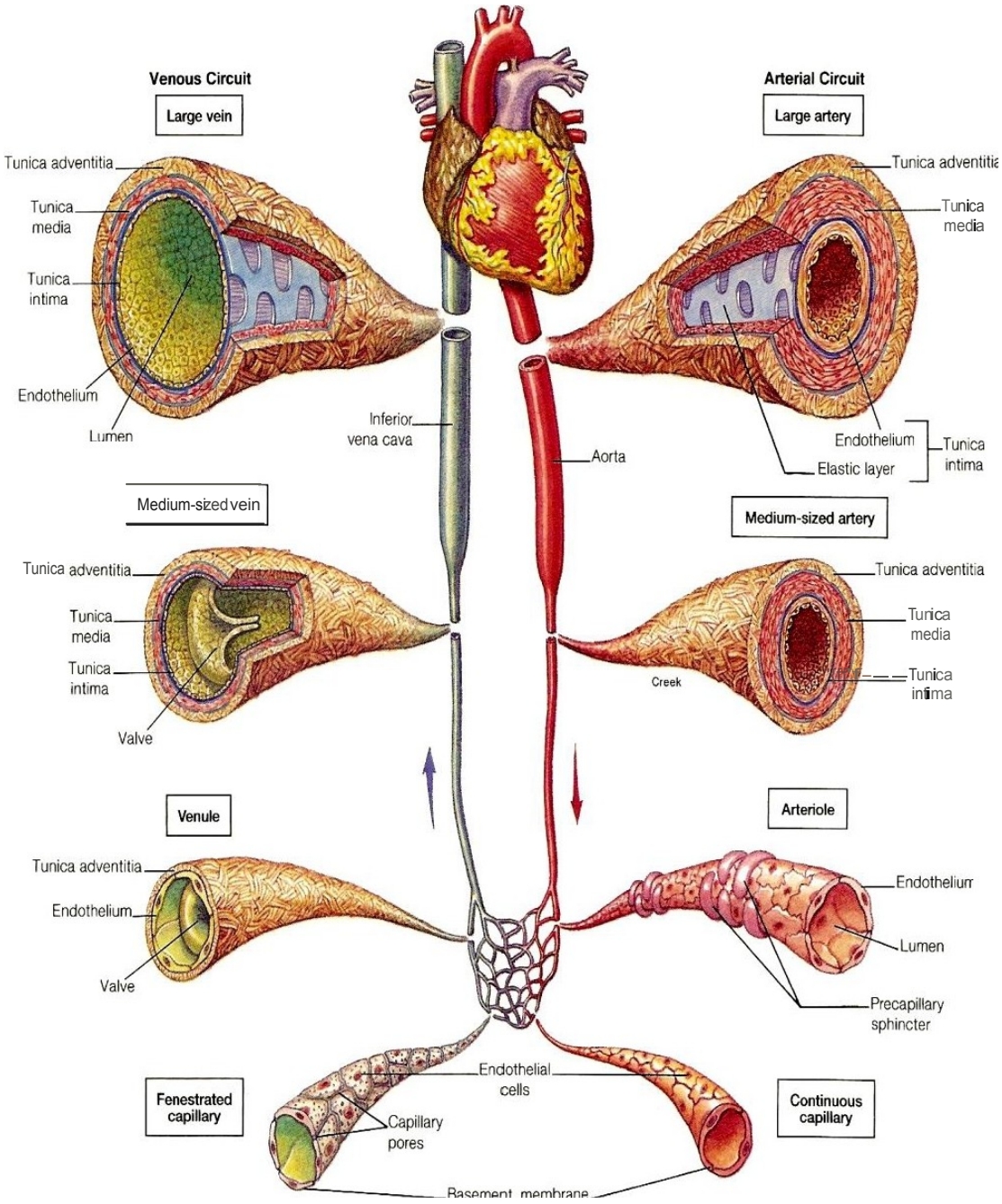

Figure 1.1 Cardia vascular system (CVS) [5]

The tunica intima, tunica media and tunica adventitia constitute the three layers of the arterial wall (figure 1.2):

- The internal layer of the artery is the tunica intima consisting of a single layer of mesenchymal endothelial cells with basement membrane and internal elastic lamina. The media and intima are attached with supportive connective tissues. Thin in healthy individuals, it becomes stiffer and thicker with age, due to pathological changes. This leads to significant alterations in the mechanical properties of the arterial wall.
- The tunica media, the middle layer of the artery, is considered the thickest layer of the arterial wall. It plays a role in modulating the arterial vascular tone and blood pressure because of the actin and myocin filaments contained in the smooth muscle cells. The media is separated from the intima and adventitia by the internal elastic lamina and the external elastic lamina, respectively. Mechanically, the media is considered to be the most important layer in a healthy artery.
- The tunica adventitia, the outer layer of the artery, consists mainly of cells that produce collagen and elastin such as fibroblasts and fibrocytes, and fibrous tissues. It is surrounded by loose connective tissues, lymphatics and the vasa vasorum, which is its own nutrient

supply. Under high blood pressure, when the collagen fibers reach their straightened lengths, the adventitia becomes stiffer to prevent the rupture and the overstretching of the artery [4, 6].

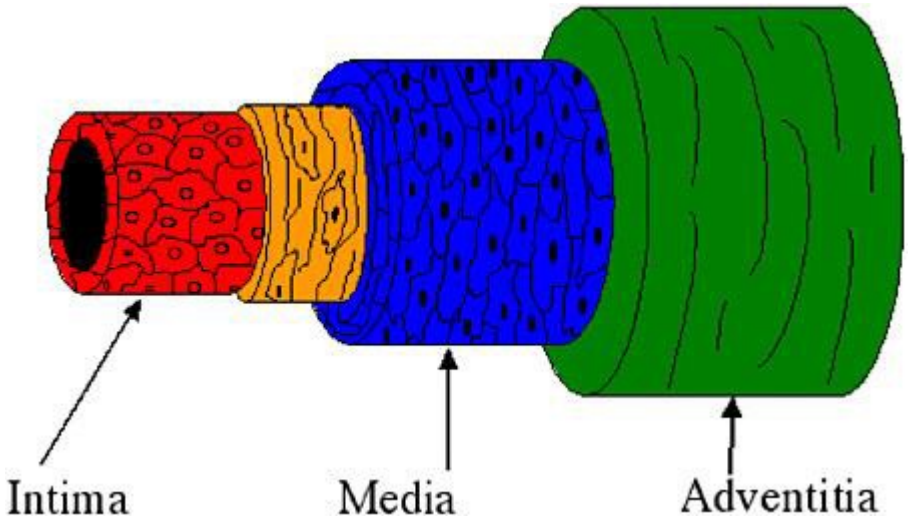

Figure 1.2 The three layers forming the arterial wall: The tunica intima, tunica media and tunica adventitia [7]

The aorta is the largest artery of the human body starting at the left ventricle of the heart (figure 1.3):

- The first part rising up from the heart is called the ascending aorta; it supplies the heart with blood through the coronary arteries.

- It curves than through the aortic arch and supplies the head, arm and neck.
- The part going through the chest is called the descending aorta. It supplies blood to the chest and some ribs.
- The abdominal aorta starts at the diaphragm and bifurcates into the paired common iliac arteries [8].

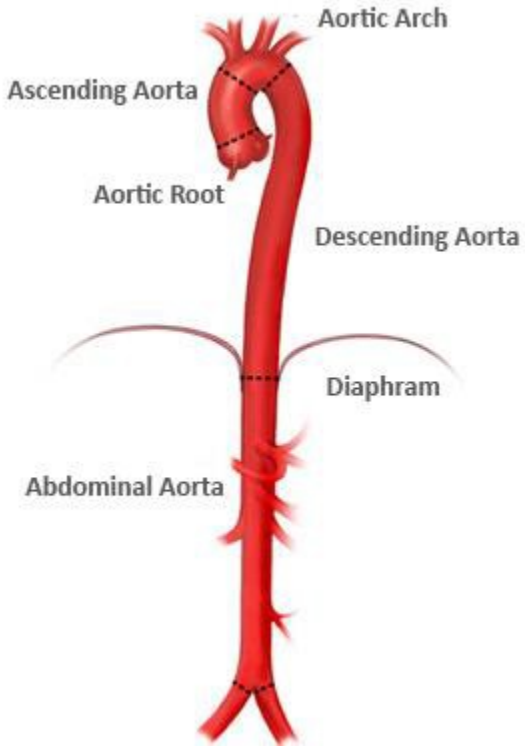

Figure 1.3 The aorta is divided in 4 sections: The ascending aorta, the aortic arch, the descending aorta and the abdominal aorta [9]

1.2.1 *Abdominal Aorta*

The abdominal aorta starts when the descending aorta passes over the twelfth thoracic vertebra (lower portion) and under the aortic hiatus of the diaphragm. It ends by bifurcating into the right and left common iliac arteries on top of the lower third of the fourth lumbar vertebra and left to the midline. The bifurcation is located using the intercrestal line, which locates an abdomen transverse plane at the fourth lumbar level. The lower portion of the abdominal aorta is located behind the peritoneum of the posterior abdominal wall (figure 1.4). To the left and right of the abdominal aorta is situated the sigmoid mesocolon and the oblique line of origin of the mesentery of the small intestine, respectively. The aorta is embedded, behind the posterior body wall peritoneum, in the extra peritoneal areolar connective tissue. Under and to the left and right of the common iliac arteries stands the left and right common iliac veins, respectively. Behind them the sympathetic trunks go down into the pelvis [10, 11].

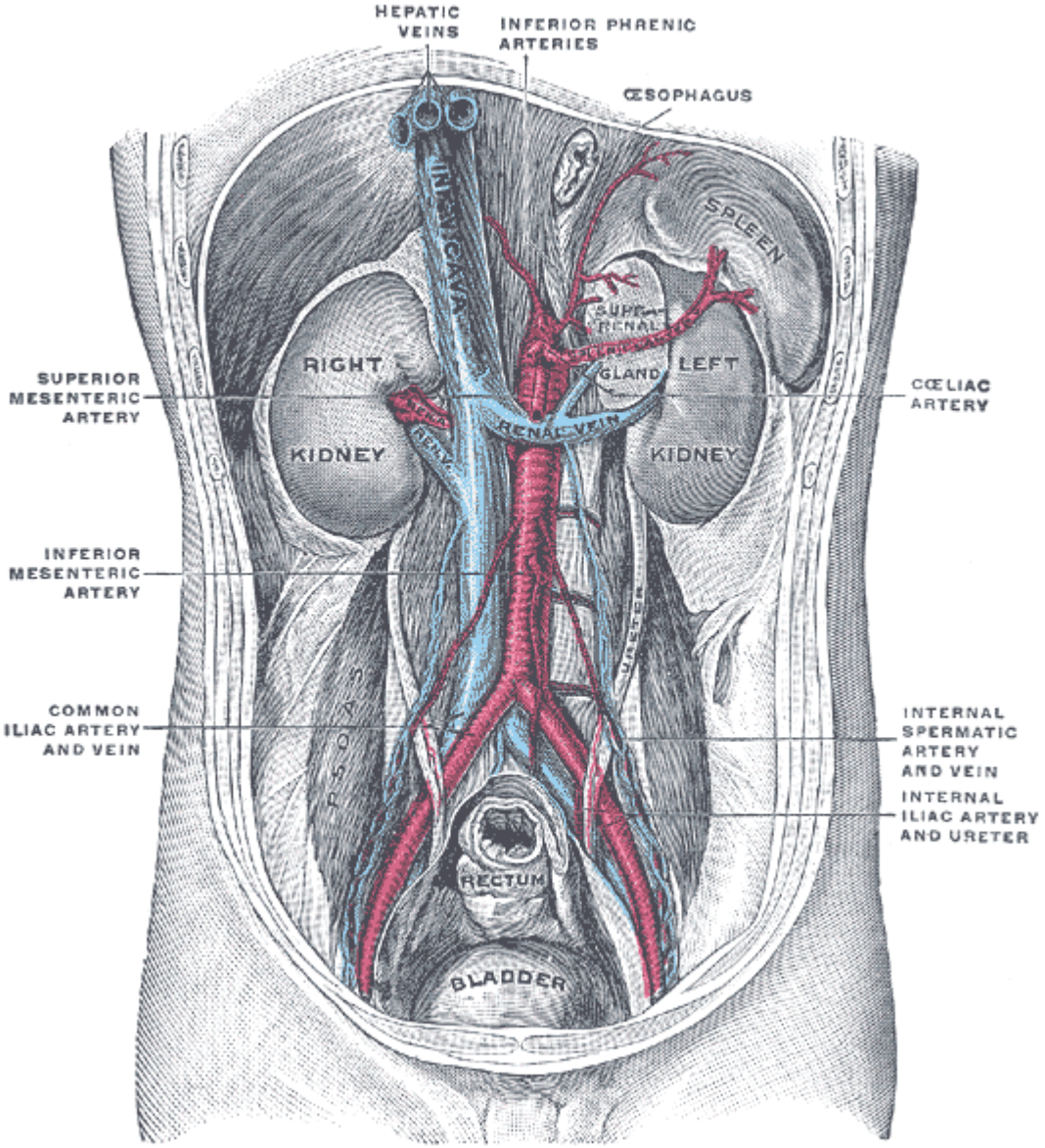

Figure 1.4 Posterior abdominal wall after removal of the peritoneum [12]

1.2.2 *Abdominal arteries and pelvic arteries*

The collateral arteries arising from the abdominal aorta divide to sub-branches in order to supply the abdomen and the pelvis (figure 1.5). These branches can be divided into five groups depending on their function:

1- The first group supplies the kidneys, diaphragm, adrenal glands, posterior abdominal wall, gonads and spinal cord. It includes the right and left renal arteries, the right and left inferior phrenic arteries, the right and left middle adrenal arteries, the right and left lumbar arteries, the right and left testicular arteries and the median sacral artery.

2- The second group made of the celiac trunk, that gives rise to the left gastric artery, the splenic artery and the common hepatic artery, supplies the liver, gallbladder, pancreas, spleen, stomach and duodenum.

3- The third group made of the superior mesenteric artery supplies the small intestine and part of the large intestine.

4- The fourth group made of the inferior mesenteric artery supplies the other part of the large intestine.

5- The fifth group supplies the pelvis through an indirect trunk arising from the common iliac artery: the internal iliac artery [13].

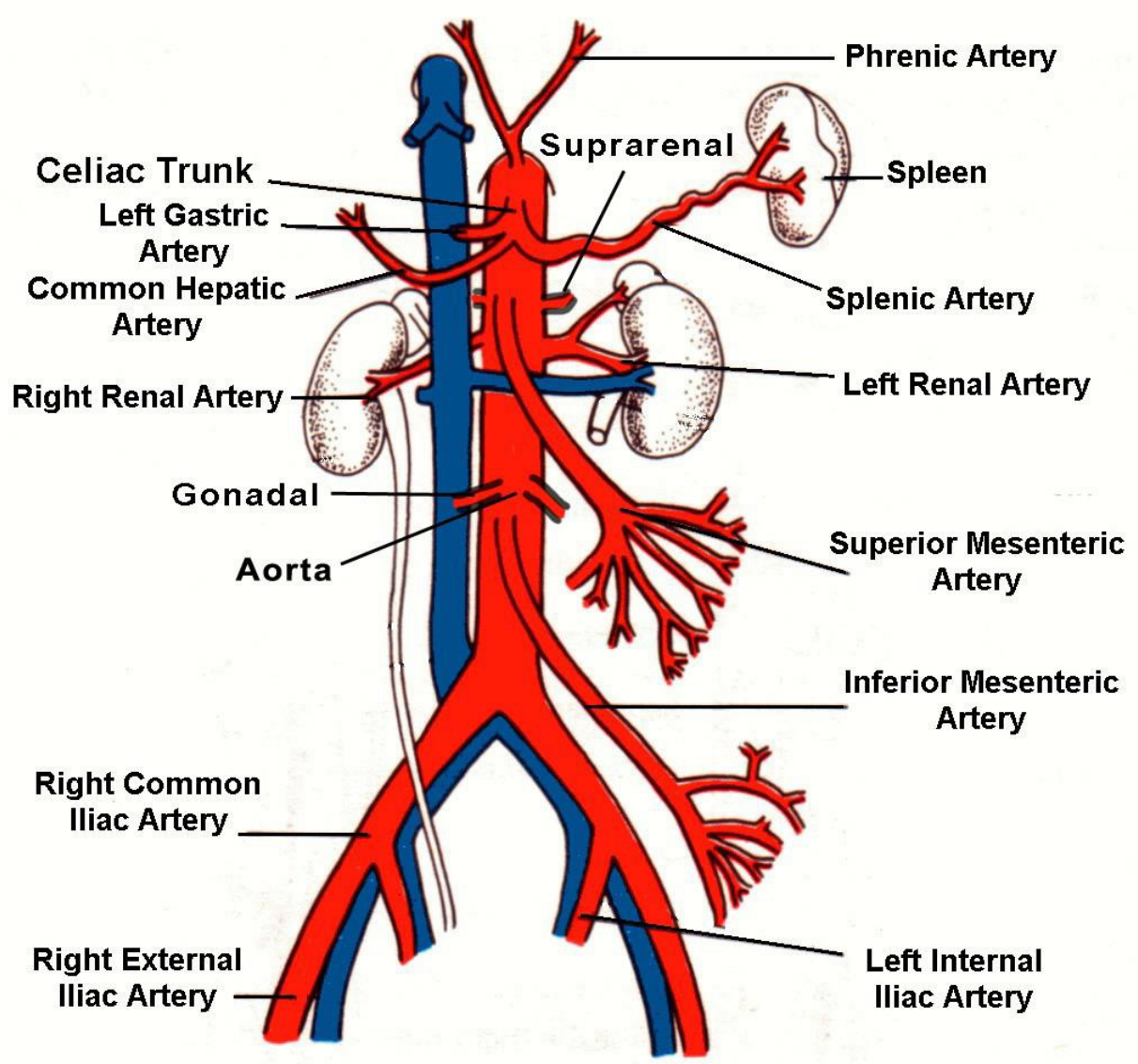

Figure 1.5 Abdominal arteries and pelvic arteries [14]

1.3 *Pathophysiology of Abdominal Aortic Aneurysm*

The arterial blood pressure imposed on the aorta is high and remains for a life time. This is why any weakness in the wall can lead to dilatation and the formation of an aneurysm, which can promote rupture and sudden death [15].

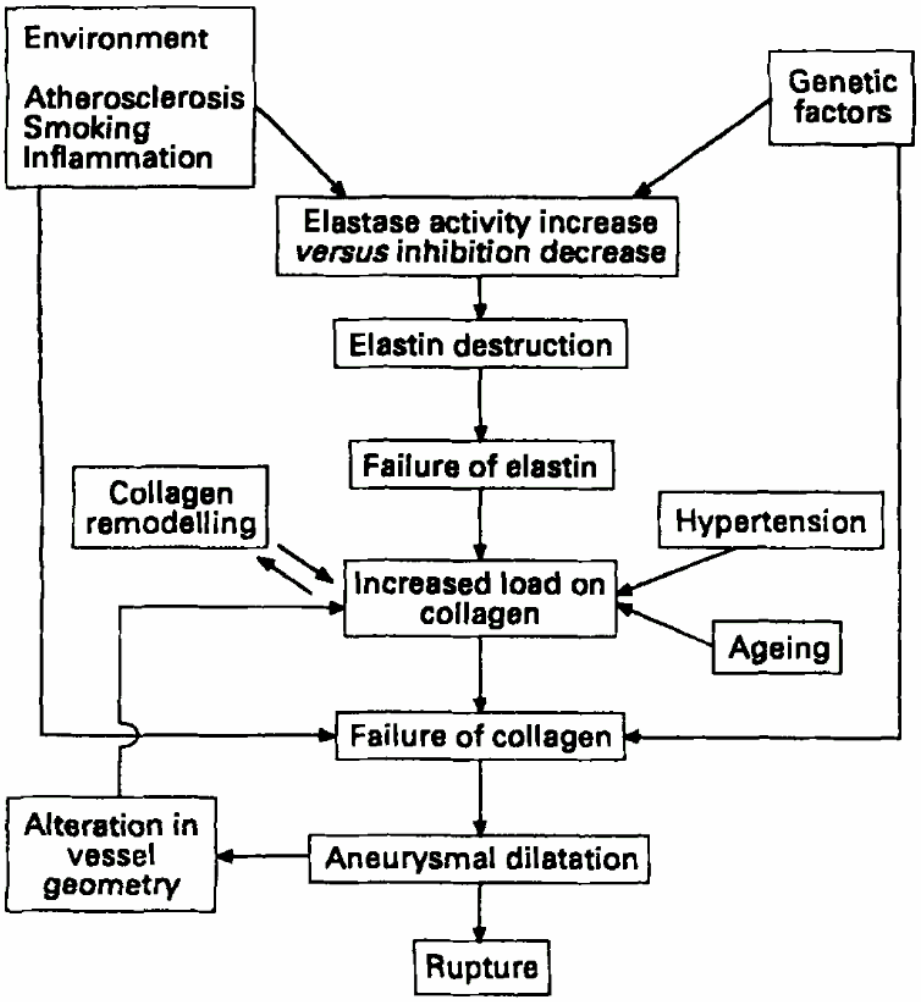

Figure 1.6 Abdominal Aortic Aneurysm pathogenesis [15]

1.3.1 *Elastin and Collagen*

Many factors involved in wall weakening and load increasing interact together leading to an aneurysm formation. Figure 1.6 represents well the sequence and reasons behind the formation of abdominal aortic aneurysms. Elastin and collagen are considered to be the aortic wall's most important

proteins that form fibers that help make up connective tissues in the body. The elastin is responsible of the elastic property that allows it to stretch during cardiac contraction and relax along with the cardiac relaxation. On the other hand, the collagen is the opposite of the elastin and it is considered to be 20 times stronger. In case of an extension that exceeds its original length, damage may occur. We can say that collagen acts as a safety net when the elastin exceeds its stretching limit [16-22].

1.3.1.1 *Elastin*

One of the reasons that aneurysms occur more frequently in the abdominal is that the elastin is less present than other parts of the aorta such as the thoracic aorta. The elastin content is lower in the aortic wall of patients with aneurysms when compared to normal abdominal aorta affecting mechanical properties that depend on the concentration of the elastin [23-28].

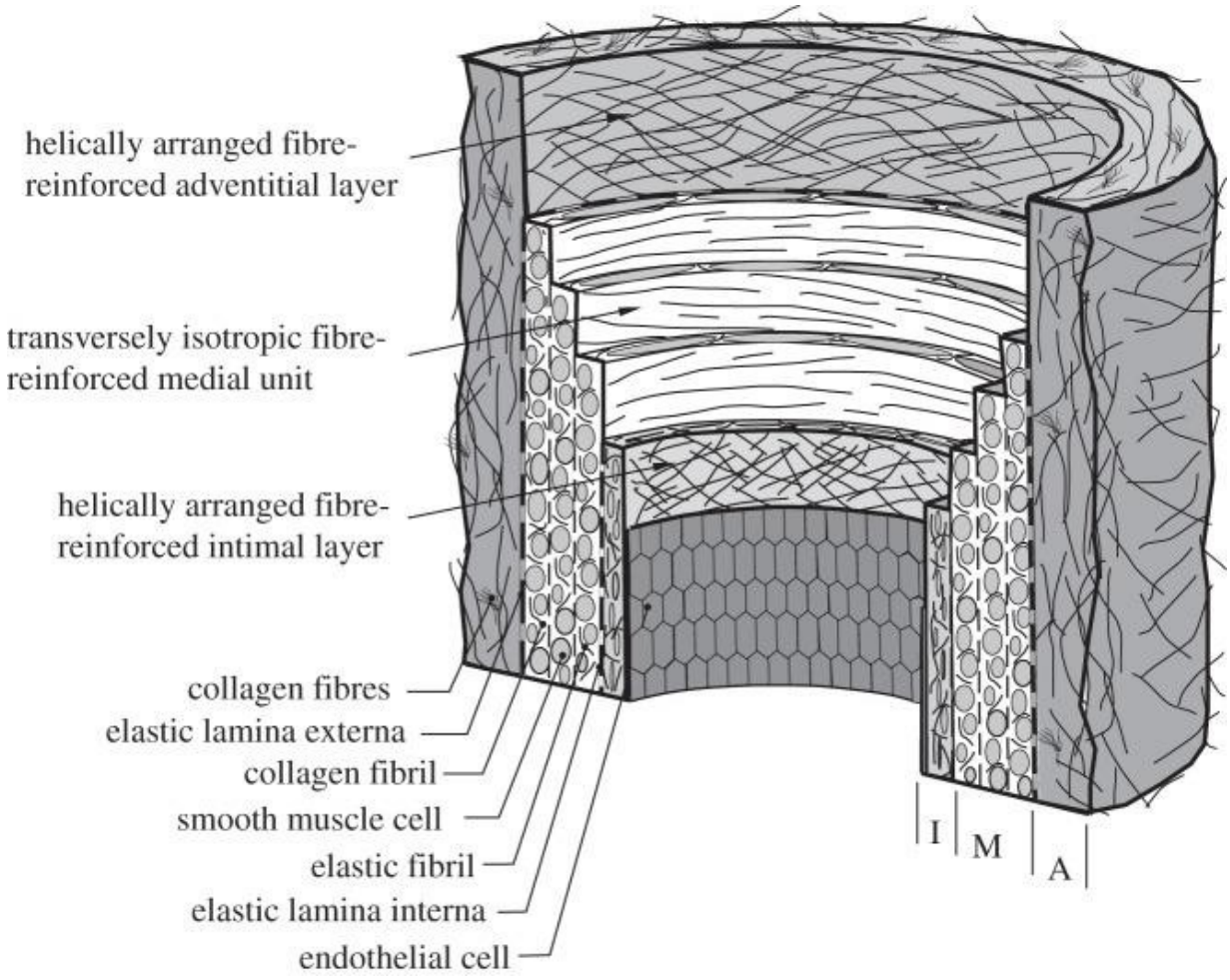

Figure 1.7 The architecture of the healthy human artery showing the elastin and collagen fibrils [29]

1.3.1.2 *Collagen*

Different from elastin, collagen is synthesized throughout life. The most important deficiency linked to aneurysms is collagen type III deficiency. It has been associated with intra-cerebral aneurysms and Ehlers-Danlos syndrome type IV, the latter including abdominal aortic aneurysms as one of its manifestations. An increase in collagen has been reported in abdominal aortic aneurysm walls. In order for the rupture to occur, the destruction of the medial collagen is required through enzymes [19, 20, 30-33].

1.3.2 *Smoking*

Abdominal aortic aneurysm has been associated to smoking since the 1960s [34]. A large study conducted in 1991 has found no relation between the number of cigarettes smoked and the risk of AAA. It has also been shown that hand-rolled cigarette smokers have higher risk than others [35]. In his study, Teun et al. has shown in 1999 that the effect of smoking on the risk of aneurysms is higher than its risk on coronary disease and peripheral vascular disease. Smokers are 7 times more likely to have an AAA than non-smokers. As for the ex-smokers, they are 3 times more likely to

develop an AAA when compared to non-smokers. Even when people quit smoking, the risk remains [35, 36].

1.3.3 *Other factors increasing the pressure on the aortic wall*

Many factors are involved in increasing the load on the aortic wall, making its dilatation, when added to other factors, easier. Hypertension is considered the most important. It increases the prevalence and the risk of rupture of an aortic wall [37-39]. It remains unclear whether arterial hypertension by itself is a major cause of AAA or whether it has to be combined with a pre-existing weakness of the aortic wall [40, 41].

Another important factor is the location of the abdominal aorta. It is the biggest artery in the body connected directly to the heart, which is the location with highest pressure. So the pulse pressure is high as the pulse wave passes through the abdominal aorta to reach the iliac bifurcation [42].

Genetic factors may also play a role with inherited defects affecting the function of elastin or collagen [43-48]. Inflammation may also cause the destruction and weakening of the aortic media. Inflammatory aneurysms are found in 4 to 10 per cent of the cases undergoing surgical treatment [49-51].

1.4 *Epidemiology*

AAA is considered as the 13th leading cause of death in the United States of America and responsible of the death of 0.8 per cent of the entire deaths in the country [52].

1.4.1 *Age and Sex*

The prevalence of AAA in men is higher than in women [53]: In England and Wales 1.36 per cent of men versus 0.45 of women die due to an abdominal aortic aneurysm [54]. In 2005, 4907 men versus 1991 women died in England because of AAA [55]. Also AAA is found more frequently at old people versus young people [53, 56-59]. As shown in figure 1.8, the prevalence increases quickly from 1 per cent when reaching the age of 60 years till it reaches its maximum at the age of 80 years. The mortality rate starts between the age of 40 and 70 years [58].

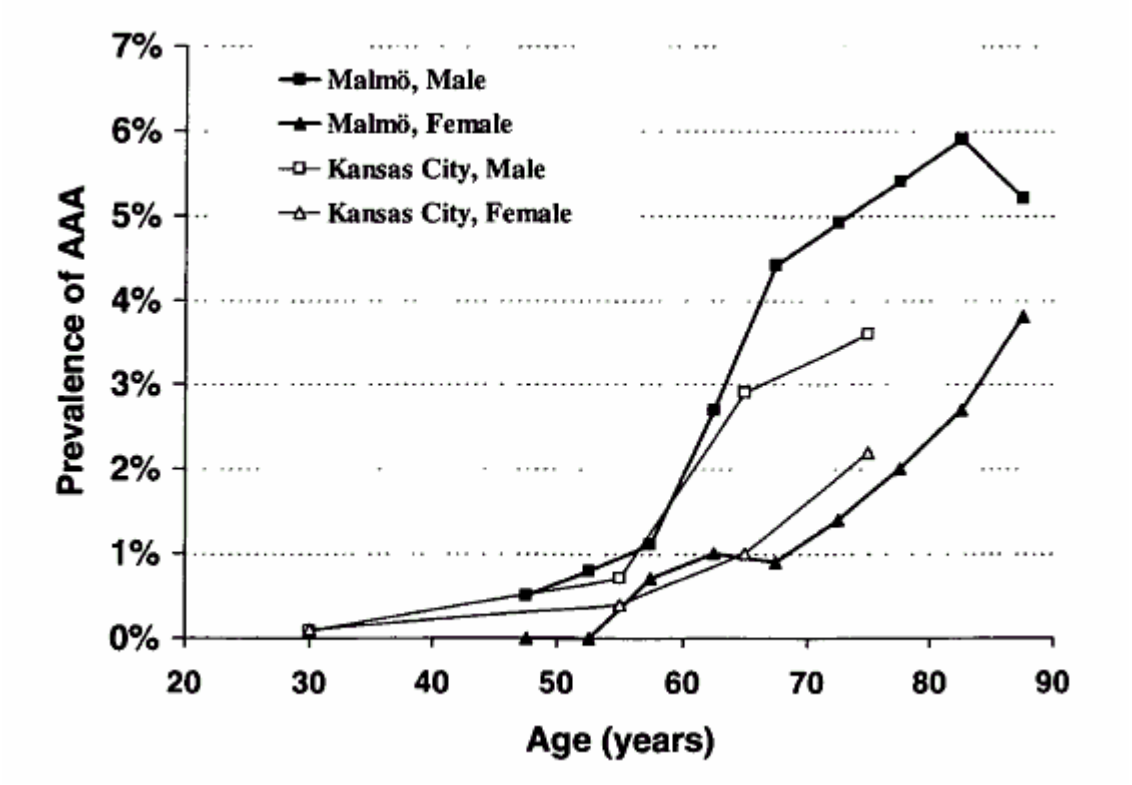

Figure 1.8 Prevalence of AAA depending on age and sex from Sweden and Kansas City [53, 57, 60]

1.5 *Abdominal Aortic Aneurysm*

1.5.1 *Rupture*

The size of the aneurysm and the growth rate are considered to be the most important factors for the assessment of the aneurysm rupture risk [61-64]. When the aortic diameter exceeds 30 mm, it is defined as an abdominal aortic aneurysm [65]. Most of the AAA ruptures occur before the patient reaches the surgical room [66]. This is why AAA has a high mortality rate of 65 to 85% of the patients [67]. When the diameter exceeds 5.5 cm, the patient should normally undergo surgery. This is why it hasn't been found a lot of data concerning the risk rupture of large abdominal aortic aneurysms. It has been shown that the rupture rate of AAAs with a diameter between 4 and 5.5 cm is between 0.7 and 1% / year [68]. When comparing the rupture rate between women and men, it has been found that women have a higher rupture rate for small AAAs and equivalent rupture rate for large AAAs (≥ 5.5 cm) [69, 70]. AAA rupture risk increases with larger diameters. A prospective cohort study performed in 47 Veterans Affairs medical centers on 198 patients revealed a 1-year incidence of rupture of 9.4% for AAA at 5.5 to 5.9 cm, 10.2% for AAA of 6.0 to 6.9 cm (19.1% for the subgroup of 6.5-6.9 cm), and 32.5% for AAA of 7.0 cm or more [71]. On the other hand many studies have shown that size is not the only significant determinant of

rupture. Expansion and rupture may occur regardless of the diameter of the AAA [61, 72].

1.5.2 *Imaging techniques for assessing AAAs*

Ultrasound is the first line examination to detect an aneurysm and assess its maximal diameter. Computed tomography is a second line examination providing reproducible measurements of maximal diameters and information on AAA extension. The choice between these two techniques depends on the indication and the accessibility of the region for ultrasound, which is often impaired in the abdomen. Obesity is a frequent factor making an ultrasound assessment of the abdominal aorta difficult [1].

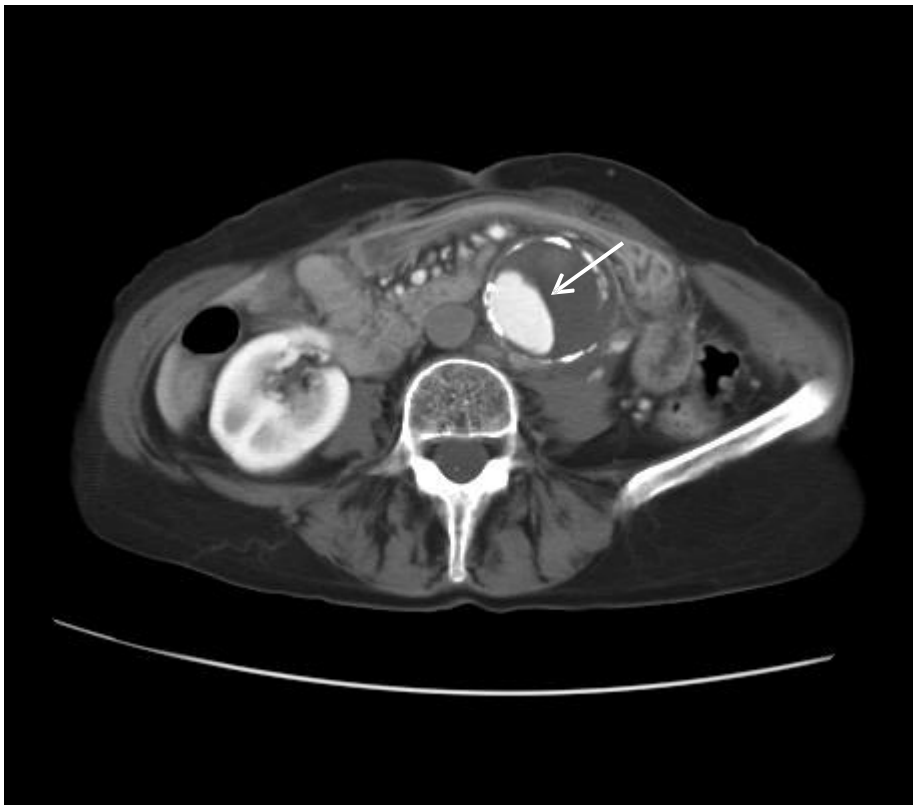

Figure 1.9 A CT scan examination showing an AAA with a contained rupture [73].

1.5.2.1 *Surveillance*

Once diagnosed, AAA of less than 55 mm in men or 50 mm in women are typically monitored every 6 months by ultrasound for changes in its maximal diameter [74, 75].

Figure 1.10 Ultrasound gray scale mode of an AAA [76].

1.5.2.2 *Screening and diagnosis*

AAA, if not discovered as an incidental findings in an abdominal scan for other indications often presents itself for the first time when it ruptures and thus have a high mortality [1]. In several countries including UK, USA and Canada, screening programs have been established to reduce AAA related mortality [77, 78].

1.5.3 *Intervention*

A CT scan is usually the technique of choice to identify patients with an indication for a surgical intervention (figure 1.9), based on diameters of 55 mm (men) or 50 mm (women). CT scan helps in determining the exact size of the aneurysm, localizing the aortic branches, identifying any calcification or inflammation and determine whether the patient can be eligible for open or endovascular repair (figure 1.11).

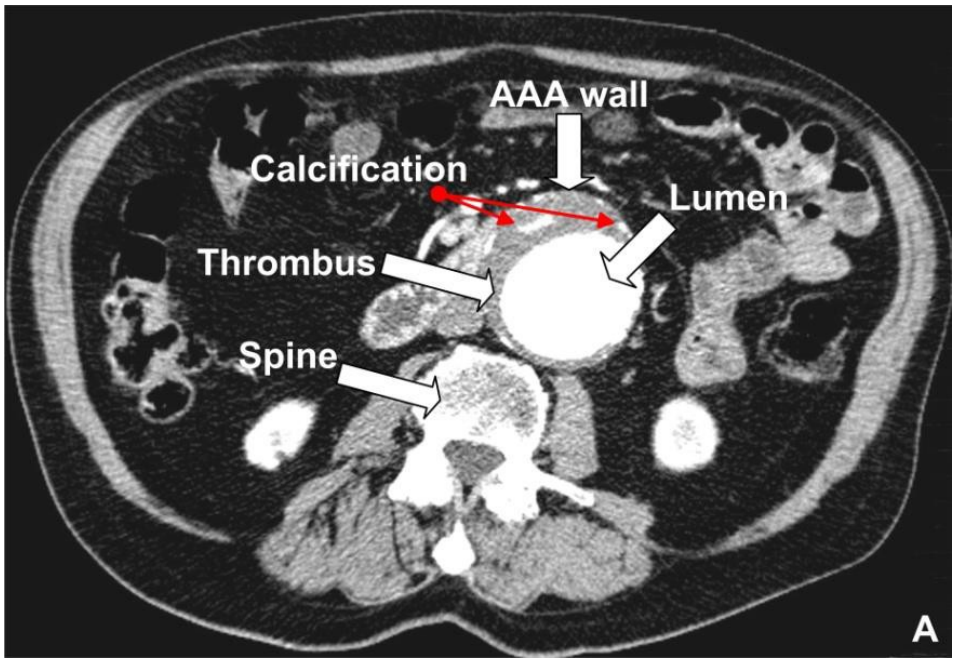

Figure 1.11 CT scan identifying the AAA lumen, wall, calcification, thrombus [79].

1.5.3.1 *Open surgical repair*

The indication for open surgical repair is based on the physician assessment of the patient surgical risk. Many factors that can increase the risk of this intervention may eliminate this option such as previous history of cardiac atherosclerotic disease (myocardial infraction and angina pectoris), stroke, diabetes and age. During the surgical operation, the aneurysm is repaired by interposing a graft through an incision at the abdomen level (figure 1.12). The mortality rate for this procedure has been recently estimated to be 4.1% - 6% [2, 80].

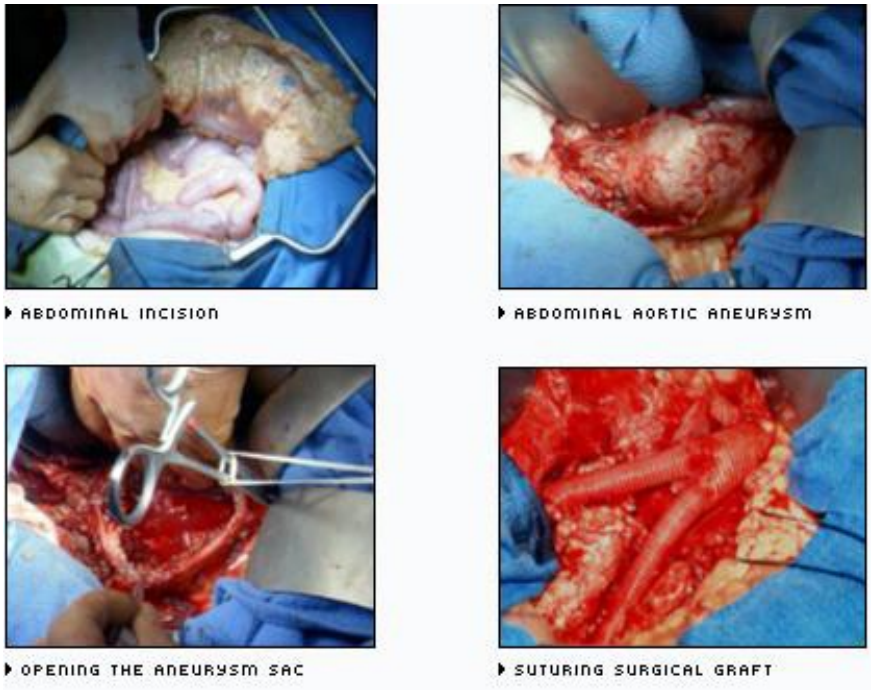

Figure 1.12 Open surgical repair [81].

1.5.3.2 *Endovascular aneurysm repair*

EVAR is less invasive and does not require any abdominal incision or exposure of the abdominal aorta. It involves the deployment of a stent graft (SG) inside the aneurysm to exclude the aneurysm sac from the blood circulation (figure 1.13) [82]. EVAR has been presented as an alternative to open surgical repair with a lower rate of post-operation mortality [2, 80]. The main limitation of EVAR is the durability of aneurysm exclusion and the occurrence of endoleaks (explained in Chapter 2). These limitations required long-term post placement surveillance (CT scan life-long follow up), diagnostic studies and possible secondary procedures, which increase the cost of EVAR by 50% [83-85].

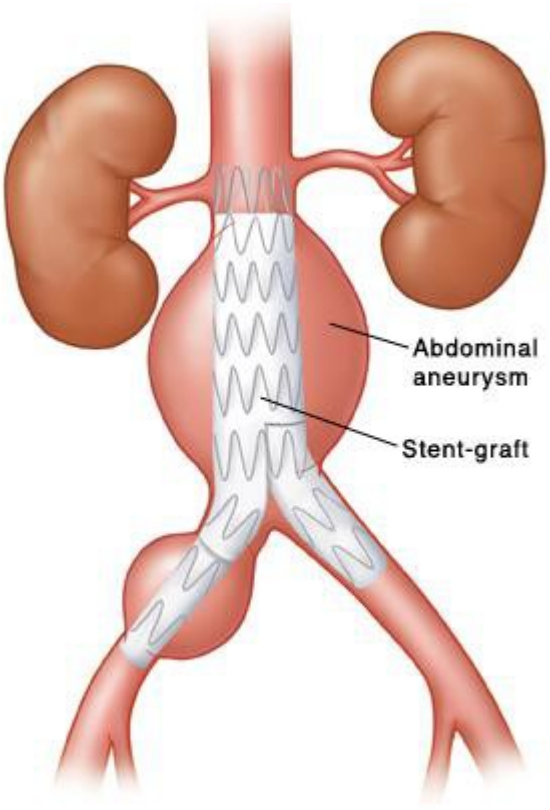

Figure 1.13 EVAR where a SG is placed inside the aneurysm without exposure of the abdominal aorta [86].

1.5.3.3 *Comparison between open surgical repair and EVAR*

EVAR has been introduced mainly to replace open surgical repair for the patients at higher surgical risk due to age, body weight and cardiac condition. As mentioned above, the post-operative mortality rate is lower than the open surgical repair but when it comes to the long term mortality rate, it has been found to be the same especially because of the occurrence of delayed rupture associated with endoleaks and the high rate of deaths non related to aneurysm disease [87].

When comparing EVAR with open surgical repair, we find less surgical complications for EVAR and higher rate of long term success for surgery [2, 88-95]. The cost of an EVAR is about 20,000$ versus 18,000$ for an open surgery (Year of 2010) [96]. But if we add the cost of secondary interventions for endoleaks (12% to 44% of the cases) and cost related to imaging follow-up, the cost of EVAR increases by 44% (a big part of the increase is due to the CT scan cost) [83, 96-98]. Even with the presence of higher cost and need for life long follow-up, patients still prefer EVAR because it is non-invasive and because of its short term success [99, 100]. This is why it has become the leading treatment for AAA disease in USA [3].

1.5.3.4 *Thrombus formation in AAA*

Thrombi are frequently observed in the peripheral portion of the AAA in areas of flow stagnation and of low shear stress condition [101]. It is essentially formed of platelets and erythrocytes and divided into 3 layers: luminal, medial and abluminal. The rigidity differs between one and another depending on the literature. Some authors find the abluminal more rigid since it is better organized and older than the others. Other authors mention the rigidity of the luminal region because of the presence of collagen [102, 103]. The thrombus can play an important role in the reduction of aortic wall stress which reduces the risk of rupture [104, 105], however major thrombus growth can also lead to the rupture by increasing the pressure on the wall [65, 106].

After endovascular repair (EVAR), complete sac thrombosis is expected due to coagulation since there is no or minimal residual flow in the aneurysm sac around the SG. If there is no residual flow or pressure, this new thrombus will mature with time and become organized.

Magnetic resonance imaging (MRI) can provide quantitative analysis of AAA healing when it comes to the size of the thrombus inside the aneurysm sac, it is also capable of differentiating between organized and unorganized thrombi [107]. MRI follow-up after EVAR has shown the presence of unorganized thrombus more than organized one inside the

aneurysm [107]. But MRI presents limited accessibility, higher cost than ultrasound, and metal artifact when using stainless-steel SG [108]. This is certainly an opportunity for the NIVE-LSME method proposed in this thesis.

CHAPTER II

Endoleak

2. Endoleak

Many types of failure occur after endovascular repair such as progressive expansion ("endotension"), infection and graft rupture, but the most common complication, observed in 10% to 36% of EVAR cases, is an endoleak. It is clinically defined as a residual aneurysm sac opacification seen on arteriography or CT scan after SG implantation caused by persisting blood flow in the aneurysm sac after EVAR [98, 109-111].

The presence of endoleaks can lead to rupture especially when associated with an expansion of the aneurysm by more than 5% [112-116]. Data of the EUROSTAR trial have shown that the risk of rupture and second interventions is higher for patients with type I or type III endoleak than with type II endoleak (explained in section 2.1). At the same time, the enlargement of the aneurysm following EVAR is lower for type II endoleak when compared to other endoleaks [117]. Other reports have shown shrinking in size of the aneurysm in the presence of an endoleak, which makes it hard to base the diagnosis based on the aneurysm size [118, 119].

2.1 *Endoleak types*

Endoleaks are classified into 5 types depending on their origin or their duration of existence (figure 2.1) [120]:

- Type I: It is defined as a blood flow between the proximal neck (type Ia) or the distal neck (type Ib) and the SG. This type of endoleak is considered dangerous because of its association with a pressurization of the aneurysm sac at systemic level, and requires detection and immediate surgical intervention or SG extension to close the gap. It is found for less than 10% of the cases [121-124]. Type I endoleak is usually related to an inaccurate SG sizing or progression of aortic degeneration in the landing zones (proximal aortic neck or common iliac). It can also be associated with SG migration caused by aneurysm sac shrinkage or inaccurate proximal SG fixation [125-129].

- Type II: This type of endoleak comes from collateral artery reverse flow (lumbar or inferior mesenteric arteries). It is the most common type of endoleak found in half of patients after EVAR [1]. Five percent of all cases are diagnosed with this type of endoleak [1, 123]. Treatment is typically deferred since it can thrombose by itself after a short period. The typical treatment is embolization when the CT scan shows an increase in the aneurysm's diameter of more than 5 mm [121, 122, 130-138].

- Type III: A gap, due to a fabric defect in the SG implanted inside the abdominal aortic aneurysm, leads to the third type of endoleak. An immediate surgical intervention closing the gap is indicated.

- Type IV: It is due to graft porosity and usually resolves itself with deposition of fibrin in the fabric. A design feature of the graft fabric may cause this type of endoleak. Usually this kind of endoleak occurs during the first 30 days following EVAR [124].

- Type V: It is an endotension observed in the aneurysm sac causing an increase of the aneurysm diameter without any evidence of endoleak on CT scan [124, 139]. The reasons behind this endotension are currently unknown, but an undetectable endoleak using conventional imaging techniques could be one of those reasons [124, 140]. Another explanation is the occurrence of sac pressurization through thrombus [124, 131, 140]. Immediate surgical intervention is required [131].

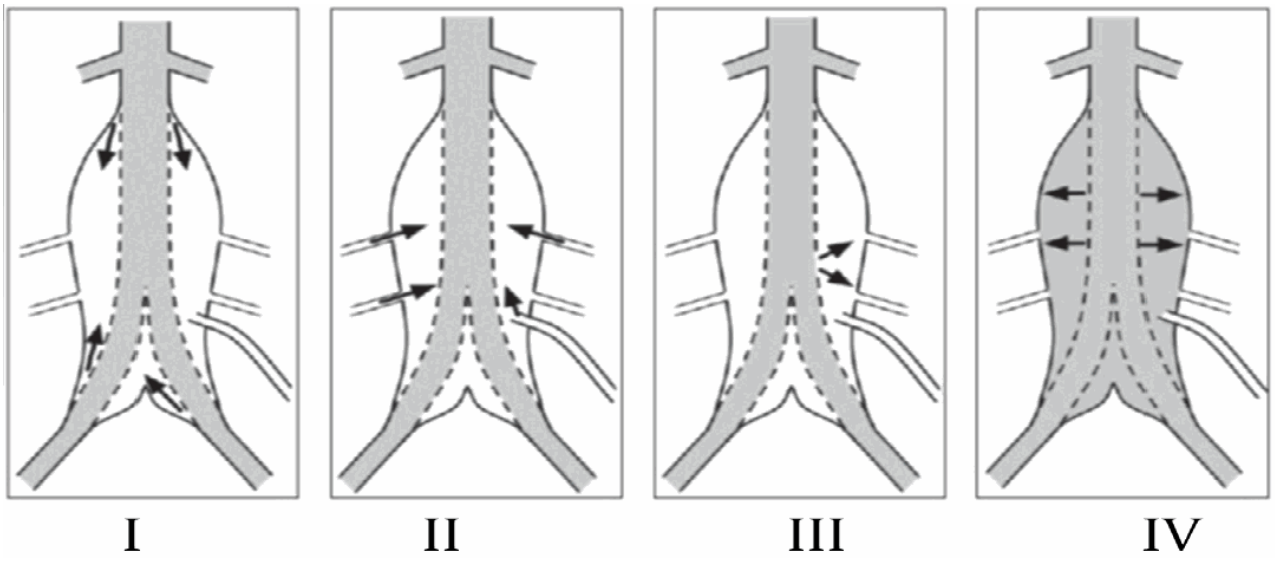

Figure 2.1 Visualization of the 4 types of endoleak. Type I: Blood flow coming from the proximal distal neck; Type II: Collateral flow coming from the collateral arteries; Type III: A gap in the SG leading to a blood flow inside the aneurysm sac; Type IV: graft porosity.

2.2 Imaging detection techniques

Different imaging modalities have been used for post-EVAR surveillance and diagnosis, but not all of them give accurate results and are capable of detecting all kinds of endoleaks with the same accuracy.

2.2.1 CT scan

Considered the gold standard for endoleak detection, CT scan provides accurate measures of aneurysm dimensions [141]. It is based on the rotation of the X-ray tube around the body to produce a 2D image through back projection filtration. The appearance of the tissue depends on its attenuation coefficient. CT is capable of producing 3D images by combining different 2D images [1]. By using a contrast agent capable of absorbing the X-ray emitted by the X-ray tube, endoleaks can be detected (figure 2.2). This technique, however, may lead to side effects related to exposure to ionizing radiation and, especially in people with renal insufficiency to contrast injection [141, 142]. Of special importance is the carcinogenic risk by frequent post-EVAR follow-up scans (each 6 months the first year and each year for the rest of his life) [143-145]. Efforts have been made to reduce the exposure dose and the frequency of exams, or even to replace it [146-148]. Despite its high overall sensitivity (86-93%), CT scan is not very sensitive to detect slow flow endoleaks, which are better

visualized by a dual phase acquisition (arterial and delayed venous phase) [149].

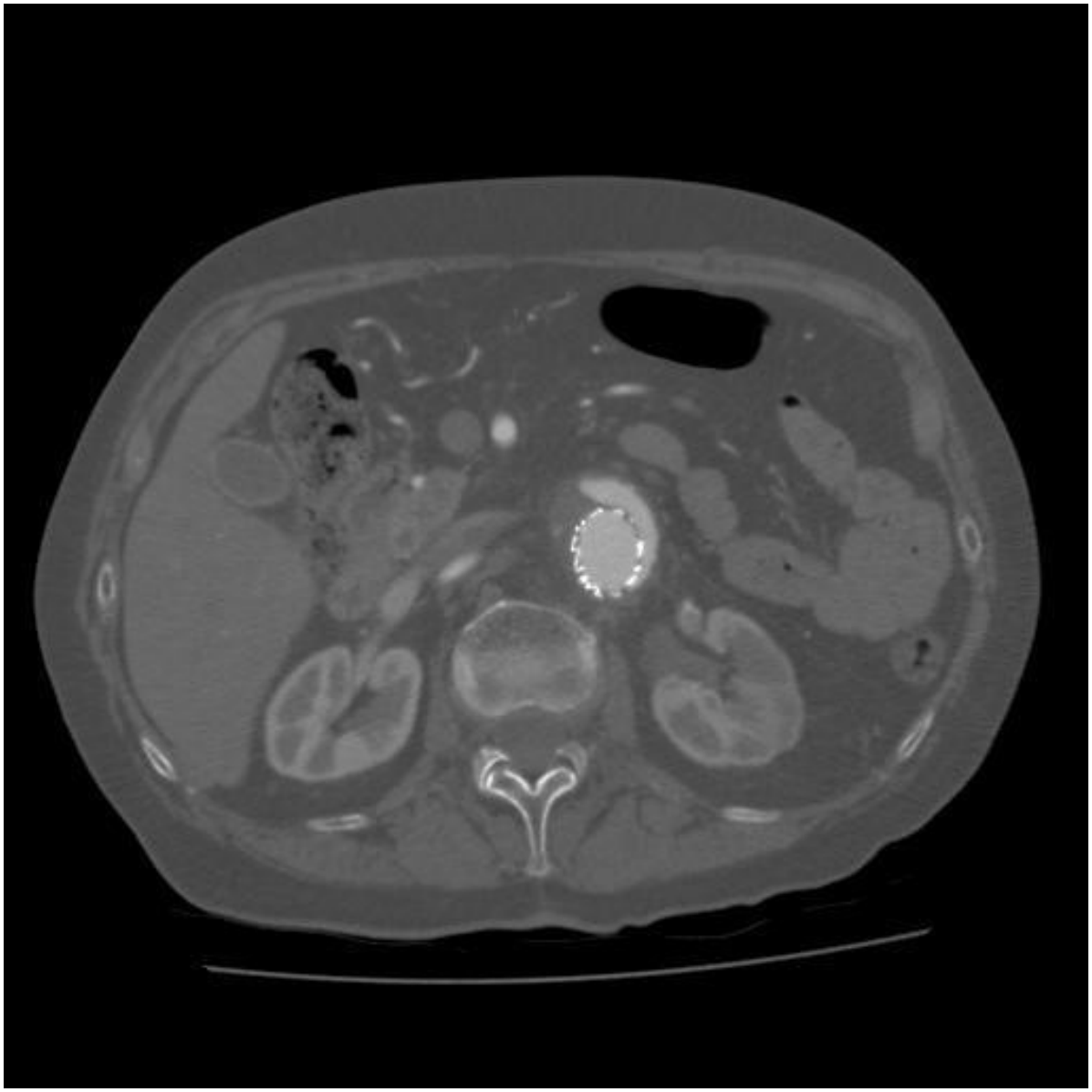

Figure 2.2 Axial CT scan image of an 80 years old female showing a type I endoleak [150].

2.2.2 Ultrasound

Ultrasound is a non-invasive and inexpensive imaging technique available in most clinics and hospitals. It can produce 2D images as well as 3D images depending on the movement of the operator handling the transducer [151]. Doppler ultrasound (DUS) is used to detect and quantify blood flow [152], whereas B-mode ultrasound is used to image structures. Both approaches are based on radio frequency (RF) waves sent into the region of interest of the body. A part of these waves are reflected, other are attenuated and the rest are scattered by small cellular structures. Part of the scattered and reflected waves reach the transducer that intermittently plays the role of a receptor. The emission time interval and the speed of RF waves determine the depth of the tissue to be imaged (depth = speed x time/2). Because of the attenuation, a gain is normally applied to compensate for it. Correlation-based techniques are used to process RF echoes in DUS, whereas envelope detection allows producing B-mode images.

Ultrasound is a good alternative to CT-scanner for post-EVAR surveillance because it is quick, easy, non-invasive and not expensive. It also provides accurate diameter measurements even if it is not as reproducible as CT imaging [153-156]. However, DUS may not detect

endoleaks in 23 to 32% of cases [149, 157]. It has shown better sensitivity to detect type I (88%) than type II (50%) endoleaks [158].

Several authors have proposed contrast-enhanced ultrasound (CEUS) to improve sensitivity [130, 131, 139, 159]. When comparing CEUS with CT, it reavealed good sensitivity but lower specificity. In addition, there is no ultrasound contrast agent that has been approved for non-cardiac use in the United States [143]. It is also time-consuming and expensive, which impairs its clinical utility [141].

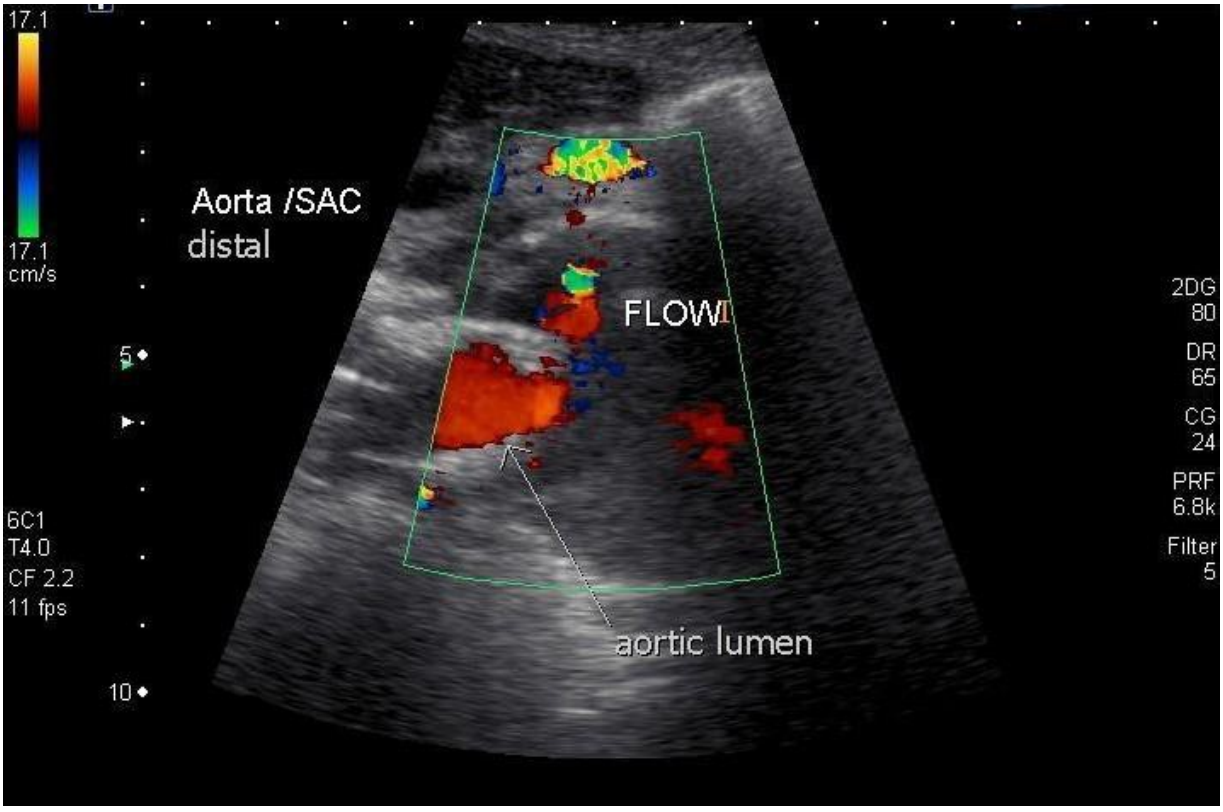

Figure 2.3 Doppler ultrasound acquisition showing a blood flow outside the SG and inside the aneurysm sac (endoleak) [160].

2.2.3 Angiography

Angiography, also known as fluoroscopy, is a widely used technique in hospitals. The technique uses cine X-ray image acquisitions during the first pass of a contrast agent. After crossing the body, these X-rays are detected and then processed to produce a real time image based on attenuation (bones have high attenuation versus tissues that have low

attenuation). For AAA characterization, the contrast agent is usually injected directly into the abdominal aorta and selectively through collateral arteries (inferior mesenteric, internal iliac and ilio-lumbar arteries through a catheter inserted in the femoral artery to detect and classify the endoleak and visualize the flow of blood inside the SG) [1]. Angiography is rarely used for endoleak detection but is performed before embolization to identify the source of endoleak to target the culprit vessel(s) [120, 121, 161-163].

Figure 2.4 Angiography acquisition of a 80 years old female showing a type I endoleak on the left side (indicated with a white arrow) [150].

2.2.4 Magnetic resonance imaging

Magnetic resonance imaging (MRI) is capable of giving high resolution images and differentiates between soft and hard tissues [164]. A major advantage is the absence of ionizing radiation unlike fluoroscopy and CT. It is based on a magnetic field that is powerful enough (1.5 or 3 tesla are common) to align protons in hydrogen atoms found in water molecules of the human body. A radiofrequency pulse is applied to induce resonant behavior of protons. The subsequent proton relaxation emits very small amounts of energy, which are used to generate images with a tissue-dependent contrast. Importantly, proton relaxation properties closely reflect tissue composition. Different factors such as field gradients, radiofrequency fields and acquisition timings affect the image quality and contrast [1].

A contrast agent can be added to alter the magnetic properties of blood and tissues and allows MRI to detect endoleaks [164]. The performance and quality of the technique is dependent on the type of SG used because of artifacts caused by its metallic composition (stainless steel SGs are not MRI compatible while nitinol SG are compatible). When the SG is compatible, the sensitivity is similar to CT for AAA size measurements. Regarding endoleaks, initial reports have shown a lower sensitivity of MRI when compared to CT angiography but recent reports have shown a better sensitivity of MRI when combined with high relaxivity

or blood pool contrast agents [165-168]. Finally, MRI is of limited use for patients with severe claustrophobia and contra-indicated in the presence of certain metallic implants, such as pacemakers or certain types of cardiac valves [108, 169-174].

Figure 2.5 Contrast enhanced MRI image showing a type II endoleak (white arrow) [173].

This page is left intentionally blank

CHAPTER III

Quasi-static elastography with the Lagrangian speckle model estimator (QSE-LSME)

3. Elastography

Palpation has been the first diagnostic method used by physicians for millennia. It is used to determine the rigidity of the tissue and locate the region of the disease. The same principle has been used in elastography where the mechanical property is measured by analyzing the response of the tissue toward a force applied to it. Often the example of the stone and sponge is used to better explain the theory of elastography: the sponge has a larger deformation than the stone because it is softer (figure 3.1). The same concept applies for hard inclusion detection in the human body [175].

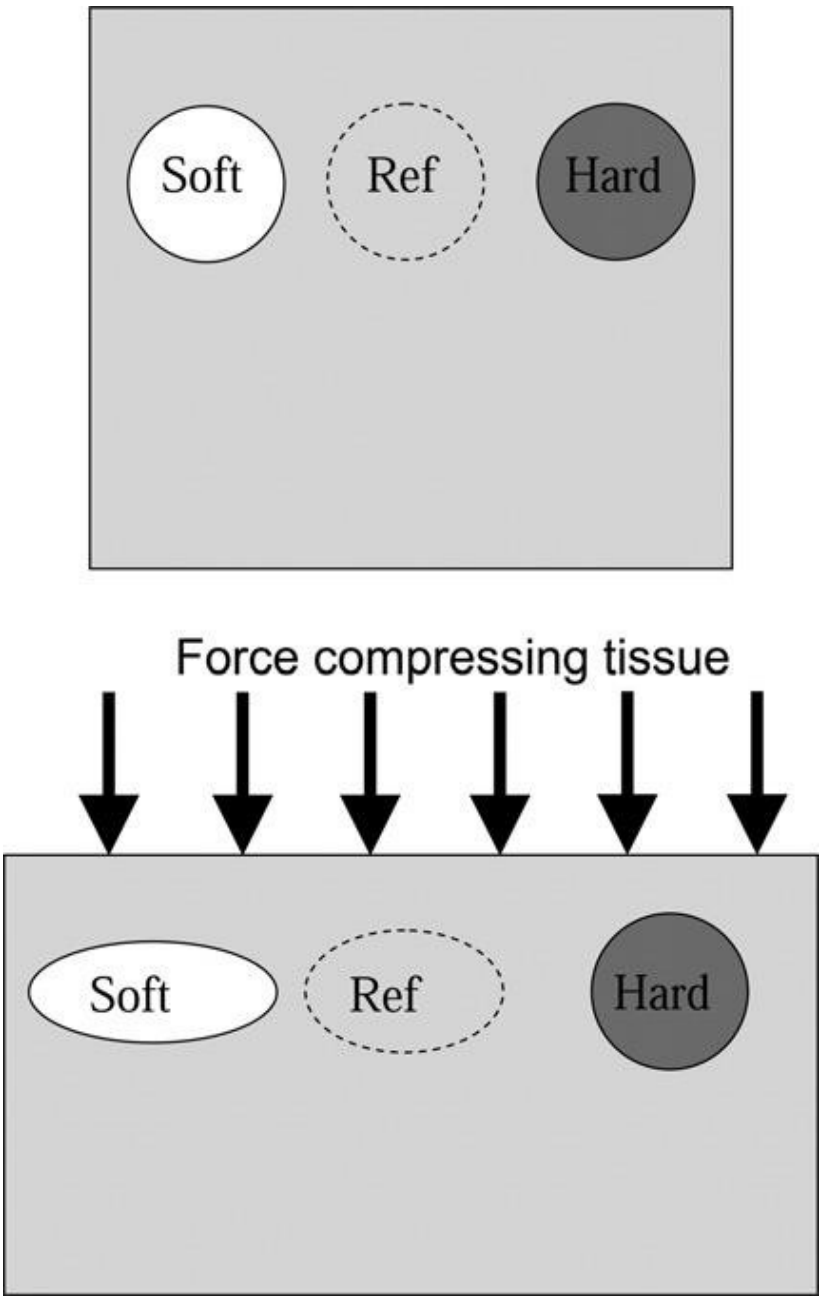

Figure 3.1 Two different tissues: Soft and hard giving different reactions toward a compression force [176].

Different elastography imaging approaches have been developed: Quasi-static elastography, harmonic elastography and transient elastography (figure 3.2). The three approaches are based on the same principles that include the perturbation of the tissue using a quasi-static pressure, harmonic or transient mechanical source, the measurement of the response or the displacement, and finally the deduction of the biomechanical properties of the tissue [177]. In this thesis, we will be focusing on the quasi-static elastography method to measure the strain of different components inside the aneurysm sac after endovascular repair (EVAR).

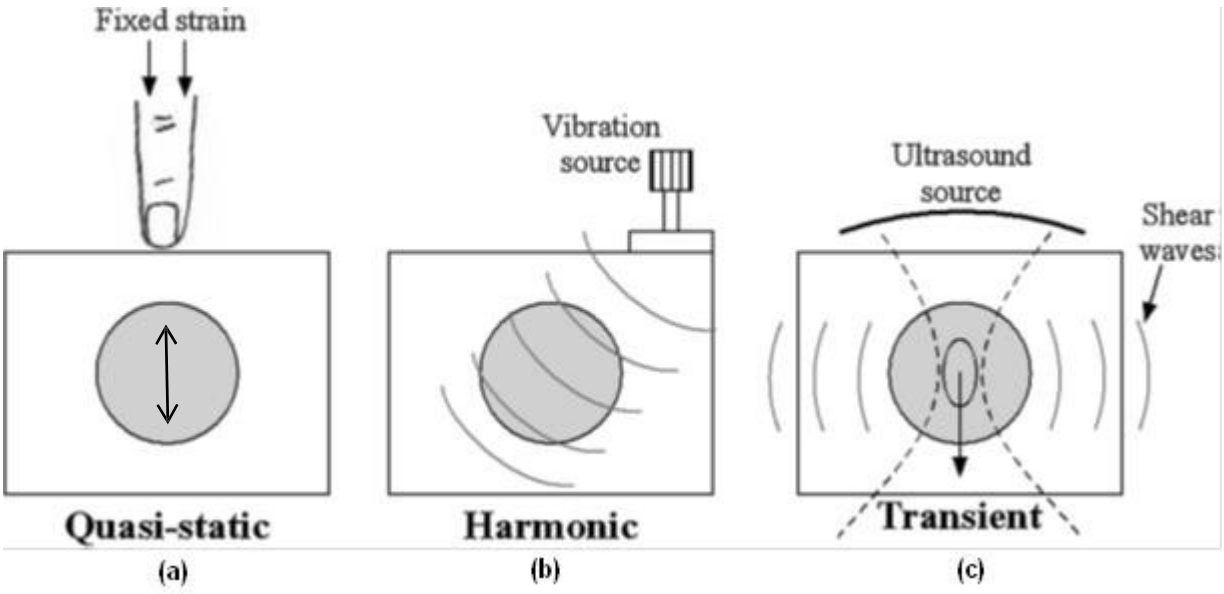

Figure 3.2 Three elastography imaging approaches: (a) Quasi-static elastography where the mechanical source is either from outside or inside the organ of interest (*e.g.*, from inside in the

case of the pulsation of an artery), (b) harmonic elastography, and (c) transient elastography [177].

3.1 Quasi-static elastography

Elastography aims to image the rigidity of a tissue, expressed as the Young's modulus in Pascal (Pa) or a strain in percent when the applied stress is unknown. In the ideal case of a linear elastic material, the Young's modulus is equivalent to the applied stress divided by the strain or deformation (figure 3.3):

E (Young's modulus) = /

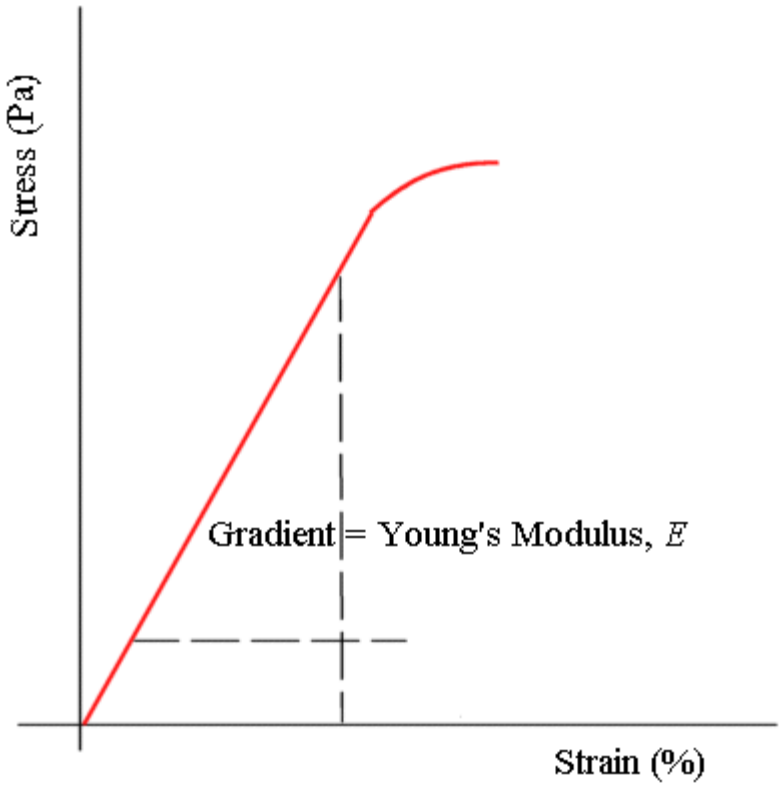

Figure 3.3 A stress/strain curve of a linear elastic material. Beyond a certain level of deformation, the material reaches an elastic limit and breaks [178].

In quasi-static elastography, images of the tissue deformation are obtained at a given stress and others at an additional incremental applied stress [179, 180]. For pulsating organs (*e.g.*, an artery), pair of images are taken at different phases of the cardiac cycle. Assuming affine deformation between applied stresses, elastography images expressed in percent of deformation are obtained. A modulus elastogram (*i.e.*, an image of the

Young's modulus) can be obtained by using an inverse problem, often based on finite element modeling [181].

3.2 Lagrangian speckle model estimator (LSME)

The Lagrangian Speckle Model Estimator (LSME), a 2-D model estimator that allows the computation of a 2-D strain tensor [182, 183], has been used to compute elastograms and estimate the 4 components of the 2D displacement matrix. Elastograms of strain and shear deformations can be computed [182, 184, 185]. In a blood vessel, the motion normally occurs radially while the ultrasound beam is projected axially. This is why there is a need for a 2-D estimator as the LSME.

- *The following tissue motion model best explains the approach:* Since vessel motion is radial, we can conclude that it is parallel to the beam at 90^0 and 270^0 for a cross-sectional or longitudinal view of the artery. The reaction of a vessel wall to a blood pressure pulsation is compression in systole and dilation in diastole. A radial strain is induced and can be measured. In order to measure the displacement in a specified zone, it is divided into small regions of interest (ROI) presented by W_{mn}. To approximate tissue motion, the LSME uses a Taylor-series expansion

where θ_i is a function of time, $[T_r]$ is the translation vector and [LT] the linear geometrical transformation of coordinates:

$$[\quad\quad\quad] = [\quad] + [\quad\quad\quad][\quad] \qquad (1)$$

In Eq. 1, $p(x,y,t)$ and $q(x,y,t)$ represent the new position of a point in the image and so the components of the displacement vector are:

$$[\quad] = [\quad\quad\quad] = [\quad] + \Delta\,[\quad]$$

and:
$$\Delta = [\quad\quad\quad] \qquad (2)$$

From Eq. 2, the strain tensor (ε) is defined as:

$$\varepsilon_{ij}(t) = -\,[\quad\quad\quad] \qquad (3)$$

where, ε_{xx} and ε_{yy} represent the lateral and axial strains, and $\varepsilon_{xy} = \varepsilon_{yy}$ are the shear strain. The elastograms reported in this study are ε_{yy} [185]. It corresponds to the deformation along the ultrasound beam.

- *The LSME is implemented using optical flow*: The speckle pattern reproduces the tissue motion with its complex kinematics because of the vascular tissue heterogeneity. Due to this observation, changes in the amplitude and phase of the backscattered ultrasound wavelets are observed. The speckle is represented as a continuum of a material property. The Lagrangian coordinate system or material coordinate system describes the speckle kinematics as:

$$\frac{dI}{dt} = \nabla I \cdot \vec{} + \frac{\partial}{\partial} = \frac{\partial}{\partial} \frac{\partial}{\partial} + \frac{\partial}{\partial} \frac{\partial}{\partial} + \frac{\partial}{\partial} = I_x \frac{\partial}{\partial} + I_y \frac{\partial}{\partial} + \frac{\partial}{\partial} \tag{4}$$

In Eq. 4, $I(x(t),y(t))$ is the speckle pattern and dI/dt is the total derivative expressing the speckle pattern rate of change of a point (x,y) when it is moving to $(x + \delta x, y + \delta y)$ in the $[t, t + \delta t]$ time interval. On the opposite, / gives the rate of change of $I(x(t), y(t))$ at a fixed observation point (x,y) [186].

Between two consecutives images for a short time interval (*i.e.*, for an affine deformation), the partial derivative $\partial I(x(t),y(t))$ can be written:

$$\partial I(x(t),y(t)) = I_x\,[\mathrm{m}_1 + \mathrm{m}_2 x + \mathrm{m}_3 y] + \mathrm{I}_y[\mathrm{m}_4 + \mathrm{m}_5 + \mathrm{m}_6 y] + (I(x(t + \delta t), y(t + \delta t)) - I(x(t), y(t))). \quad (5)$$

In order to implement the optical flow-based implementation of the LSME, we assume that $\partial I(x(t), y(t)) = 0$ inside the ROI (Mw), which allow us to write the discrete from of Eq. 5 as ($p \times q$ represent the size of the MWs):

[ ]

X

[ ]

=

[ ]

This page is left intentionally blank

Section II

Abdominal aortic aneurysm follow-up after endovascular repair in a canine model with non-invasive vascular elastography

This page is left intentionally blank

CHAPTER IV

Abdominal aortic aneurysm follow-up after endovascular repair in a canine model with non-invasive vascular elastography

4. Aortic aneurysm in a canine model

Animal models for AAA creation (figure 4.0), should mimic pathological features of AAA in humans. Canine or porcine models have been used mostly to test the endovascular exclusion techniques because of the similarity in shape, size and dimension with the human's AAA [187].

In our project a canine model has been chosen since endoleak can be created for a long period of time and are more persistent than the porcine model and thus more suitable for our follow up imaging protocol [188]. The absence of significant growth during follow-up facilitates animal handling for imaging. An approval from the institutional Animal Committee in accordance with guidelines of the Canadian Council on Animal Care is required. AAAs, type I and type II endoleaks were created following the protocol previously published by Lerouge et al. [188].

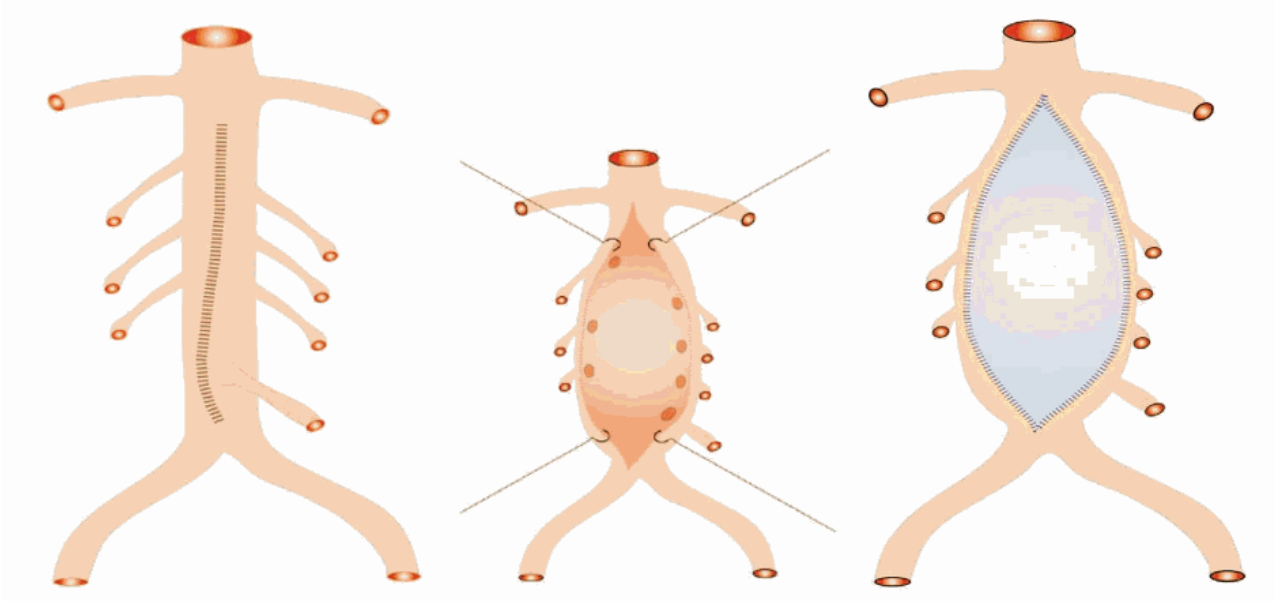

Figure 4.0 Representation of the AAA reconstruction [188]

4.1 Abdominal Aortic Aneurysm follow-up after Endovascular Repair in a canine model with Non-Invasive Vascular Elastography

4.1.1 Introduction to Manuscript

The goal of this master's thesis research project is to apply and optimize Non-Invasive Vascular Elastography (NIVE) of abdominal aortic aneurysm (AAA) after Endovascular Aneurysm Repair (EVAR) with Stent-Graft (SG) in a canine model to detect endoleaks and characterize thrombus organization. In order to do so, we conducted a correlation study between abdominal aortic aneurysm strain, Doppler ultrasound, CT and macroscopic examination. CT was chosen to be the gold standard for endoleak detection, whereas macroscopic tissue slides were the gold standard for thrombus differentiation (Organized and fresh thrombus). The accuracy of NIVE in detecting endoleak and differentiate the thrombus was assessed, leading to a comparison in strain values between type I and type II endoleak.

The effect of blood pressure on the strain results was studied by correlating the strain measurements and the aneurysm sac pressure. Furthermore a correlation between the sac measurements and strain results was evaluated to investigate the effect of size on the strain.

A comparison between DUS and NIVE was evaluated by taking CT and macroscopic cuts as reference.

NIVE could provide valuable information on the biomechanical aspects of the thrombus inside the aneurysm sac and the healing progression. It can also detect the presence of endoleaks as detected by CT scan.

4.1.2 Role of authors

The following is the order of authors for this submitted article and corresponding affiliations:

Elie Salloum[1,3,4,5]; Antony Bertrand-Grenier[1,3,4,5], MSc; Sophie Lerouge[2,6], PhD; Claude Kauffman[3,5,], PhD; Hélène Héon[1,3],DVM, MSc; Eric Therasse[1,2,3], MD; Marie Hélène Roy Cardinal[3,4], PhD; Guy Cloutier[1,3,4], PhD; Gilles Soulez[1,2,3,4,], MD, MSc

1. Department of Radiology, Radio-Oncology and Nuclear Medicine, and Institute of Biomedical Engineering, Université de Montréal, Montreal, Quebec, Canada
2. Department of Radiology, Centre hospitalier de l'Université de Montréal (CHUM), Montreal, Quebec, Canada
3. Centre de recherche de l'Université de Montréal (CRCHUM), Montreal, Quebec, Canada
4. Laboratory of Biorheology and Medical Ultrasonics (LBUM), Université de Montréal's Hospital Research Centre (CRCHUM), Montreal, Quebec, Canada
5. Clinical Image Processing Laboratory (LCTI), Univertité de Montréal's Hospital Research Centre (CRCHUM), Montreal, Quebec, Canada
6. École de technologie supérieure, Montreal, Quebec, Canada

The role of all authors of the submitted article is detailed below.

Elie Salloum: First author of this project. Performed: Imaging acquisition protocol modifications, data collection, US-NIVE data collection, Ultrasound imaging interpretation and segmentation, preparation of

macroscopic tissue slides, preparation of necropsy, optimization of the ORS plugin software, literature review, presentation of the project at multiple conferences in 2013 (International Tissue Elasticity Conference (Lingfield, UK), Radiological Society of North America (Chicago, IL); writer of manuscript submitted to *Radiology Journal* on the first of September 2014.

Antony Bertrand-Grenier: Performed data collection, preparation of macroscopic tissue slides, literature review; correction of the manuscript for submission.

Sophie Lerouge: Supervision of the histology and macroscopic slides; correction of the manuscript for submission.

Claude Kauffman: Performed optimization and development of the CT scan platform; correction of the manuscript for submission.

Hélène Héon: Performed follow up of the dogs before and after implantation; correction of the manuscript for submission.

Eric Therasse: Clinical context, stent graft and endoleak clinical parameters; correction of the manuscript for submission.

Marie Hélène Roy Cardinal: Performed optimizations to the platform, contributed to troubleshooting of technical issues for calculation of elastograms; correction of the manuscript for submission.

Guy Cloutier: Co-director and supervisor of my studies and this research project; correction of the manuscript for submission.

Gilles Soulez: Director and supervisor of my studies and this research project; supervised the Ultrasound, CT scan acquisitions, performed angiography, review of segmentation and correlation of imaging tests; correction of manuscript.

4.1.3 Thesis format of Submitted Manuscript

In section 4.2, the manuscript submitted to X for publication is presented. The list of references following the conclusion of this manuscript is the same as what was submitted, and the article's reference numbers have been kept in round brackets and italicized *"(1)"* throughout the manuscript. In addition, for efficient navigation and homogeneity of this thesis, appropriate reference numbers in square brackets "[1]", with links to the reference section of this thesis, have been maintained.

4.2 Manuscript submitted to Radiology Journal

The manuscript starts on the following page.

Abbreviated Title page

Manuscript title:

Abdominal aortic aneurysm follow-up after endovascular repair in a canine model with non-invasive vascular elastography

Manuscript Type:

Original Research

Advances in Knowledge:

1- Ultrasound Non-Invasive Vascular Elastography (NIVE) has the potential of being a complementary follow-up imaging technique to detect endoleaks after EVAR and to characterize the thrombus organization based on its mechanical property

2- NIVE was capable of characterizing the endoleak and thrombus organization inside the aneurysm sac and thus possibly detect an endotension after EVAR

3- Strain measurements are independent from the systemic pressure and the pressure inside the aneurysm sac, as well as from the size of the endoleak and the thrombus.

Implications for patient care:

NIVE is feasible and has the potential to characterize thrombus organization inside the aneurysm. No hardware modification is needed and can be a useful adjunct during Doppler examination after EVAR. It could reduce the need for CT angiography, the cost and the exposition to ionizing radiation and contrast agents for the follow up of AAA after EVAR.

Summary Statement:

NIVE technique could detect aneurysmal elasticity tissue properties not seen on B-mode and color Doppler and reduce the need for CT angiography, for the follow up of AAA after EVAR

List of authors:

Elie Salloum[1,3,4,5]; Antony Bertrand-Grenier[1,3,4,5], MSc; Sophie Lerouge[3,6], PhD; Claude Kauffman[1,3,5], PhD; Hélène Héon[3],DVM, MS; Eric Therasse[1,2,3], MD; Marie Hélène Roy Cardinal[3,4], PhD; Guy Cloutier[1,3,4], PhD; Gilles Soulez[1,2,3,5], MD, MSc

1. Department of Radiology, Radio-Oncology and Nuclear Medicine, and Institute of Biomedical Engineering, Université de Montréal, Montreal, Quebec, Canada
2. Department of Radiology, Centre Hospitalier de l'Université de Montréal (CHUM), Montreal, Quebec, Canada

3. Centre de recherche de l'Université de Montréal (CRCHUM), Montreal, Quebec, Canada
4. Laboratory of Biorheology and Medical Ultrasonics, Centre de recherche de l'Université de Montréal (CRCHUM), Montreal, Quebec, Canada
5. Clinical Image Processing Laboratory (LCTI), Centre de recherche de l'Université de Montréal (CRCHUM), Montreal, Quebec, Canada
6. Department of mechanical engineering, École de technologie supérieure, Montreal, Quebec, Canada

PURPOSE

To assess the ability of non-invasive vascular elastography (NIVE) to characterize endoleaks and thrombus organization in a canine model of abdominal aortic aneurysm (AAA) after endovascular aneurysm repair (EVAR) with stent-graft (SGs).

METHODS AND MATERIALS

SGs were implanted in a group of 18 dogs with an aneurysm created in the abdominal aorta. Type I endoleak was created in 4 aneurysms, type II in 13 aneurysms and no endoleak in 1 aneurysm. Doppler ultrasound (DUS) and NIVE examinations were performed at baseline, 1-week, 1-month, 3-month and 6-month follow-up. Angiography, CT-scan and macroscopic tissue slides were performed at sacrifice. Strain values were computed using the Lagrangian Speckle Model Estimator (LSME). Areas of endoleak, solid organized thrombus and fresh thrombus were identified and segmented by comparing the results of CT scan and macroscopic tissue slides. Strain values in areas with endoleak, organized and fresh thrombi were compared.

RESULTS

Maximal axial strains over consecutive heart cycles in endoleak, organized and fresh thrombus areas were respectively 0.78 ± 0.22, 0.23 ± 0.02, 0.10 ± 0.04 %.

Strain values were significantly different between endoleak and organized or fresh thrombus areas (p = 5,136E-09) and between organized and fresh thrombus areas (p = 0.00063). All endoleaks were clearly depicted on elastography examinations. No correlation was found between strain values and type of endoleak, sac pressure, endoleak size and aneurysm size.

CONCLUSION

NIVE can characterize endoleak and thrombus organization regardless of the size, pressure and the type of endoleak.

Introduction

Endovascular aneurysm repair (EVAR) using stent grafts (SGs) is a promising alternative to surgery with lower peri-operative mortality and morbidity rates (2.1 – 4 % versus 5.7 – 7 %), and shorter hospitalization time [2, 3, 96, 189] *(1-4)*. The main limitation of this method is, however, the durability of the aneurysm exclusion and the occurrence of endoleaks requiring regular follow-up imaging [190] *(5)*. For EVAR surveillance, different modalities such as computed tomography (CT) scanning, Doppler ultrasound (DUS), and magnetic resonance imaging (MRI) have been adopted [159] *(6)*. CT-scan is considered the gold standard for follow-up after EVAR but leads to cost increase and exposition to ionizing radiation and contrast agents [141] *(7)*. Approximately 65% of follow-up costs have been attributed to CT scanning [85] *(8)*. An effort was made for DUS to replace CT scan (or MRI) but the main concern is the lower sensitivity and specificity of the former method to detect endoleaks (failure in 23 to 32% of cases) [149, 158, 191-194] *(9-14)*.

The Lagrangian Speckle Model Estimator (LSME) is becoming established to non-invasively map vascular tissue deformations with a standard array transducer [195-198] *(15-18)*. This technique, labeled non-invasive vascular elastography (NIVE), was first developed to characterize carotid atherosclerotic lesions. Then, a study conducted by Fromageau et al. reported preliminary data using the LSME in a type I

endoleak canine aneurysm model [199] *(19)*. In the latter study, it was possible to characterize the axial strain of the aneurysm wall and differentiate the venous patch used to create the model from the native artery, and detect endoleaks as areas of strain decorrelation (equivalent to aliasing on Doppler ultrasound). However, this study was limited by the small sample size, the absence of CT examinations as gold standard for endoleak diagnosis, and the absence of correlation with thrombus organization.

Strain measurement with NIVE has thus the potential of being a complementary follow-up imaging technique for EVAR to detect endoleaks and to characterize the thrombus organization based on its mechanical property. The objectives of the present study were: 1) to correlate NIVE elastographic measurements with CT-scan, DUS, angiography, sac pressure measurements and histomorphometric data from macroscopic tissue slides; 2) to define elastographic patterns associated with type I and II endoleaks, and 3) to characterize the endoleak properties and organization of the thrombus based on strain measurements.

Methods

A. Aneurysm Creation in a Canine Model

In order to test NIVE for the detection of endoleaks and the characterization of thrombi within the covered aneurysm sac, aortic aneurysms were created in 18 mongrel dogs between September 2011 and November 2013. The surgical construction of aneurysms was done with preservation of the collateral vessel patency (collateral flow) or ligation of all collateral vessels arising from the sac (absence of collateral flow). A SG was implanted after a recovery period of 8 weeks (3 dogs: TFLE - Zenith Flex® AAA Endovascular Graft, 15 dogs: ZFLE - Zenith Flex® AAA Endovascular Graft (Cook Medical, Bloomington, IN). The animals were planned to be divided into 3 groups: 5 dogs with type I endoleaks (short landing zone) with collateral flow, 7 dogs with type II endoleaks (adequate landing zone) with collateral flow, and 6 dogs with neither endoleak nor collateral flow (adequate landing zone and collateral arteries ligated). All protocols were approved by the Animal Care Committee in accordance with the guidelines of the Canadian Council of Animal Care. At the end of the study, each dog was sacrificed and a necropsy was performed. The aneurysms were collected and fixed in buffered formalin.

B. Imaging Protocols

DUS and elastography examinations were performed at baseline, 1-week, 1-month, 3-month and 6-month follow-up. Angiography, CT-scan and macroscopic tissue cuts were also performed at sacrifice. All acquisitions were conducted under general anesthesia and by the same 20-year experienced technologist supervised by a 22-year experienced vascular radiologist. Before sacrifice, after dissection of the abdomen, the sac and aortic pressure were measured by introducing a Spiral needle (22G x 3–´´) inside the aneurysm sac and the aorta, and connecting it to a pressure sensor. Between baseline and sacrifice, measurements of the aneurysm's length, maximum and minimum diameters of the aneurysm, areas of the SG and aneurysm were taken during DUS acquisitions in order to correlate them with strain parameters, and to study the size evolution in the presence and absence of endoleak.

B.1. Doppler Ultrasound Acquisitions

All DUS examinations were performed using an Aixplorer scanner (Supersonic Imagine, Aix en Provence, France) equipped with a 256 elements (SuperLinear™ SL15-4) 7.5 MHz linear array transducer (pulse repetition frequency = 1.95 KHz, scale = 10 cm/s, sound speed = 1540 m/s). The high definition frame rate (HD/FR) was set to middle, the wall filter to low and the smoothing to 0. Ultrasound sequences were

acquired on longitudinal and three axial planes (proximal, mid and distal parts of the aneurysm).

B.2 Radio Frequency (RF) Acquisitions

Ultrasound RF data were acquired using a Sonix Touch scanner (Ultrasonix Corp., Vancouver, Canada) equipped with a 128-element L14-5/38 10 MHz linear array transducer. This probe had a 60% bandwidth at a frame rate of 25 Hz, RF data were sampled at 40 MHz, and acquisitions were performed over approximately 5 sec for each plane. Systemic pressures and pulse rates were measured at the beginning, middle and end of RF acquisitions (LifeWindow™ 6000V), as these variables potentially affect strain measures. The acquisitions were acquired on the same planes as DUS.

B.3 Angiography

Digital subtraction angiography (Koordinat 3D, Siemens Medical, Forcheim, Germany) was performed at baseline, before and during implantation of the SG, and at sacrifice by the same interventional radiologist. A pigtail catheter (4 or 5 French) was inserted in the abdominal aorta at the level of renal arteries. Acquisitions were performed during injection of 20 ml at 10 ml/s of iodine contrast agent (Iopamidol Isovue 200, Bracco Imaging Canada, Anjou, Quebec, Canada, during implantation and Conray 60, Mallinckrodt Canada, Pointe-Claire, Quebec, Canada, during

sacrifice) to detect type Ia and II endoleaks. A second injection was performed after pulling the catheter at the distal portion of the aorta in order to detect type Ib endoleaks.

B.4 CT-Scan

At sacrifice, a contrast-enhanced CT-scan (Somatom 64, Siemens Medical, Erlangen, Germany) was acquired before and after contrast injection (69 ml of Iohexol, Omnipaque 300 mg, GE healthcare, Mississauga, Ontario, Canada, iodine concentration at 4 ml/s) in arterial and venous phases to detect and classify the endoleak using recognized criteria [200] *(20)*. All CT angiograms were acquired on a 64 multi-detector scanner, with a retrospective gating, a tube voltage of 120 KV, a collimation of 0.6 mm and a pitch of 0.2. The reconstruction of 70% of the cardiac cycle was typically used for analysis. A bolus tracking method was utilized to start the arterial phase, whereas the venous phase was acquired 10 seconds after the end of the arterial phase.

B.5 Macroscopic Tissue Slides

After sacrifice, the aorta was perfused by 10% buffered formalin at 150 mmHg for 1 hour before being harvested and fixed in formalin for 24h. For correlation with CT scans and US, axial macroscopic sections including the intact tissue/SG interface

were prepared every 3 mm using an Exakt cutting system (Exakt GmbH, Norderstedt, Germany).

B.6 Segmentation and Post-processing

Based on the cranio caudal level of axial acquisitions, maximum diameter of the aneurysm and SG orientation inside the aneurysm, a registration between CT-scan, DUS, macroscopic cuts and RF ultrasound images was performed after sacrifice. The CT-scan was taken as reference to define the endoleak area. The areas of organized and fresh thrombi were delimited on macroscopic tissue slides after matching all the information coming from the 3 techniques (DSA, CT scanner, B-mode and color Doppler DUS) (see Figure 4.1). A fresh thrombus was defined on macroscopic cuts as areas of loose thrombus with black brown coloration, which corresponds to fibrin blood clot containing phantoms of red blood cells and no visible fibrous organization according to histology (Figure 4.2). Organized thrombus presented a dense and yellowish appearance indicative of fibrous organization.

Once identified, manual segmentations of the endoleak area, organized and fresh portions of thrombi were performed in all imaging modalities, except for RF ultrasound acquisitions. An application developed by our team for carotid artery segmentation [201] *(21)* was adapted for the segmentation of regions of interest (endoleak, organized and fresh thrombi) on RF acquisitions. All segmentations were performed

by the same technologist and verified by the same radiologist. The LSME-NIVE method was applied to compute time-varying curves of axial strain averaged over segmented areas for 3 or more consecutive cardiac cycles (Figure 4.3) [202] *(22)*. Figure 4 explains the protocol adopted for the segmentation in each imaging modality.

C. Strain Parameters

Five NIVE strain parameters were investigated: the maximum and minimum axial strains (Max/MinAxStrain), maximum cumulated axial strain (MaxCumAxStrain), and maximum and minimum strain rates (Max/MinStrainRate). MaxAxStrain and MinAxStrain represent the mean value, over acquired cardiac cycles, of positive and negative peaks of the time varying instantaneous axial strain curve, respectively (see Figure 4.3a). The maximum positive axial strain corresponds to the peak dilatation, whereas the minimum negative axial strain represents the peak compression of the tissue. MaxCumAxialStrain is the average, over acquired cardiac cycles, of maximum positive values of the cumulated axial strain curve, corresponding to peak dilatation (see Figure 4.3b). The last 2 parameters, defined as the speed of deformation during a cardiac cycle, were computed from the time derivative of the instantaneous filtered axial strain curve, as previously defined [202] *(22)*. MaxStrainRate is the time averaged positive peaks of the strain rate curve, whereas MinStrainRate represents the mean of negative peaks.

D. Statistical Analysis

Statistical tests were performed using SigmaStat (version 3.11, Systat Software Inc. San Jose, CA). Outcome comparisons of NIVE parameters (*e.g.*, MaxAxStrain, MinAxStrain, etc …) between endoleak, organized thrombus and fresh thrombus strain groups were analyzed using the Kruskal-Wallis method. All 2x2 multiple comparisons were estimated using Wilcoxon rank sum test, where statistical significance was adjusted using a Bonferroni correction. For each group (endoleak, organized and fresh thrombi), comparisons were performed between types I and II strain results using Wilcoxon rank sum test.

For the correlation between strain and aneurysm sac pressure and systemic pressure measurements, as well between the aneurysm size (maximal diameter and area) at sacrifice, Pearson correlation tests were performed. Statistical significance was set at $p < 0.05$.

Results

A. Technical feasibility and accuracy of NIVE for endoleak and thrombus characterization

Eighteen mongrel dogs were studied after implantation of a SG. No complications occurred during the study. Four dogs had a type I endoleak, 13 dogs had a type II endoleak, and 1 dog had no endoleak and thus a perfect seal of the aneurysm sac. One type I converted in a type II endoleak probably due to an inadequate undersizing of the SG. Five EVARs aiming for a complete sealing eventually presented type II endoleaks, probably because of the presence of lumbar arteries that were not accessible for ligation. In total, all 18 dogs had solid thrombus in the sac; 6 of these dogs also had fresh thrombus.

Strain measurements were successfully processed in all areas of interest defined after the process of segmentation and intermodal registration. As introduced earlier, 5 NIVE strain parameters were investigated: Max/MinAxStrain, MaxCumAxialStrain, and Max/MinStrainRate [202] (22). All 5 parameters showed statistically significant differences ($p < 0.001$) when comparing results in areas corresponding to an endoleak versus a solid or a fresh thrombus. Only the MaxAxStrain and MinStrainRate parameters showed significant differences ($p <$

0.001) between solid and fresh thrombi (Table 4.1). Figure 4.5 is reporting those differences for the case of the parameter MaxAxStrain.

B. Comparison between type I and type II endoleaks

We further compared strain parameters for the three categories of aneurysmal sac tissue properties (*i.e.*, endoleak, fresh and organized thrombus) for AAA presenting type I and type II endoleaks. As summarized in Table 4.2, all 5 strain parameters showed no statistically significant differences between the two endoleak groups.

C. Correlation between strain, sac pressure and systemic pressure measurements

Table 4.3 summarizes geometric and mean sac pressure measurements for each dog. The mean sac pressure in AAA with type I and II endoleaks were respectively estimated at 67.5 ± 20.6 and 51.9 ± 19.8 mmHg ($p = 0.2$). Because MaxAxStrain and MeanStrainRate could discriminate aneurysmal sac tissue properties (see Section A), those measures were correlated with mean pressure values within the sac and systemic pressure as well. None of these parameters presented a significant correlation ($p > 0.05$); as an example we present in Figure 4.6 correlations for MaxAxStrain.

D. Correlation between strain measurements and aneurysm size

Geometric measures in Table 4.3 were correlated with strain parameters. No significant correlations were found ($p > 0.05$). Figures 4.7 and 4.8 show the absence of correlations between MaxAxStrain and the maximum aneurysm and endoleak areas respectively.

Discussion

With this preclinical model, we could confirm the feasibility of NIVE for the characterization of endoleaks and thrombus organization after EVAR. The LSME algorithm estimated the strain transmitted by the cardiac pulsation inside the aneurysm sac. No external compression or radiation force was needed.

The results showed that the endoleak area, organized and fresh thrombi characteristics display different values on NIVE. Thus, this technique could be capable of detecting the presence of an endoleak in addition of being able characterizing the thrombus region. In this setting, NIVE could be a tool to monitor the healing process inside the aneurysm sac after EVAR [203] *(23)*. The high strains obtained within the endoleak area are due to the highly heterogeneous content inside the region segmented; it indeed consists of a slow blood flow inducing some RF signal decorrelation mixed with immature soft thrombus promoting high deformations [199] *(19)*. On the other hand, the organized thrombus is a solid homogeneous tissue.

This stiffer tissue expresses lower strain values and rates of deformation when submitted to blood pulsation. The fresh thrombus, a region of immature structuring displayed strain values lower than the solid thrombus and higher than the endoleak results. Reported strain results may be used to identify specific aneurysm regions and possibly follow its healing with time [102, 204, 205] *(24-26)*. Indeed, the characterization of the thrombus organization has been presented as a new concept of follow-up using MRI [206, 207] *(27, 28)*. It was shown that the thrombus organization and identification of the different components inside the aneurysm sac could be used for the detection of endotension [206] *(27)*. But MRI presents limited accessibility, higher cost than ultrasound, and metal artifact when using stainless-steel SG [108] *(29)*. This is certainly an opportunity for the NIVE-LSME method.

Differences in strain values could be expected when comparing aneurysms with type I and II endoleaks. Indeed, those endoleaks generally have different sac pressure regiments, as type I are typically at systemic pressure whereas retrograde flow in type II endoleak have lower pressure values [208-210] *(30-32)*. Nevertheless, in our study no statistically significant difference was observed between measured sac pressures for type I and II endoleaks. This explains why there was no statistically significant difference between any strain parameters for the two types of endoleak.

Another unexpected observation is the independence of strain results with the sac pressure. There was no correlation between the pressure measured inside the

aneurysm sac and strain values for the endoleak, organized and fresh thrombus areas. This may be explained by the fact that the strain is measured between two consecutive RF images at different pressures [195] *(15)*. It is thus mainly influenced by the systolic and diastolic amplitude range, and less by the mean pressure. As most biological tissues display non-linear stress-strain relationships, the mean pressure is, at a lesser extent, a potential cofounding factor that should be considered. Note that we could not measure the pulse pressure amplitude within aneurysm sacs with available pressure sensors.

It is logical to observe larger endoleak areas in larger aneurysms [211] *(33)*. However, the leak size had no impact on strain measurements, which is an intrinsic property of the tissue under examination.

This study was aiming to validate the NIVE technique and report typical strain values for the 3 AAA components (endoleaks, organized and fresh thrombi). This technique still requires approximately 5 minutes of post processing and elastograms are not displayed in real time. Thus, the operator was not able to have a visual feedback of strain values during image acquisitions. In this setting, it was not possible to compare directly the diagnostic accuracy of elastography with DUS or CT scanner. Furthermore, to enable detection of endoleaks or thrombus characteristics, diagnostic thresholds would need to be defined. This will be under investigation in a phase II clinical study [212] *(34)*. In a clinical workflow, we believe NIVE acquisition could be

easily acquired at the end of a complete B-mode and color Doppler examination to characterize thrombus organization and possibly detect slow flow endoleaks and endotension that cannot be seen on Doppler examination [149, 158, 191] *(9,13,14)*.

Conclusion

The results showed that different values of NIVE parameters were displayed in endoleak and thrombus with different grade of thrombus organization inside the aneurysm sac and thus possibly detect an endotension. Even though, NIVE could not differentiate type I and II endoleaks. This new technique could be a good addition to the radiology arsenal for detecting aneurysmal tissue properties not seen on B-mode and color Doppler. It could reduce the need for CT angiography for the follow up of AAA after EVAR.

Acknowledgments

This study has received funding by clinical research scholarship to GS from Fonds de la recherche en santé du Québec (FRSQ) and operating grants from the Canadian Institute of Health Research (CIHR/MOP-115099) and Fonds de la Recherche en santé du Québec (FRQ-S-22951).

We like to thank Mrs Jocelyne Lavoie and Michel Gouin research technicians for their assistance in animal experimentation and image acquisition, staff members involved in the animal research platform for their tremendous work and Martin Ladouceur for his assistance in statistical analyses.

Table 4.1. NIVE strain parameters in segmented regions

	Endoleak (Mean ± SD) (%)	Organized Thrombus (Mean ± SD) (%)	Fresh Thrombus (Mean ± SD) (%)	P Value *		
				E Vs. OT	E Vs. FT	OT Vs. FT
MaxAxStrain	0,78 ± 0.22	0,10 ± 0,04	0,23 ± 0,02	< 0.001	< 0.001	< 0.001
MinAxStrain	-0,44 ± 0,30	-0,17 ± 0,06	-0,17 ± 0,05	0.004	0.023	0.818
MaxCumAxStrain	0,85 ± 0,56	0,16 ± 0,10	0,20 ± 0,08	<0.001	0.002	0.316
MaxStrainRate	5,61 ± 3,75	1,16 ± 0,60	1,66 ± 0,69	<0.001	0.006	0.11
MinStrainRate	-6,00 ± 3,71	-1,10 ± 0,53	-1,76 ± 0,81	<0.001	0.006	0.033

Note: Max/MinAxStrain = maximum and minimum axial strains; MaxCumAxStrain = maximum cumulated axial strain; Max/MinStrainRate = maximum and minimum strain rates; E = Endoleak; OT = Organized Thrombus; FT = Fresh Thrombus; * = Wilcoxon rank sum test

Table 4.2. Comparison as a function of endoleak type (aneurysms with type I vs. type II endoleak)

		Type I (average ± SD)	Type II (average ± SD)	P value
MaxAxStrain	**Endoleak**	0,87 ± 0,34	0,74 ± 0,21	P = 0.39
	O.T	0,10 ± 0,03	0,10 ± 0,04	P = 0.93
	F.T	0,25	0,23 ± 0,02	N/A
MinAxStrain	**Endoleak**	-0,68 ± 0,32	-0,47 ± 0,40	P = 0.41
	O.T	-0,19638 ± 0,07	-0,17 ± 0,06	P = 0.49
	F.T	-0,16	-0,17 ± 0,05	N/A
MaxCumAxStrain	**Endoleak**	0,96 ± 0,54	0,83 ± 0,56	P = 0.72
	O.T	0,19 ± 0,09	0,15 ± 0,09	P = 0.46
	F.T	0,30	0,19 ± 0,08	N/A
MaxStrainRate	**Endoleak**	6,55 ± 3,74	5,55 ± 3,77	P = 0.68
	O.T	1,10 ± 0,21	1,18 ± 0,69	P = 0.95
	F.T	1,35	1,72 ± 0,75	N/A
MinStrainRate	**Endoleak**	-8,77 ± 5,17	-5,38 ± 3,10	P = 0.14
	O.T	-1,23 ± 0,42	-1,06 ± 0,57	P = 0.59
	F.T	-1,40	-1,82 ± 0,89	N/A

Table 2: Comparison of strain values in endoleak, organized thrombus and fresh thrombus regions as a function of endoleak type (aneurysms with Type I vs type II endoleak). No statistical significant difference was found for any of the parameters

Table 4.3. Aneurysm and endoleak size measurements

Dog	Type of endoleak	Area of the leak (Min-Max) CT (mm2)	Area of the aneurysm (Min-Max) CT (mm2)	Diameter of the aneurysm CT (mm)	Diameter variation between sacrifice/1 week post US %	Mean sac pressure (mmHg)
1	IB	124 - 59	153 – 487	26.7 - 11.9	+ 8.6%	88
2	II	14 - 20	104 – 284	20.9 - 11.2	- 4.7%	49
3	II	7 - 18	102 – 348	23.9 - 10.9	- 13.1%	55
4	II	1 – 5	113 – 322	21.7 - 12.6	- 16.4%	45
5	II	5 - 79	121 – 274	21.1 - 12.9	- 1.57%	33
6	II	4 - 11	105 – 274	20.4 - 11.2	- 7.7%	70
7	II	5 - 36	132 – 303	20.8 - 11	- 3.19%	70
8	II	1 – 9	131 – 456	27.2 - 12.2	- 8.4%	89
9	II	Fail	106 – 246	19.7 - 10.2	- 2.07%	67
10	II	9 - 48	147 – 345	23.4 - 11	- 22.9%	54
11	II	1 - 10	129 – 265	20.0 - 11.2	- 7.3%	45
12	II	4 - 74	169 – 290	20.8 - 10.4	- 4.6%	54
13	IB	4 – 4	105 – 246	20.9 - 11.8	+ 13.2%	60
14	IB	5 - 85	143 – 371	23.7 - 10.7	+ 6.42%	80
15	0	-	102 – 235	19.2 - 10.5	- 5.5%	NA
16	IA	1 - 13	101 – 228	18.6 - 10.3	- 9.13%	42
17	II	4 - 5	63 – 228	16.1 - 8.4	- 2.58%	24
18	II	3 - 8	142 – 433	25.5 - 12.5	- 19.03%	23

Note: Type of endoleak according to the Society of Vacular Surgery Classification (0= no endoelak). (ref). The % of difference in aneurysm diameter is measured between sacrifice

and 1 week after implantation of the SG on DUS. A (+) sign indicates that the diameter has increased whether a (-) sign indicates a shrinkage in the aneurysm diameter. The dog number 15 had no endoleak detected through CT scan, DUS and macroscopic tissue slides

Figure Captions

Figure 4.1. The macroscopic tissue slide is first analyzed to detect the presence of an endoleak through a defect/gap in the aneurysm sac. If the presence of the defect correlates with CT scan contrast enhancement in the same region, presence of an endoleak is confirmed. The rest of the tissue in the aneurysmal sac is characterized as organized or fresh thrombus according to its appearance on macroscopic cuts. Note: C+ means contrast on CT scanner.

Figure 4.2. Example of macroscopic tissue slide (a) with endoleak (1), fresh thrombus (2) and organized thrombus (3). Corresponding histology with Movat staining (b) and immunostaining of alpha smooth muscle actin (αSMA, in brown)) (c and d). The brown region corresponds to the dense fibrous connective tissues (organized thrombus). The blue region corresponds to the fresh thrombus (c and d) which confirms the areas of fresh thrombus (loose thrombus with black brown coloration and absence of fibrous organization) and organized thrombus (dense fibrous organization with a yellowish appearance) on the macroscopic tissue slides

Figure 4.3a. LSME was applied to compute time varying strain curves for 3 or more consecutive cardiac cycles. This figure shows the instantaneous axial strain curve on 90 frames (7 cycles). MaxAxStrain and MinAxStrain represent the mean value, over

acquired cardiac cycles, of positive and negative peaks of the time varying instantaneous axial strain curve, respectively.

Figure 4.3b. A cumulated axial strain curve over the same 90 frames (7 cycles). MaxCumAxialStrain is the average, over acquired cardiac cycles, of maximum positive values of the cumulated axial strain curve, corresponding to peak dilatation.

Figure 4.4a. CT scan image of dog 1 (A Stena Labrador female, 6 years old and weights 30.5 Kg) taken before sacrifice and showing a large type I endoleak at the proximal neck. CT scan is used as a reference for endoleak segmentation and registration on elastogram.

Figure 4.4b. Transverse acquisition of Doppler Ultrasound at the same level than CT scan (Figure 4.4a).

Figure 4.4c. A macroscopic tissue slide at the same level shown in figure 4.4a and 4.4b. The endoleak area is well visible (dashed arrow). A small area of fresh thrombus seen as a soft black brown area is depicted (white arrow). The organized thrombus is seen at the upper portion (thin arrow with an oval head) of the macroscopic cut. These 3 regions of interest located on the macroscopic tissue slide are segmented and registered on the elastogram for computation of strain parameters.

Figure 4.4d**.** Cumulated axial strain elastogram of the entire aneurysm sac at the same level that Figure 4.4,a,b,c The region of accumulation of very high and low strain values on the middle left of the elastogram (white arrow) corresponds to the region of endoleak.

Figure 4.4e. Cumulated axial strain elastogram of the endoleak region of the same dog 1 at the same level segmented based on the CT scan and macroscopic results showed in figure 4.4a and 4.4c.

Figure 4.4f**.** Cumulated axial strain elastogram of the fresh thrombus region of the same dog 1 at the same level segmented based on the macroscopic results showed in figure 4.3c.

Figure 4.4g. Cumulated axial strain elastogram of the organized thrombus region of the same dog 1 at the same level segmented based on the macroscopic results showed in figure 4.3c.

Figure 4.5. Mean and SD Maximum Axial Strain values for the three regions of interest. A statistical significant difference was found when comparing the endoleak, organized and fresh thrombi.

Figure 4.6. No correlation has been found between the pressure measured inside the aneurysm sac and the maximum axial strain parameter results.

Figure 4.7. No correlation has been found between the aneurysm area measured on CT scan and the maximum axial strain parameter results.

Figure 4.8**.** No correlation has been found between the endoleak area measured on CT scan and the maximum axial strain parameter results.

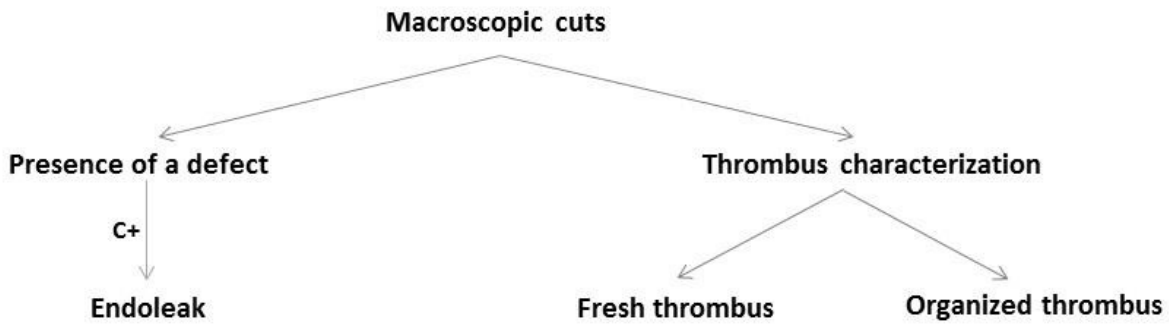

Figure 4.1. The macroscopic tissue slide is first analyzed to detect the presence of an endoleak through a defect/gap in the aneurysm sac. If the presence of the defect correlates with CT scan contrast enhancement in the same region, presence of an endoleak is confirmed. The rest of the tissue in the aneurysmal sac is characterized as organized or fresh thrombus according to its appearance on macroscopic cuts.

Note: C+ means contrast on CT scanner

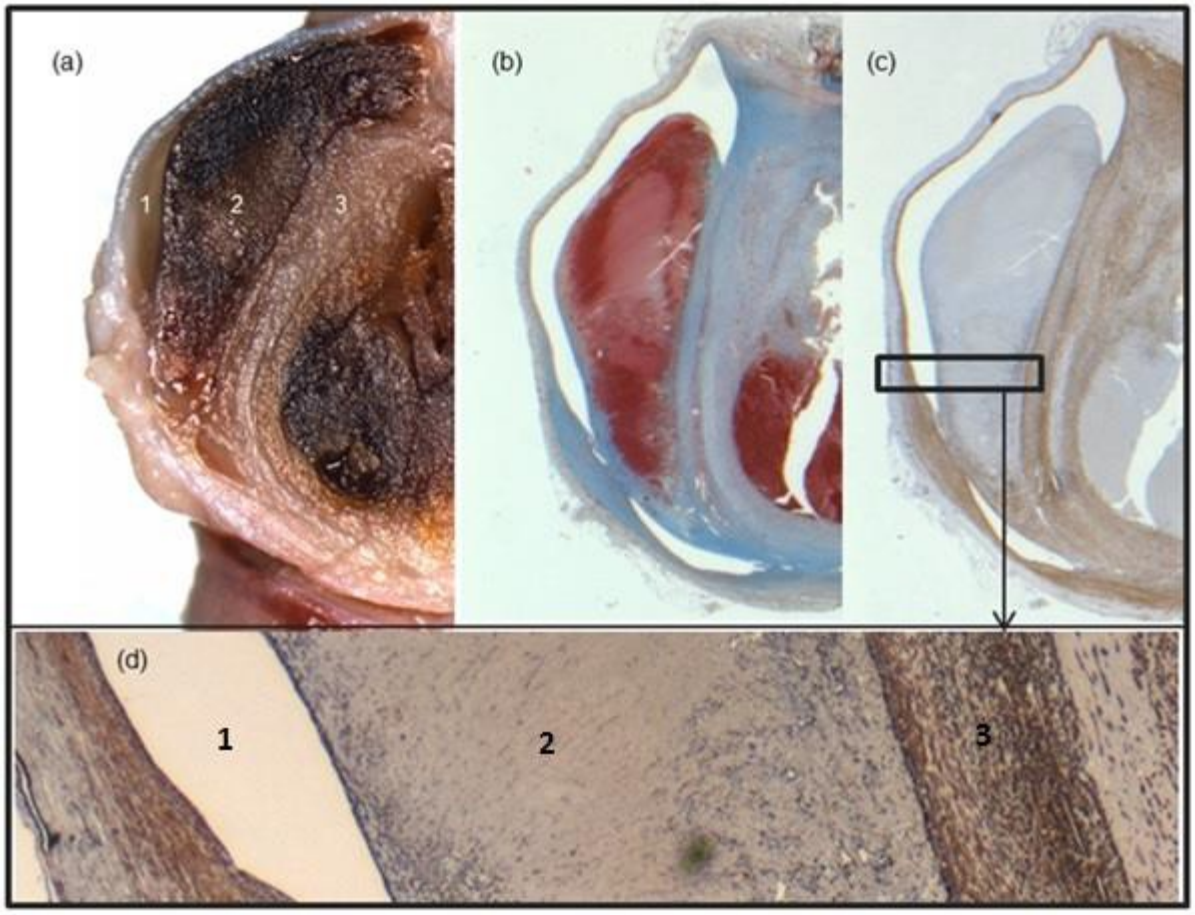

Figure 4.2. Example of macroscopic tissue slide (a) with endoleak (1), fresh thrombus (2) and organized thrombus (3). Corresponding histology with Movat staining (b) and immunostaining of alpha smooth muscle actin (αSMA, in brown)) (c and d). The brown region corresponds to the dense fibrous connective tissues (organized thrombus). The blue region corresponds to the fresh thrombus (c and d) which confirms the areas of fresh thrombus (loose thrombus with black brown coloration and absence of fibrous organization) and organized thrombus (dense fibrous organization with a yellowish appearance) on the macroscopic tissue slides.

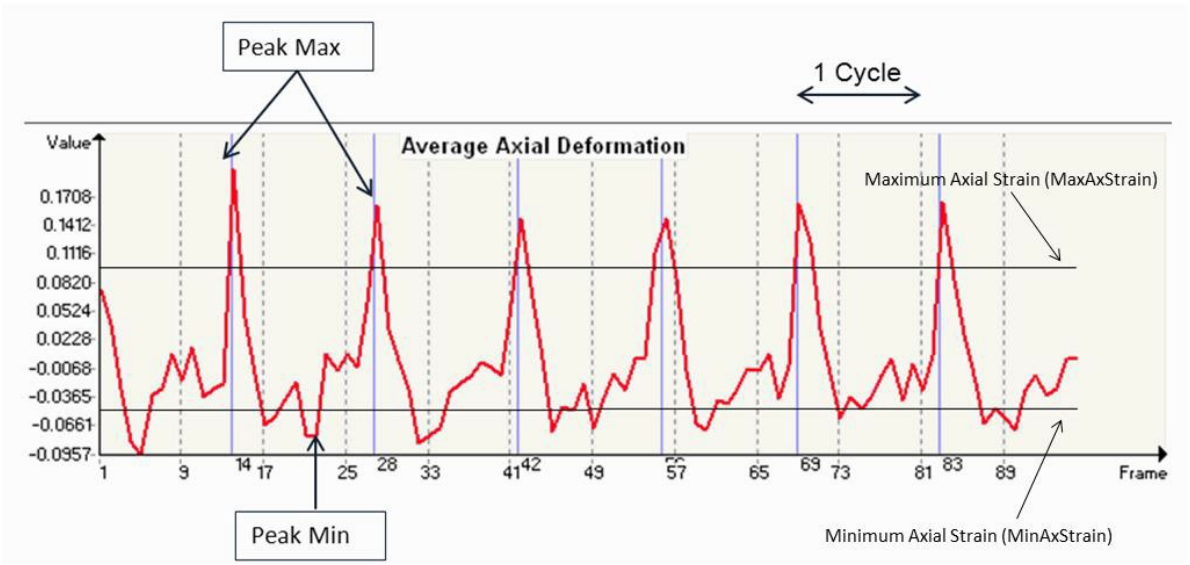

Figure 4.3a. LSME was applied to compute time varying strain curves for 3 or more consecutive cardiac cycles. This figure shows the instantaneous axial strain curve on 90 frames (7 cycles). MaxAxStrain and MinAxStrain represent the mean value, over acquired cardiac cycles, of positive and negative peaks of the time varying instantaneous axial strain curve, respectively.

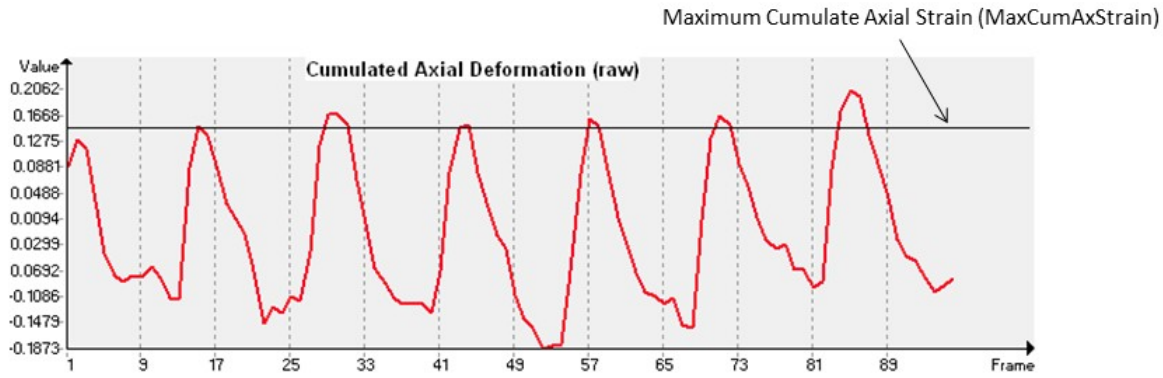

Figure 4.3b. A cumulated axial strain curve over the same 90 frames (7 cycles). MaxCumAxialStrain is the average, over acquired cardiac cycles, of maximum positive values of the cumulated axial strain curve, corresponding to peak dilatation.

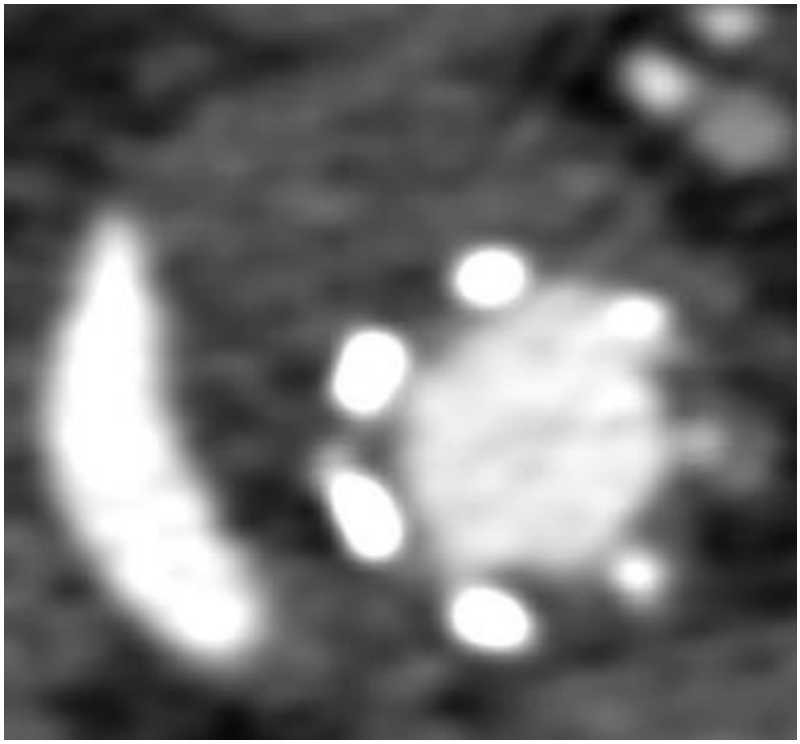

Figure 4.4a.: CT scan image of dog 1 (A Stena Labrador female, 6 years old and weights 30.5 Kg) taken before sacrifice and showing a large type I endoleak at the proximal neck. CT scan is used as a reference for endoleak segmentation and registration on elastogram.

23x25mm (300 x 300 DPI)

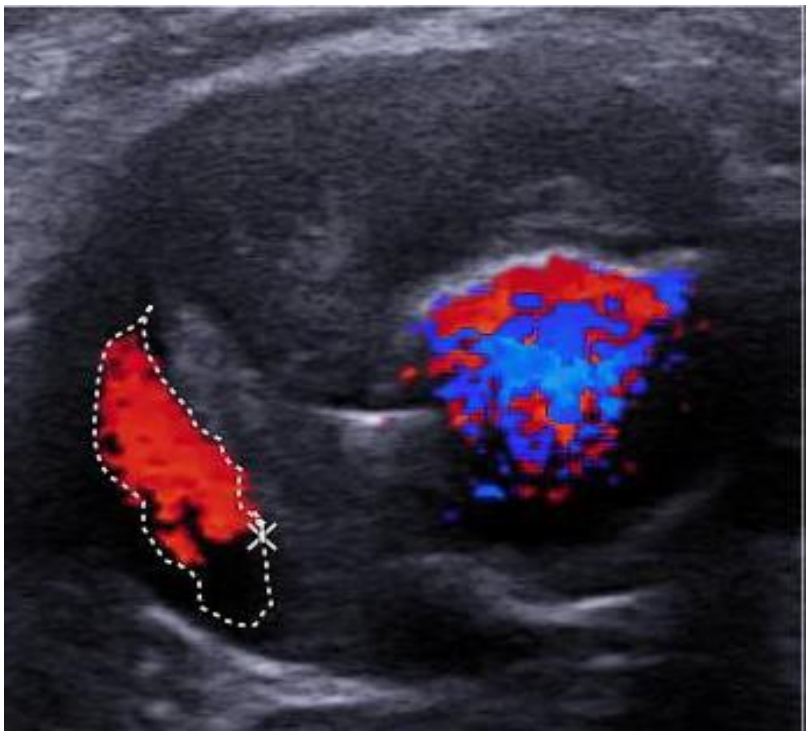

Figure 4.4b. Transverse acquisition of Doppler Ultrasound at the same level than CT scan (Figure 4a).

26x25mm (300 x 300 DPI)

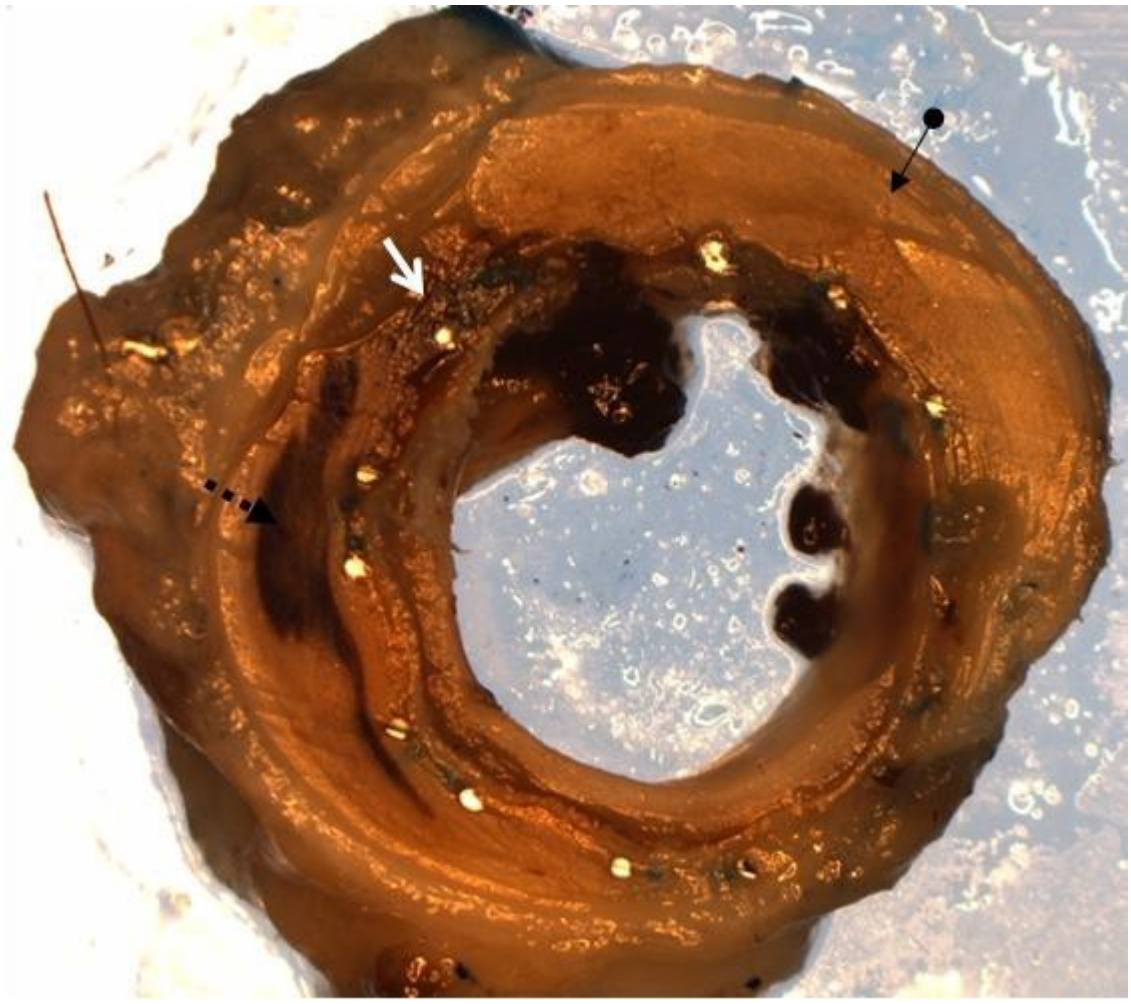

Figure 4.4c. A macroscopic tissue slide at the same level shown in figure 4a and 4b. The endoleak area is well visible (dashed arrow). A small area of fresh thrombus seen as a soft black brown area is depicted (white arrow). The organized thrombus is seen at the upper portion (thin arrow with an oval head) of the macroscopic cut. These 3 regions of interest located on the macroscopic tissue slide are segmented and registered on the elastogram for computation of strain parameters.

24x25mm (300 x 300 DPI)

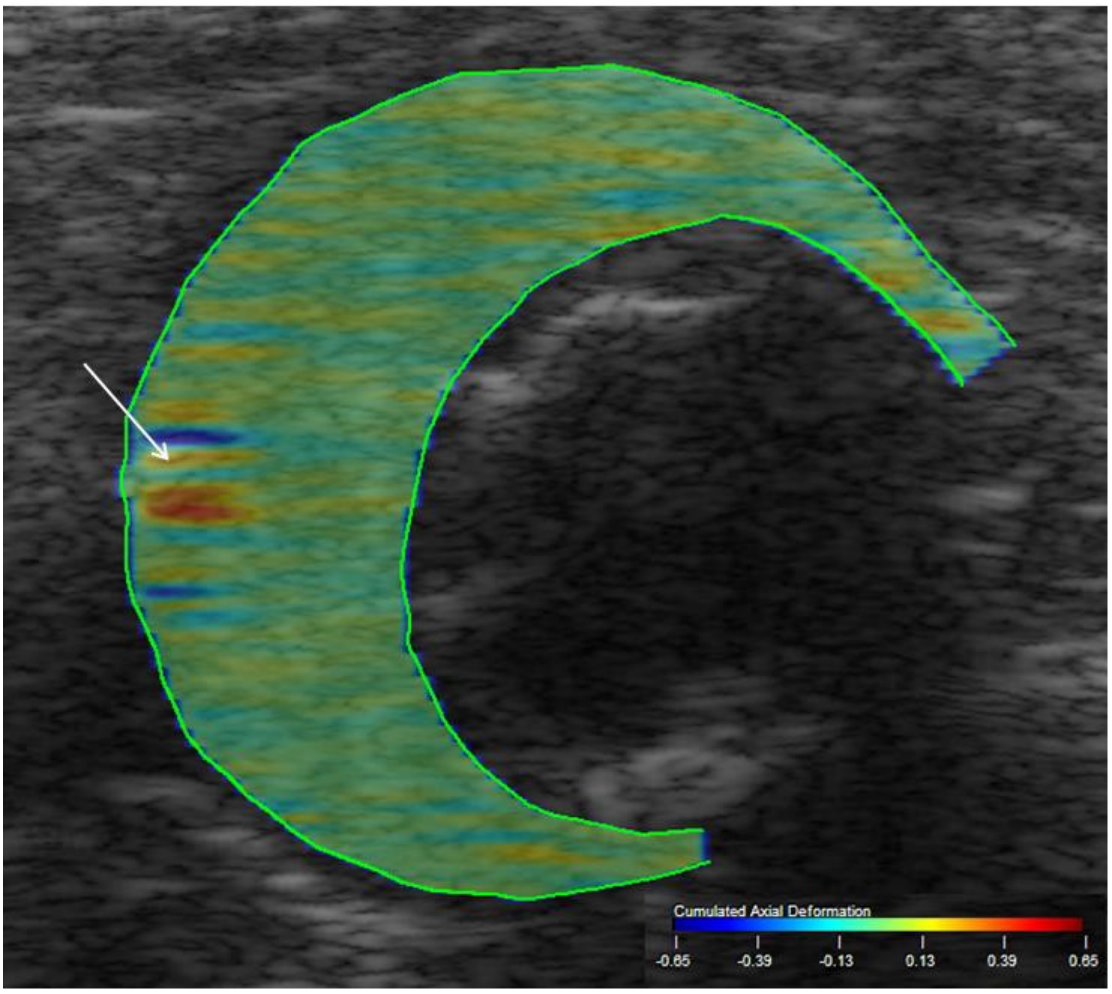

Figure 4.4d. Cumulated axial strain elastogram of the entire aneurysm sac at the same level that Figure 4,a,b,c The region of accumulation of very high and low strain values on the middle left of the elastogram (white arrow) corresponds to the region of endoleak.

28x27mm (300 x 300 DPI)

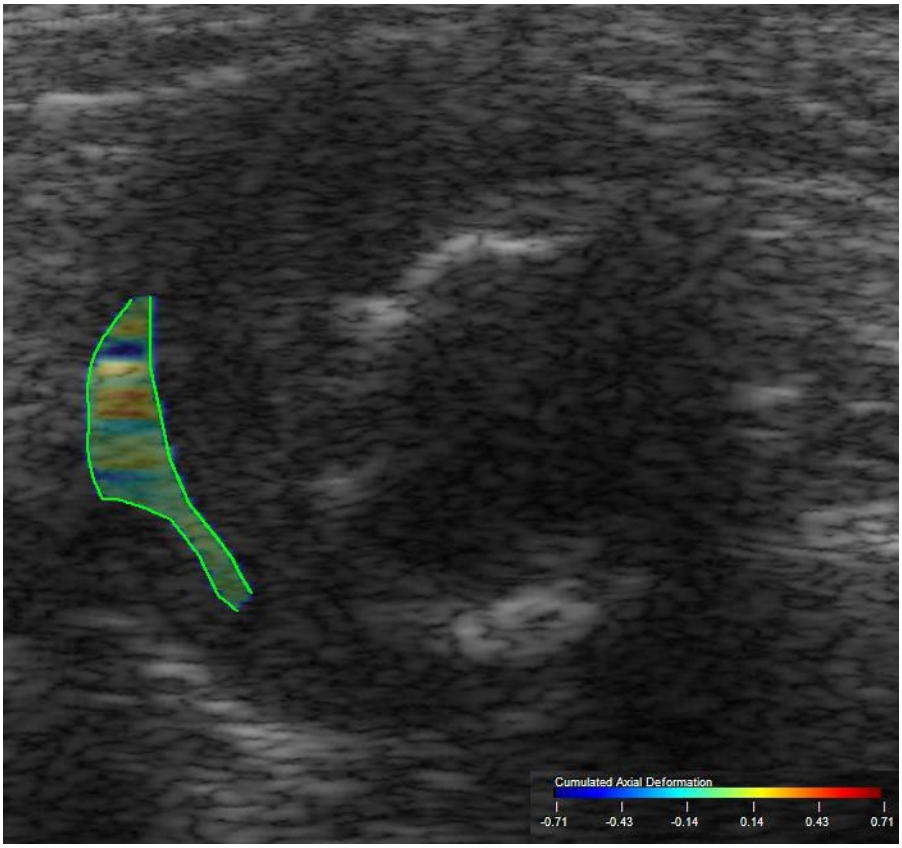

Figure 4.4e. Cumulated axial strain elastogram of the endoleak region of the same dog 1 at the same level segmented based on the CT scan and macroscopic results showed in figure 4a and 4c.

28x27mm (300 x 300 DPI)

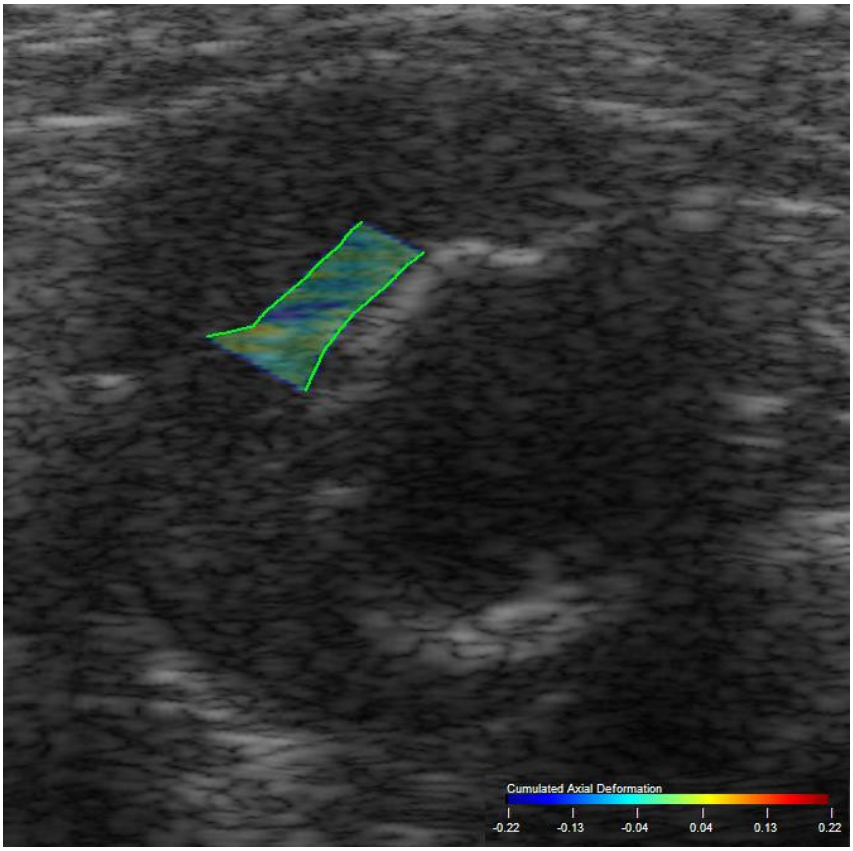

Figure 4.4f. Cumulated axial strain elastogram of the fresh thrombus region of the same dog 1 at the same level segmented based on the macroscopic results showed in figure 3c.

28x27mm (300 x 300 DPI)

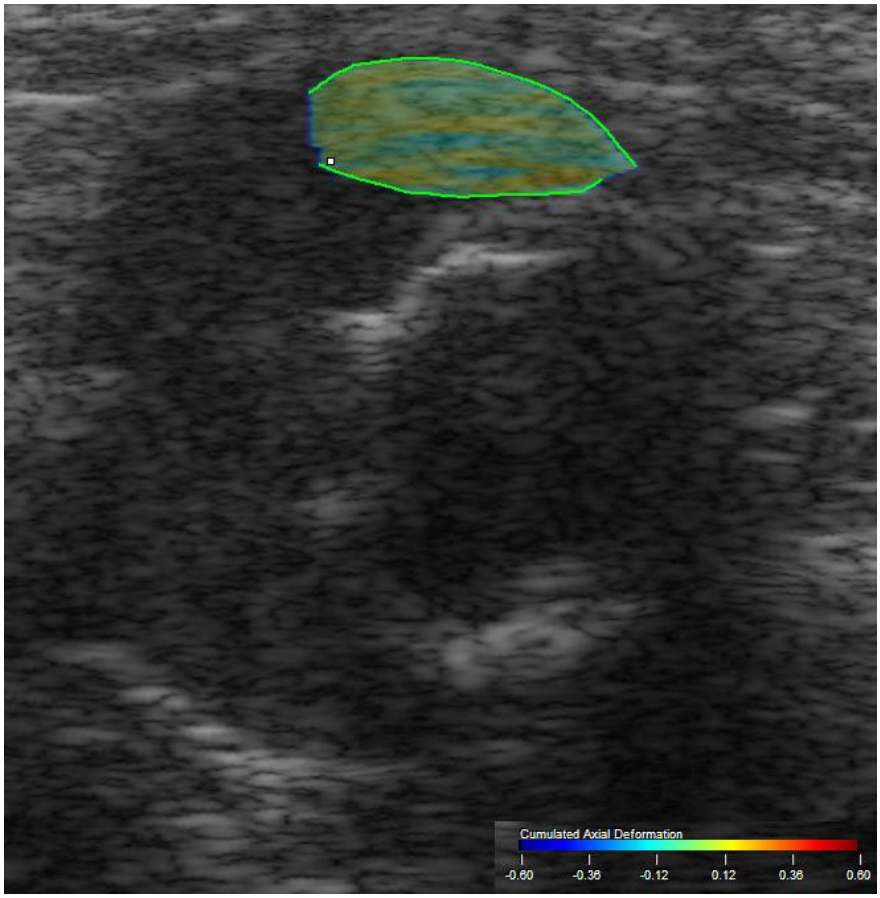

Figure 4.4g. Cumulated axial strain elastogram of the organized thrombus region of the same dog 1 at the same level segmented based on the macroscopic results showed in figure 3c.

28x27mm (300 x 300 DPI)

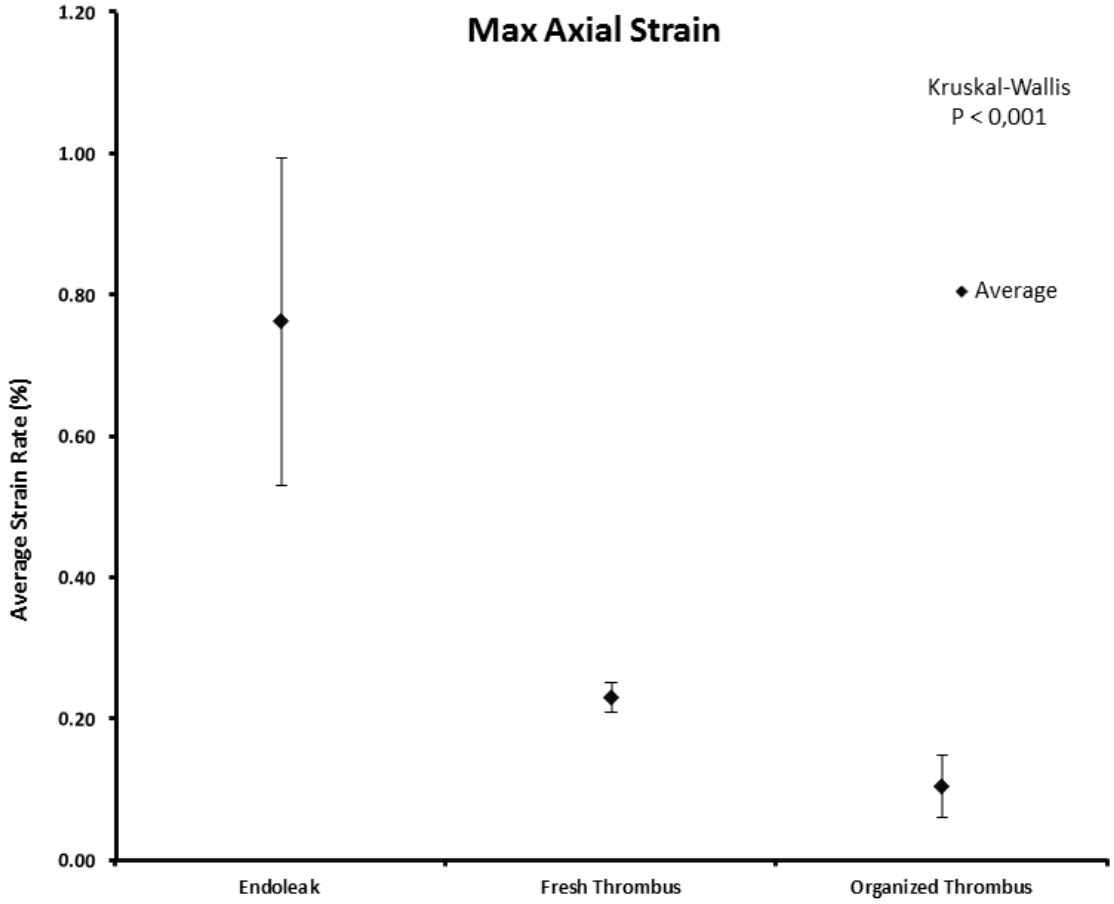

Figure 4.5. Mean and SD Maximum Axial Strain values for the three regions of interest. A statistical significant difference was found when comparing the endoleak, organized and fresh thrombi.

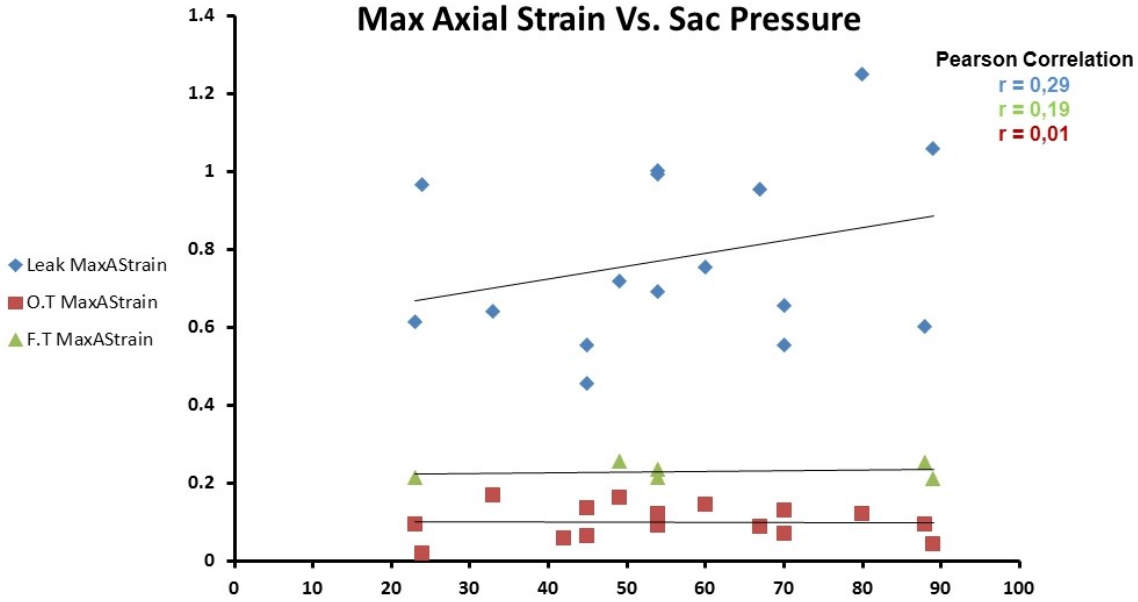

Figure 4.6. No correlation has been found between the pressure measured inside the aneurysm sac and the maximum axial strain parameter results.

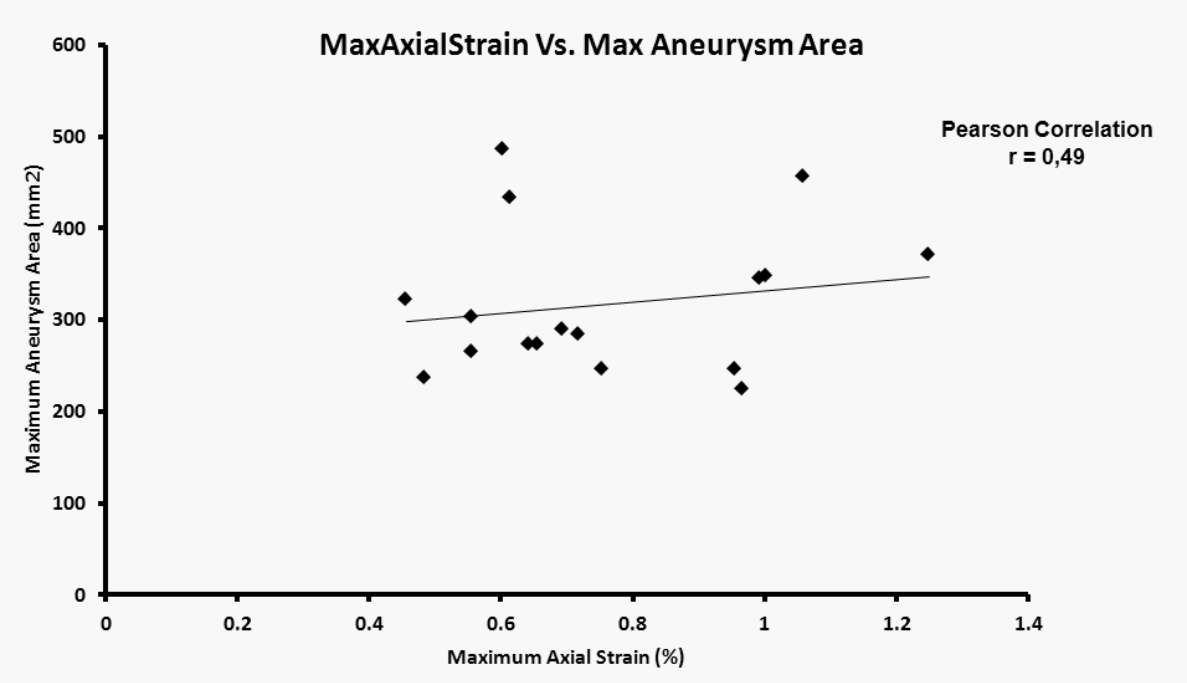

Figure 4.7. No correlation has been found between the aneurysm area measured on CT scan and the maximum axial strain parameter results.

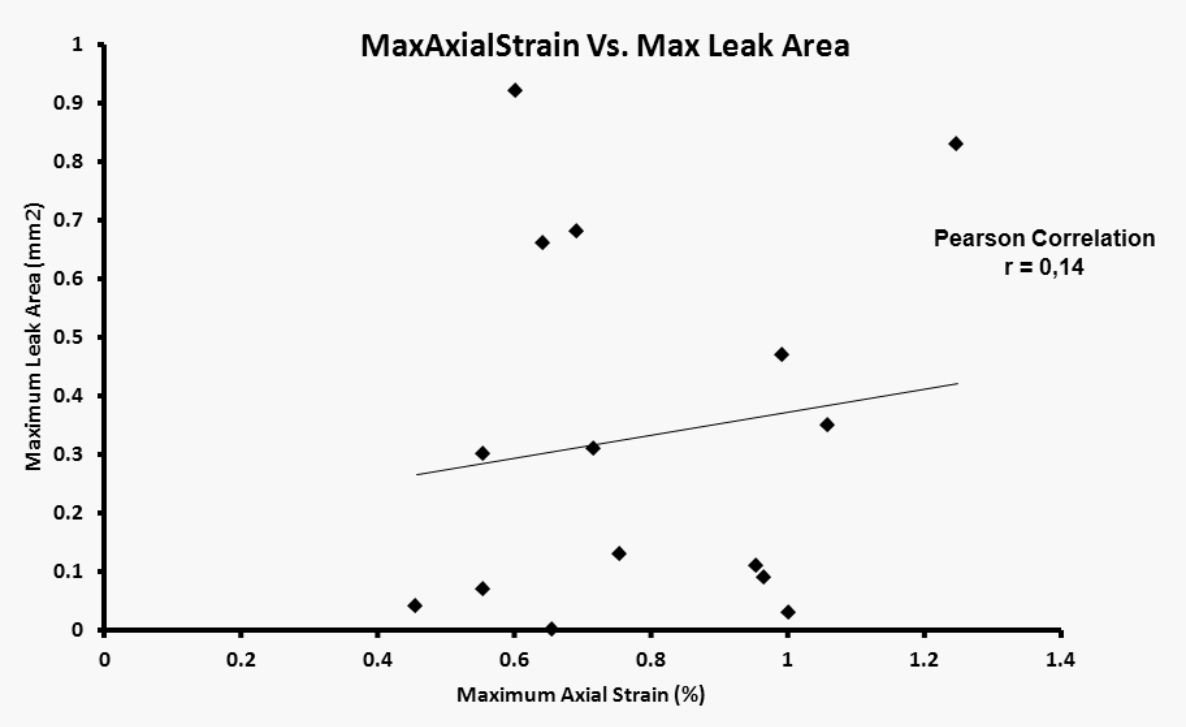

Figure 4.8. No correlation has been found between the endoleak area measured on CT scan and the maximum axial strain parameter results.

References

1. Greenhalgh, R.M., et al., *Comparison of endovascular aneurysm repair with open repair in patients with abdominal aortic aneurysm (EVAR trial 1), 30-day operative mortality results: randomised controlled trial.* Lancet, 2004. **364**(9437): p. 843-8.
2. Prinssen, M., et al., *A randomized trial comparing conventional and endovascular repair of abdominal aortic aneurysms.* The New England journal of medicine, 2004. **351**(16): p. 1607-18.
3. participants, E.t., *Endovascular aneurysm repair versus open repair in patients with abdominal aortic aneurysm (EVAR trial 1): randomised controlled trial.* Lancet, 2005. **365**(9478): p. 2179-86.
4. Blankensteijn, J.D., et al., *Two-Year Outcomes after Conventional or Endovascular Repair of Abdominal Aortic Aneurysms.* New England Journal of Medicine, 2005. **352**(23): p. 2398-2405.
5. Tadros, R.O., et al., *The impact of stent graft evolution on the results of endovascular abdominal aortic aneurysm repair.* Journal of Vascular Surgery, 2014(0): p. 1518 - 1527.
6. Nordon, I.M., et al., *Secondary interventions following endovascular aneurysm repair (EVAR) and the enduring value of graft surveillance.* European Journal of Vascular & Endovascular Surgery, 2010. **39**(5): p. 547-54.
7. Brown, L.C.P., et al., *Renal Function and Abdominal Aortic Aneurysm (AAA): The Impact of Different Management Strategies on Long-Term Renal Function in the UK EndoVascular Aneurysm Repair (EVAR) Trials. [Article]*. Annals of Surgery May 2010;251(5):966-975.
8. Prinssen, M., et al., *Surveillance after endovascular aneurysm repair: diagnostics, complications, and associated costs.* Annals of Vascular Surgery, 2004. **18**(4): p. 421-7.
9. Sun, Z., *Diagnostic value of color duplex ultrasonography in the follow-up of endovascular repair of abdominal aortic aneurysm.* J Vasc Interv Radiol, 2006. **17**(5): p. 759-64.
10. Beeman, B.R., et al., *Duplex ultrasound imaging alone is sufficient for midterm endovascular aneurysm repair surveillance: a cost analysis study and prospective comparison with computed tomography scan.* Journal of Vascular Surgery, 2009. **50**(5): p. 1019-24.
11. Go, M.R., et al., *What is the clinical utility of a 6-month computed tomography in the follow-up of endovascular aneurysm repair patients?* 2008: Journal of Vascular Surgery. 47 (6) (pp 1181-1187), 2008. Date of Publication: June 2008.
12. Sternbergh, I.W.C., et al., *Redefining postoperative surveillance after endovascular aneurysm repair: Recommendations based on 5-year follow-up in the US Zenith multicenter trial*. 2008: Journal of Vascular Surgery. 48 (2) (pp 278-285), 2008. Date of Publication: August 2008.
13. AbuRahma, A.F., et al., *Computed tomography versus color duplex ultrasound for surveillance of abdominal aortic stent-grafts.* J Endovasc Ther, 2005. **12**(5): p. 568-73.
14. Elkouri, S., et al., *Computed tomography and ultrasound in follow-up of patients after endovascular repair of abdominal aortic aneurysm.* Annals of Vascular Surgery, 2004. **18**(3): p. 271-9.

15. Maurice, R.L., et al., *Noninvasive vascular elastography: theoretical framework.* IEEE Trans Med Imaging, 2004. **23**(2): p. 164-80.
16. Maurice, R.L., et al., *Noninvasive vascular elastography for carotid artery characterization on subjects without previous history of atherosclerosis*. Medical Physics. 35 (8) (pp 3436-3443), 2008. Date of Publication: 2008.
17. Schmitt, C., et al., *Noninvasive vascular elastography: toward a complementary characterization tool of atherosclerosis in carotid arteries.* Ultrasound Med Biol, 2007. **33**(12): p. 1841-58.
18. Destrempes, F., et al., *Segmentation method of intravascular ultrasound images of human coronary arteries.* Computerized Medical Imaging and Graphics, 2014. **38**(2): p. 91-103.
19. Fromageau, J., et al., *Noninvasive vascular ultrasound elastography applied to the characterization of experimental aneurysms and follow-up after endovascular repair.* Phys Med Biol, 2008. **53**(22): p. 6475-90.
20. Stavropoulos, S.W. and S.R. Charagundla, *Imaging techniques for detection and management of endoleaks after endovascular aortic aneurysm repair*. 2007: Radiology. 243(3). JUN 2007. 641-655.
21. Destrempes, F., *Segmentation of plaques in sequences of ultrasonic B - mode images of carotid arteries based on motion estimation and a bayesian model.* IEEE Transactions on Biomedical Engineering, 2011. **58**(8): p. 2202.
22. Mercure, E., et al., *A local angle compensation method based on kinematics constraints for non-invasive vascular axial strain computations on human carotid arteries.* Computerized Medical Imaging and Graphics, 2014. **38**(2): p. 123-136.
23. Kulcsár, Z., et al., *Intra-Aneurysmal Thrombosis as a Possible Cause of Delayed Aneurysm Rupture after Flow-Diversion Treatment.* American Journal of Neuroradiology, 2011. **32**(1): p. 20-25.
24. Ashton, J.H., et al., *Compressive mechanical properties of the intraluminal thrombus in abdominal aortic aneurysms and fibrin-based thrombus mimics.* Journal of Biomechanics, 2009. **42**(3): p. 197-201.
25. Wang, D.H., et al., *Mechanical properties and microstructure of intraluminal thrombus from abdominal aortic aneurysm.* Journal of biomechanical engineering, 2001. **123**(6): p. 536-539.
26. Gasser, T.C., et al., *Failure properties of intraluminal thrombus in abdominal aortic aneurysm under static and pulsating mechanical loads.* Journal of Vascular Surgery, 2008. **48**(1): p. 179-188.
27. Cornelissen, S.A., et al., *Use of Multispectral MRI to Monitor Aneurysm Sac Contents After Endovascular Abdominal Aortic Aneurysm Repair.* Journal of Endovascular Therapy, 2011. **18**(3): p. 274-279.
28. Engellau, L., et al., *Magnetic resonance imaging and MR angiography of endoluminally treated abdominal aortic aneurysms.* European Journal of Vascular and Endovascular Surgery, 1998. **15**(3): p. 212-219.

29. Weigel, S., et al., *Thoracic aortic stent graft: comparison of contrast-enhanced MR angiography and CT angiography in the follow-up: initial results.* European Radiology, 2003. **13**(7): p. 1628-1634.
30. Dayal, R., et al., *Characterization of retrograde collateral (type II) endoleak using a new canine model.* Journal of vascular surgery, 2004. **40**(5): p. 985-994.
31. Dias, N.V., et al., *Intra-aneurysm sac pressure measurements after endovascular aneurysm repair: Differences between shrinking, unchanged, and expanding aneurysms with and without endoleaks*. Journal of Vascular Surgery. 39 (6) (pp 1229-1235), 2004. Date of Publication: June 2004.
32. Dias, N.V., et al., *Endoleaks after endovascular aneurysm repair lead to nonuniform intra-aneurysm sac pressure*. Journal of Vascular Surgery. 46 (2) (pp 197-203), 2007. Date of Publication: August 2007.
33. Ellozy, S.H., et al., *Abdominal aortic aneurysm sac shrinkage after endovascular aneurysm repair: correlation with chronic sac pressure measurement.* J Vasc Surg, 2006. **43**(1): p. 2-7.
34. (CHUM), C.h.d.l.U.d.M. *Abdominal Aortic Aneurysm Follow-up After Endovascular Repair by Non-invasive Vascular Elastography* 2013; Available from: http://clinicaltrials.gov/ct2/show/NCT01907386?term=abdominal+aortic+aneurysm&recr=Not+yet+recruiting&rslt=Without&type=Intr&titles=abdominal+aortic+aneurysm+follow-up+after+endovascular+repair+by+non-invasive+vascular+elastography&cntry1=NA%3ACA&state1=NA%3ACA%3AQC&locn=Montreal&rank=1.

4.3 Further discussion and future perspectives

A further discussion on the methodology, results and future work is provided in this postscript.

4.3.1 Study Methodology

The first applications of ultrasound elastography were developed for breast cancer (figure 4.9) to complement conventional B-mode ultrasound [213]. A tumor region is usually harder than healthy tissues, which allows elastography to detect the elasticity difference. As another non-vascular application, renal elasticity has presented another success by providing the possibility of detecting early state kidney transplant rejection [214] or liver elastography to grade liver fibrosis [101].

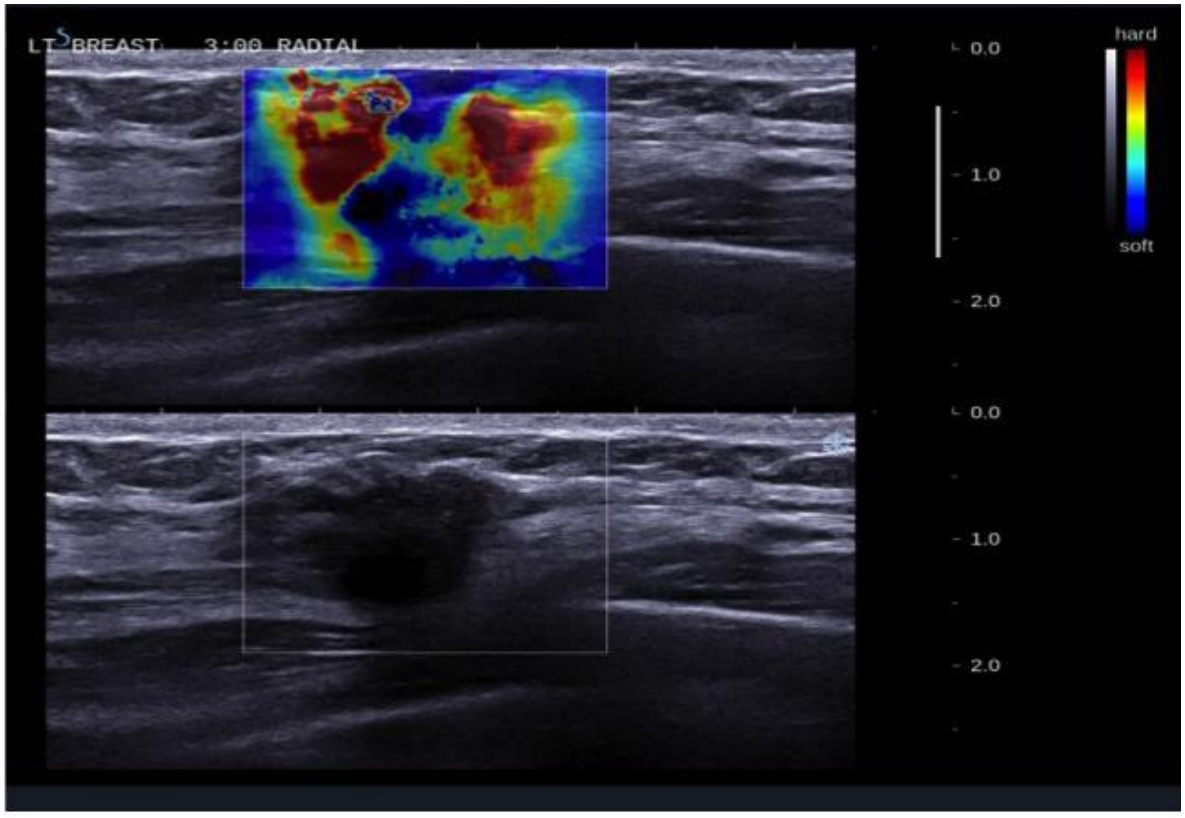

Figure 4.9. Quasi-static compression elastography examination of a breast carcinoma. The color indicates the relative stiffness (red to blue) [215].

Vascular elastography using IVUS (intravascular ultrasound) has shown the ability to distinguish between fiber, fibro fatty and fatty plaques in coronary and carotid arteries [216-220]. A small US emitter is attached to the top of a catheter, introduced either through femoral or brachial arterial approach to reach the coronary or carotid arteries. This technique permits to the physician to see the lumen and wall of the artery and evaluate

accurately the plaque characteristics with B-mode ultrasound. Ultrasound waves are emitted towards the artery and the reflection of these sound waves can be translated to images [221]. IVUS is more expensive than angiography and is used to evaluate SG apposition in the landing zone during EVAR [222-224].

IVUS combined with elastographic examination (endovascular elastography or EVE) was first reported in 1998 by Chris L. de Korte *et al*. [116]. Its clinical applications are still limited because it is expensive and invasive and it is mainly used for research purpose in coronary arteries.

Quasi-static elastography was subsequently adapted to non-invasive acquisitions with an extracorporeal probe; it was labeled non-invasive vascular elastography (NIVE). NIVE was originally proposed for characterizing the mechanical properties of the carotid artery wall [225]. The force causing the deformation in NIVE is applied by the blood pulsation radially, where the ultrasound beam propagates axially. The main advantage of NIVE when compared to shear wave elastography (SWE, Supersonic Imagine) or acoustic radiation force impulse (ARFI, Siemens) is the penetration depth. NIVE is capable of reaching higher penetration depth since it is based on the RF data and the blood pulsation. On the other hand, SSI and ARFI are less reliable at depths greater than 6 cm (figure 4.10) [117]. This is an important advantage for any elastography study

concerning the abdominal aortic region, which is usually deeper than 10 cm.

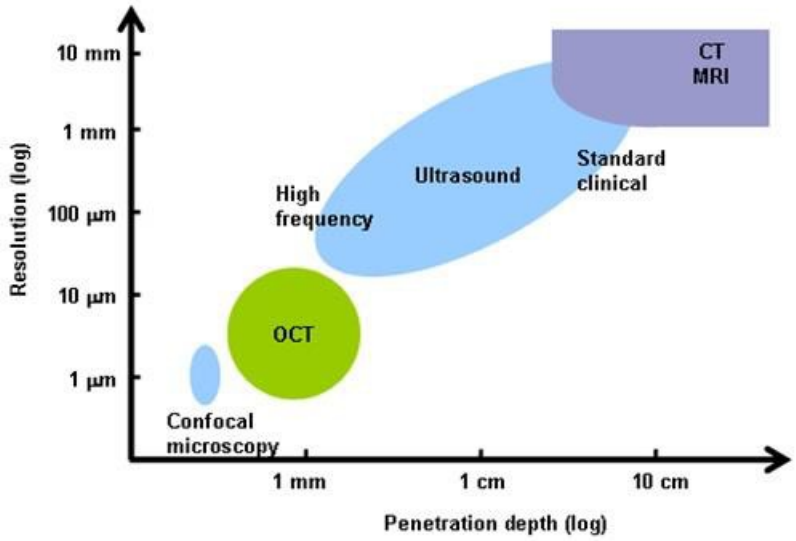

Figure 4.10. The resolution and penetration of some imaging modalities [117].

In the current project, we used a version of NIVE that had been optimized and implemented in a post processing and visualization platform (Visual, Object Research System ORS, Montreal, Canada) [201]. The RF raw data acquired during the dog examinations were loaded to the platform, where a B-mode image was reconstructed allowing image segmentation and registration between elastograms to obtain images of different vascular components (lumen, thrombus, aneurysm wall and stent-graft).

The segmentation was performed only on one frame and an algorithm developed by our team propagated the segmentation on the subsequent frames acquired during the cine loop acquisition [201, 202]. The time needed to obtain the elastography results for an acquisition of 90 frames was approximately 5 minutes. The different strain parameters were exported in an Excel sheet for analyzing and investigating.

When it comes to the acquisition of the RF data, the total time needed for acquiring 90 frames was approximately 5 seconds. This is why a further development of the platform toward a real time NIVE is needed to provide real time feed-back to allow the detection by the operator of areas with higher strain values that can be associated with endoleaks or fresh thrombus. In the future, DUS and NIVE should be combined in the same examination to improve the sensitivity for endoleak detection and give new information on thrombus organization. It could reduce the need for long term CT scan follow-up.

4.3.2 Limitations

We have faced different limitations in our study:

- Some of the dogs had a fast breathing rate during the acquisition, which caused motion artifacts, altering segmentation propagation.

- A difficulty of segmentation of couple of subjects because of the poor quality of the B-mode image.

4.3.3 Future work

We recently started the clinical phase of the study, where 3 groups of 15 patients will be selected based on clinical and CT-angiography criteria. Group 1 will include patients without endoleak and AAA volume decrease of more than 20% following EVAR, group 2 patients will consist in AAA without endoleak and no more than 10% sac volume variation, and group 3 will include patients with endoleak or endotension and more than 20% sac volume increase. Ultrasound B-mode RF acquisitions will be acquired. We will compare strain values of the different AAA components in the three groups. Thresholds on strain parameters will be tested to detect endoleaks. Then strain values will be correlated with diameter, volume and stretch index variation between baseline and contemporary CT scans.

A second prospective study to validate strain elasticity thresholds for endoleak detection and characterization of thrombus organization over time will take place. The goal of this second clinical feasibility study is to collect longitudinal strain and elasticity measurements in the early post EVAR period (before one-year). We will include 15 patients with AAA scheduled

for EVAR. These patients will have a baseline CT and baseline QSE-LSME examination. Doppler ultrasound with QSE-LSME examinations will then be performed at 3 and 12 months. The variation of strain values over time frames will be analyzed and correlated with volume progression and endoleak occurrence on CT scans.

4.3.4 Final Conclusion

Ultrasound Non-Invasive Vascular Elastrography is a technique which is feasible in a preclinical model of EVAR with endoleak, and has potential to detect endoleak and characterize thrombus organization. Further developments are needed to enable real-time elastograms optimized for AAA follow-up after EVAR. It could play an important role when combined to other ultrasound techniques such as Doppler ultrasound examinations. This provides important data for translating experimental data to clinical practice.

Section III

References

This page is left intentionally blank

Reference List

1. **McGloughlin, T.,** ***Biomechanics and mechanobiology of aneurysms*****. Springer.**
2. **Prinssen, M., et al.,** ***A randomized trial comparing conventional and endovascular repair of abdominal aortic aneurysms.*** **The New England journal of medicine, 2004. 351(16): p. 1607-18.**
3. **Greenhalgh, R.M., et al.,** ***Comparison of endovascular aneurysm repair with open repair in patients with abdominal aortic aneurysm (EVAR trial 1), 30-day operative mortality results: randomised controlled trial.*** **Lancet, 2004. 364(9437): p. 843-8.**
4. **Cowling, M.,** ***Vascular Interventional Radiology: Current Evidence in Endovascular Surgery*****. 2012.**
5. ***Blood sucking hookworms inhabit 700 million people worldwide.***
6. **Holzapfel, G., T. Gasser, and R. Ogden,** ***A New Constitutive Framework for Arterial Wall Mechanics and a Comparative Study of Material Models.*** **Journal**

of elasticity and the physical science of solids, 2000. 61(1-3): p. 1-48.

7. ***Frontiers of Engineering: Reports on Leading-Edge Engineering from the 2004 NAE Symposium on Frontiers of Engineering*. 2005: The National Academies Press.**

8. **Sinai, I.S.o.M.a.M. *About Aortic Aneurysms*. Available from: http://www.mountsinai.org/patient-care/service-areas/heart/procedures-and-services/aortic-aneurysm-repair/about-aortic-aneurysms.**

9. **Segreti, D. *About Aortic Aneurysms* Available from: http://www.mountsinai.org/patient-care/service-areas/heart/procedures-and-services/aortic-aneurysm-repair/about-aortic-aneurysms.**

10. **Feller, I., *Surgical anatomy of the abdominal aorta.* Annals of surgery, 1961. 154(6)Suppl: p. 239-52.**

11. **Marieb, E., *Human anatomy & physiology*.**

12. **B.Y., R., *Lesson No 14: THEME 1. TRACHEA. BROCHI. LUNGS*.**

13. **Gilroy, *Atlas of anatomy*.**

14. Pakistan, S.S.o., *Abdominal Arteries and Pelvic Arteries*. 2012.

15. MacSweeney, S.T.R., J.T. Powell, and R.M. Greenhalgh, *Pathogenesis of abdominal aortic aneurysm.* British Journal of Surgery, 1994. 81(7): p. 935-941.

16. Dobrin, P., *Mechanics of normal and diseased blood vessels.* Annals of Vascular Surgery, 1988. 2(3): p. 283-294.

17. Thubrikar, M.J., *Vascular Mechanics and Pathology*. 2007.

18. Caro, *The mechanics of the circulation*.

19. Menashi, S., et al., *Collagen in abdominal aortic aneurysm: Typing, content, and degradation.* Journal of Vascular Surgery, 1987. 6(6): p. 578-582.

20. Rizzo, R.J., et al., *Collagen types and matrix protein content in human abdominal aortic aneurysms.* Journal of Vascular Surgery, 1989. 10(4): p. 365-373.

21. Roy, C.S., *The Elastic Properties of the Arterial Wall.* Journal of physiology, 1881. 3(2): p. 125-59.

22. **Burton, A.C., *Relation of structure to function of the tissues of the wall of blood vessels.* Physiological reviews, 1954. 34(4): p. 619-42.**

23. **Wolinsky, H., *STRUCTURAL BASIS FOR THE STATIC MECHANICAL PROPERTIES OF THE AORTIC MEDIA.* Circulation research, 1964. 14: p. 400-13.**

24. **Zatina, M.A., et al., *Role of medial lamellar architecture in the pathogenesis of aortic aneurysms.* Journal of Vascular Surgery, 1984. 1(3): p. 442-448.**

25. **Campa, J.S., R.M. Greenhalgh, and J.T. Powell, *Elastin degradation in abdominal aortic aneurysms.* Atherosclerosis, 1987. 65(1–2): p. 13-21.**

26. **Powell, J.T., N. Vine, and M. Crossman, *On the accumulation of d-aspartate in elastin and other proteins of the ageing aorta.* Atherosclerosis, 1992. 97(2–3): p. 201-208.**

27. **Dobrin, P.B., W.H. Baker, and W.C. Gley, *Elastolytic and collagenolytic studies of arteries: Implications for the mechanical properties of aneurysms.* Archives of Surgery, 1984. 119(4): p. 405-409.**

28. Anidjar, S., et al., *Elastase-induced experimental aneurysms in rats.* Circulation, 1990. 82(3): p. 973-81.

29. Tsamis, A., J.T. Krawiec, and D.A. Vorp, *Elastin and collagen fibre microstructure of the human aorta in ageing and disease: a review.* J R Soc Interface, 2013. 10(83): p. 20121004.

30. Pope, F.M., et al., *Type III collagen mutations in Ehlers Danlos Syndrome type IV and other related disorders.* Clinical and Experimental Dermatology, 1988. 13(5): p. 285-302.

31. Østergaard, J.R. and H. Oxlund, *Collagen type III deficiency in patients with rupture of intracranial saccular aneurysms.* Journal of Neurosurgery, 1987. 67(5): p. 690-696.

32. Powell, J.T., et al., *Influence of type III collagen genotype on aortic diameter and disease.* British Journal of Surgery, 1993. 80(10): p. 1246-1248.

33. Powell, J. and R.M. Greenhalgh, *Cellular, enzymatic, and genetic factors in the pathogenesis of abdominal aortic aneurysms.* Journal of Vascular Surgery, 1989. 9(2): p. 297-304.

34. Hammond, E.C. and L. Garfinkel, *Coronary heart disease, stroke, and aortic aneurysm.* Archives of environmental health, 1969. 19(2): p. 167-182.

35. Strachan, D.P., *Predictors of death from aortic aneurysm among middle-aged men: The Whitehall study.* British Journal of Surgery, 1991. 78(4): p. 401-404.

36. Wilmink, T.B.M., C.R.G. Quick, and N.E. Day, *The association between cigarette smoking and abdominal aortic aneurysms.* Journal of Vascular Surgery, 1999. 30(6): p. 1099-1105.

37. Turk, K.A., *The post-mortem incidence of abdominal aortic aneurysm.* Proc R Soc Med, 1965. 58(11 Part 1): p. 869-70.

38. Cronenwett, J.L., et al., *Variables that affect the expansion rate and outcome of small abdominal aortic aneurysms.* J Vasc Surg, 1990. 11(2): p. 260-8; discussion 268-9.

39. Spittell, J.J.A., *Hypertension and arterial aneurysm.* Journal of the American College of Cardiology, 1983. 1(2s1): p. 533-540.

40. Twomey, A., et al., *Unrecognised aneurysmal disease in male hypertensive patients.* Int Angiol, 1986. 5(4): p. 269-73.

41. Bengtsson, H., et al., *A population based screening of abdominal aortic aneurysms (AAA).* European Journal of Vascular Surgery, 1991. 5(1): p. 53-57.

42. Dobrin, P.B., *Pathophysiology and pathogenesis of aortic aneurysms. Current concepts.* Surg Clin North Am, 1989. 69(4): p. 687-703.

43. Webster, M.W., et al., *Abdominal aortic aneurysm: Results of a family study.* Journal of Vascular Surgery, 1991. 13(3): p. 366-372.

44. Clifton, M.A., *Familial abdominal aortic aneurysms.* British Journal of Surgery, 1977. 64(11): p. 765-766.

45. Webster, M.W., et al., *Ultrasound screening of first-degree relatives of patients with an abdominal aortic aneurysm.* Journal of Vascular Surgery, 1991. 13(1): p. 9-14.

46. Tilson, M.D. and M.R. Seashore, *Human genetics of the abdominal aortic aneurysm.* Surg Gynecol Obstet, 1984. 158(2): p. 129-32.

47. Johansen, K. and T. Koepsell, *FAmilial tendency for abdominal aortic aneurysms.* JAMA, 1986. 256(14): p. 1934-1936.

48. Powell, J.T. and R.M. Greenhalgh, *Multifactorial inheritance of abdominal aortic aneurysm.* European Journal of Vascular Surgery, 1987. 1(1): p. 29-31.

49. Crawford, J.L., et al., *Inflammatory aneurysms of the aorta.* Journal of Vascular Surgery, 1985. 2(1): p. 113-124.

50. Walker, D.I., et al., *Inflammatory aneurysms of the abdominal aorta.* British Journal of Surgery, 1972. 59(8): p. 609-614.

51. Sterpetti, A.V., et al., *Inflammatory aneurysms of the abdominal aorta: Incidence, pathologic, and etiologic considerations.* Journal of Vascular Surgery, 1989. 9(5): p. 643-650.

52. Patel, M.I., et al., *Current views on the pathogenesis of abdominal aortic aneurysms.* Journal of the American College of Surgeons, 1995. 181(4): p. 371-382.

53. Bengtsson, H., D. Bergqvist, and N.H. Sternby, *Increasing prevalence of abdominal aortic aneurysms. A*

necropsy study. **The European journal of surgery = Acta chirurgica, 1992. 158(1): p. 19-23.**

54. ***2005 Mortality statistics: cause (England and Wales).*** **Health statistics quarterly, 2007(33): p. 89-92.**

55. Vardulaki, K.A., et al., ***Growth rates and risk of rupture of abdominal aortic aneurysms.*** **British Journal of Surgery, 1998. 85(12): p. 1674-1680.**

56. Alcorn, H.G., et al., ***Risk Factors for Abdominal Aortic Aneurysms in Older Adults Enrolled in the Cardiovascular Health Study.*** **Arteriosclerosis, Thrombosis, and Vascular Biology, 1996. 16(8): p. 963-970.**

57. McFarlane, M.J., ***THe epidemiologic necropsy for abdominal aortic aneurysm.*** **JAMA, 1991. 265(16): p. 2085-2088.**

58. Lilienfeld, D.E., et al., ***Epidemiology of aortic aneurysms: I. Mortality trends in the United States, 1951 to 1981.*** **Arteriosclerosis, Thrombosis, and Vascular Biology, 1987. 7(6): p. 637-43.**

59. Pleumeekers, H.J.C.M., et al., ***Aneurysms of the Abdominal Aorta in Older Adults: The Rotterdam Study.***

American Journal of Epidemiology, 1995. 142(12): p. 1291-1299.

60. Blanchard, J.F., *Epidemiology of Abdominal Aortic Aneurysms.* Epidemiologic Reviews, 1999. 21(2): p. 207-221.

61. Glimåker, H., et al., *Natural history of patients with abdominal aortic aneurysm.* European Journal of Vascular Surgery, 1991. 5(2): p. 125-130.

62. Nevitt, M.P., D.J. Ballard, and J.W. Hallett, *Prognosis of Abdominal Aortic Aneurysms.* New England Journal of Medicine, 1989. 321(15): p. 1009-1014.

63. Griepp, R.B., et al., *Natural history of descending thoracic and thoracoabdominal aneurysms.* The Annals of Thoracic Surgery, 1999. 67(6): p. 1927-1930.

64. Lobato, A.C. and P. Puech-Leão, *Predictive factors for rupture of thoracoabdominal aortic aneurysm.* Journal of Vascular Surgery, 1998. 27(3): p. 446-453.

65. Stenbaek, J., B. Kalin, and J. Swedenborg, *Growth of Thrombus may be a Better Predictor of Rupture than Diameter in Patients with Abdominal Aortic Aneurysms.* European Journal of Vascular and Endovascular Surgery, 2000. 20(5): p. 466-469.

66. Wilmink, T.B.M., et al., *The influence of screening on the incidence of ruptured abdominal aortic aneurysms.* Journal of Vascular Surgery, 1999. 30(2): p. 203-208.

67. Kniemeyer, H.W., et al., *Treatment of Ruptured Abdominal Aortic Aneurysm, a Permanent Challenge or a Waste of Resources? Prediction of Outcome Using a Multi-organ-dysfunction Score.* European Journal of Vascular and Endovascular Surgery, 2000. 19(2): p. 190-196.

68. Lederle, F., *In the clinic. Abdominal aortic aneurysm.* Annals of Internal Medicine, 2009. 150(9): p. ITC5-1-15;quizITC5-16.

69. Powell, J., *The rupture rate of large abdominal aortic aneurysms: is this modified by anatomical suitability for endovascular repair?* Annals of surgery, 2008. 247(1): p. 173-9.

70. Brown, L.C., *Risk factors for aneurysm rupture in patients kept under ultrasound surveillance. UK Small Aneurysm Trial Participants.* Annals of surgery, 1999. 230(3): p. 289-96;discussion296-7.

71. Lederle, F.A., et al., *RUpture rate of large abdominal aortic aneurysms in patients refusing or unfit for elective repair.* JAMA, 2002. 287(22): p. 2968-2972.

72. Limet, R., *Determination of the Expansion Rate and Incidence of Rupture of Abdominal Aortic Aneurysms.* 1991.

73. Medscape, *Abdominal Aortic Aneurysm Rupture Imaging* 2013.

74. Uk Small Aneurysm Trial, P., *Mortality results for randomized controlled trial of early elective surgery or ultrasonographic surveillance for small abdominal aortic aneurysms.* Lancet (North American ed.), 1998. 352(9141): p. 1649-1655.

75. Lanne, *Improved reliability of ultrasonic surveillance of abdominal aortic aneurysms.* European journal of vascular and endovascular surgery, 1997. 13(2): p. 149-153.

76. Gaughan, S., *Developing a Method of Determining Abdominal Aortic Aneurysm Geometry and Rupture Threat from Standard 2D Ultrasound Images*. 2010: Centre for Applied Biomedical Engineering Research.

77. Fillinger, M., *Screening for Abdominal Aortic Aneurysm: Recommendation Statement.* Perspectives in Vascular Surgery and Endovascular Therapy, 2006. 18(1): p. 71-73.

78. Scott, R.A.P., *The Multicentre Aneurysm Screening Study (MASS) into the effect of abdominal aortic aneurysm screening on mortality in men: a randomised controlled trial.* The Lancet, 2002. 360(9345): p. 1531-1539.

79. Sandor, B.I., et al., *An analysis of blood flow dynamics in AAA*. Etiology, Pathogenesis and Pathophysiology of Aortic Aneurysms and Aneurysm Rupture. 2011.

80. Bush, R.L., et al., *Performance of endovascular aortic aneurysm repair in high-risk patients: results from the Veterans Affairs National Surgical Quality Improvement Program.* Journal of Vascular Surgery, 2007. 45(2): p. 227-233; discussion 233-5.

81. Endologix, *Treatment options*. 2011.

82. Thompson, M.M., R.D. Sayers, and P.R. Bell, *Endovascular aneurysm repair.* Bmj, 1997. 314(7088): p. 1139-40.

83. Buth, J. and R.J.F. Laheij, *Early complications and endoleaks after endovascular abdominal aortic aneurysm repair: Report of a multicenter study.* Journal of Vascular Surgery, 2000. 31(1): p. 134-146.

84. Noll, R.E., Jr., et al., *Long-term postplacement cost after endovascular aneurysm repair.* Journal of Vascular Surgery, 2007. 46(1): p. 9-15; discussion 15.

85. Prinssen, M., et al., *Surveillance after endovascular aneurysm repair: diagnostics, complications, and associated costs.* Annals of Vascular Surgery, 2004. 18(4): p. 421-7.

86. Center, T.N.M., *Abdominal Aortic Aneurysm Repair*.

87. *Endovascular aneurysm repair and outcome in patients unfit for open repair of abdominal aortic aneurysm (EVAR trial 2): randomised controlled trial.* The Lancet. 365(9478): p. 2187-2192.

88. Adriaensen, M.E.A.P.M., et al., *Elective Endovascular versus Open Surgical Repair of Abdominal Aortic Aneurysms: Systematic Review of Short-term Results.* Radiology, 2002. 224(3): p. 739-747.

89. Anderson, P.L., et al., *A statewide experience with endovascular abdominal aortic aneurysm repair: Rapid diffusion with excellent early results.* Journal of Vascular Surgery, 2004. 39(1): p. 10-18.

90. Lee, W.A., et al., *Perioperative outcomes after open and endovascular repair of intact abdominal aortic*

aneurysms in the united states during 2001. **Journal of Vascular Surgery, 2004. 39(3): p. 491-496.**

91. Maher, M.M., et al., *Abdominal Aortic Aneurysms: Elective Endovascular Repair versus Conventional Surgery—Evaluation with Evidence-based Medicine Techniques.* Radiology, 2003. 228(3): p. 647-658.

92. Zarins, C.K., et al., *AneuRx stent graft versus open surgical repair of abdominal aortic aneurysms: Multicenter prospective clinical trial.* Journal of Vascular Surgery, 1999. 29(2): p. 292-308.

93. Matsumura, J.S., et al., *A multicenter controlled clinical trial of open versus endovascular treatment of abdominal aortic aneurysm.* Journal of Vascular Surgery, 2003. 37(2): p. 262-271.

94. Moore, W.S., et al., *Five-year interim comparison of the guidant bifurcated endograft with open repair of abdominal aortic aneurysm.* Journal of Vascular Surgery, 2003. 38(1): p. 46-55.

95. Greenberg, R.K., et al., *Zenith AAA endovascular graft: intermediate-term results of the US multicenter trial.* Journal of Vascular Surgery, 2004. 39(6): p. 1209-1218.

96. participants, E.t., *Endovascular aneurysm repair versus open repair in patients with abdominal aortic aneurysm (EVAR trial 1): randomised controlled trial.* Lancet, 2005. 365(9478): p. 2179-86.

97. Noll Jr, R.E., et al., *Long-term postplacement cost after endovascular aneurysm repair.* Journal of Vascular Surgery, 2007. 46(1): p. 9-15.

98. Steingruber, I.E., et al., *Technical and clinical success of infrarenal endovascular abdominal aortic aneurysm repair: A 10-year single-center experience.* European Journal of Radiology, 2006. 59(3): p. 384-392.

99. Winterborn, R.J., et al., *Preferences for endovascular (EVAR) or open surgical repair among patients with abdominal aortic aneurysms under surveillance.* Journal of Vascular Surgery, 2009. 49(3): p. 576-581.e3.

100. Reise, J.A., et al., *Patient Preference for Surgical Method of Abdominal Aortic Aneurysm Repair: Postal Survey.* European Journal of Vascular and Endovascular Surgery, 2010. 39(1): p. 55-61.

101. Sandrin, L., et al., *Transient elastography: a new noninvasive method for assessment of hepatic fibrosis.*

Ultrasound in Medicine & Biology, 2003. 29(12): p. 1705-1713.

102. Wang, D.H., et al., *Mechanical properties and microstructure of intraluminal thrombus from abdominal aortic aneurysm.* Journal of biomechanical engineering, 2001. 123(6): p. 536-539.

103. Busuttil, *Elastase activity: The role of elastase in aortic aneurysm formation.* The Journal of surgical research, 1982. 32(3): p. 214-217.

104. Roy, D., et al., *A literature review of the numerical analysis of abdominal aortic aneurysms treated with endovascular stent grafts.* Computational and mathematical methods in medicine, 2012. 2012: p. 820389-820389.

105. Georgakarakos, E., et al., *Aneurysm sac shrinkage after endovascular treatment of the aorta: Beyond sac pressure and endoleaks.* Vascular Medicine, 2012. 17(3): p. 168-173.

106. Bosman, W.-M.P.F., et al., *Effect of Stent-Graft Compliance on Endotension After EVAR.* Journal of Endovascular Therapy, 2009. 16(1): p. 105-113.

107. Cornelissen, S.A., et al., *Lack of thrombus organization in nonshrinking aneurysms years after endovascular abdominal aortic aneurysm repair.* Journal of Vascular Surgery, 2012. 56(4): p. 938-942.

108. Weigel, S., et al., *Thoracic aortic stent graft: comparison of contrast-enhanced MR angiography and CT angiography in the follow-up: initial results.* European Radiology, 2003. 13(7): p. 1628-1634.

109. Hiramoto, J.S., et al., *Long-term outcome and reintervention after endovascular abdominal aortic aneurysm repair using the Zenith stent graft.* Journal of Vascular Surgery, 2007. 45(3): p. 461-466.

110. Seriki, D.M., et al., *Midterm Follow-up of a Single-center Experience of Endovascular Repair of Abdominal Aortic Aneurysms with Use of the Talent Stent-Graft.* Journal of Vascular and Interventional Radiology, 2006. 17(6): p. 973-977.

111. Thomas, S.M., et al., *Results from the Prospective Registry of Endovascular Treatment of Abdominal Aortic Aneurysms (RETA): Mid Term Results to Five Years.* European Journal of Vascular and Endovascular Surgery, 2005. 29(6): p. 563-570.

112. Chuter, T., et al., *Aneurysm pressure following endovascular exclusion.* European Journal of Vascular and Endovascular Surgery, 1997. 13(1): p. 85-87.

113. Chaikof, E., et al., *Reporting standards for endovascular aortic aneurysm repair.* Journal of vascular surgery, 2002. 35(5): p. 1048-1060.

114. Matsumura, J.S., et al., *Reduction in aortic aneurysm size: Early results after endovascular graft placement.* Journal of Vascular Surgery, 1997. 25(1): p. 113-123.

115. White, R.A., et al., *Regression of an abdominal aortic aneurysm after endograft exclusion.* Journal of Vascular Surgery, 1997. 26(1): p. 133-137.

116. de Korte, C.L., et al., *Intravascular Ultrasound Elastography in Human Arteries: Initial Experience In Vitro.* Ultrasound in Medicine & Biology, 1998. 24(3): p. 401-408.

117. Boppart, S.A., *Elastography*. 2014, Biophotonics Imaging Laboratory

118. Gilling-Smith GL, C.P., Buth, et al, *The significance of endoleaks after endovascular aneurysm repair : Results of a large European multicenter study.* Endovascular Surgery, 1998.

119. DH, D., *Results of a multicenter trial of the EVT Endovascular Grafting System.* Endovascular Surgery, 1999.

120. White, G.H., et al., *Endoleak as a Complication of Endoluminal Grafting of Abdominal Aortic Aneurysms: Classification, Incidence, Diagnosis,and Management.* Journal of Endovascular Surgery, 1997. 4(2): p. 152-168.

121. Fearn, S., et al., *Follow-Up After Endovascular Aortic Aneurysm Repair: The Plain Radiograph Has an Essential Role in Surveillance.* Journal of Endovascular Therapy, 2003. 10(5): p. 894-901.

122. Hodgson, R., et al., *Migration Versus Apparent Migration: Importance of Errors Due to Positioning Variation in Plain Radiographic Follow-up of Aortic Stent-Grafts.* Journal of Endovascular Therapy, 2003. 10(5): p. 902-910.

123. Fransen, G.A.J., et al., *Rupture of Infra-renal Aortic Aneurysm after Endovascular Repair: A Series from EUROSTAR Registry.* European Journal of Vascular and Endovascular Surgery, 2003. 26(5): p. 487-493.

124. Veith, F.J., et al., *Nature and significance of endoleaks and endotension: summary of opinions expressed at an*

international conference. **J Vasc Surg, 2002. 35(5): p. 1029-35.**

125. Czermak, B.V., et al., *Serial CT Volume Measurements After Endovascular Aortic Aneurysm Repair.* Journal of Endovascular Therapy, 2001. 8(4): p. 380-389.

126. Dattilo, J.B., et al., *Clinical failures of endovascular abdominal aortic aneurysm repair: Incidence, causes, and management.* Journal of Vascular Surgery, 2002. 35(6): p. 1137-1144.

127. Zarins, C.K., et al., *Stent graft migration after endovascular aneurysm repair: importance of proximal fixation.* Journal of Vascular Surgery, 2003. 38(6): p. 1264-1272.

128. Resch, T., et al., *Distal Migration of Stent-Grafts after Endovascular Repair of Abdominal Aortic Aneurysms.* Journal of Vascular and Interventional Radiology, 1999. 10(3): p. 257-264.

129. Engellau, L., et al., *Long-Term Results After Endovascular Repair of Abdominal Aortic Aneurysms with the Stentor and Vanguard Stent-graft.* Acta Radiologica, 2004. 45(3): p. 275-283.

130. Gelfand, D.V., G.H. White, and S.E. Wilson, *Clinical Significance of Type II Endoleak after Endovascular Repair of Abdominal Aortic Aneurysm.* Annals of Vascular Surgery, 2006. 20(1): p. 69-74.

131. Marrewijk, C.v., et al., *Significance of endoleaks after endovascular repair of abdominal aortic aneurysms: The EUROSTAR experience.* Journal of Vascular Surgery, 2002. 35(3): p. 461-473.

132. Nevala, *Finnish Multicenter Study on the Midterm Results of Use of the Zenith Stent-Graft in the Treatment of an Abdominal Aortic Aneurysm.* Journal of vascular and interventional radiology, 2009. 20(4): p. 448-454.

133. Muller, W., *Prediction of inferior mesenteric artery (IMA)-related type II endoleaks after EVAR.* Cardiovascular and interventional radiology, 2013. 36: p. S231.

134. Muller, W., *Embolization of endoleaks using ethylene vinyl alcohol copolymer.* Cardiovascular and interventional radiology, 2013. 36: p. S389.

135. Khaja, M., et al., *Treatment of Type II Endoleak Using Onyx With Long-Term Imaging Follow-Up.*

CardioVascular and Interventional Radiology, 2014. 37(3): p. 613-622.

136. Massis, K., et al., *Treatment of Type II Endoleaks With Ethylene-Vinyl-Alcohol Copolymer (Onyx).* Vascular and Endovascular Surgery, 2012. 46(3): p. 251-257.

137. Conrad, M.F., et al., *Secondary Intervention After Endovascular Abdominal Aortic Aneurysm Repair.* Annals of Surgery, 2009. 250(3): p. 383-389 10.1097/SLA.0b013e3181b365bd.

138. Abularrage, C.J., et al., *Improved results using Onyx glue for the treatment of persistent type 2 endoleak after endovascular aneurysm repair.* Journal of Vascular Surgery, 2012. 56(3): p. 630-636.

139. Gilling-Smith, G., et al., *Endotension after endovascular aneurysm repair: definition, classification, and strategies for surveillance and intervention.* J Endovasc Surg, 1999. 6(4): p. 305-7.

140. Mennander, A., et al., *Nonoperative approach to endotension.* Journal of Vascular Surgery, 2005. 42(2): p. 194-198.

141. Brown, L.C.P., et al., *Renal Function and Abdominal Aortic Aneurysm (AAA): The Impact of Different*

Management Strategies on Long-Term Renal Function in the UK EndoVascular Aneurysm Repair (EVAR) Trials. [Article]. **Annals of Surgery May 2010;251(5):966-975.**

142. Gleeson, T.G. and S. Bulugahapitiya, *Contrast-Induced Nephropathy.* American Journal of Roentgenology, 2004. 183(6): p. 1673-1689.

143. Eskandari, M.K., et al., *Surveillance after endoluminal repair of abdominal aortic aneurysms.* Cardiovascular Surgery, 2001. 9(5): p. 469-71.

144. Jones, C., et al., *The impact of radiation dose exposure during endovascular aneurysm repair on patient safety.* Journal of Vascular Surgery, 2010. 52(2): p. 298-302.

145. WHITE, et al., *Estimating risk associated with radiation exposure during follow-up after endovascular aortic repair (EVAR)*. Vol. 51. 2010, Torino, ITALIE: Minerva medica. 10.

146. Go, M.R., et al., *What is the clinical utility of a 6-month computed tomography in the follow-up of endovascular aneurysm repair patients?* Journal of Vascular Surgery, 2008. 47(6): p. 1181-1187.

147. Sternbergh Iii, W.C., et al., *Redefining postoperative surveillance after endovascular aneurysm repair: Recommendations based on 5-year follow-up in the US Zenith multicenter trial.* Journal of Vascular Surgery, 2008. 48(2): p. 278-285.

148. Bargellini, I., et al., *Ultrasonographic Surveillance With Selective CTA After Endovascular Repair of Abdominal Aortic Aneurysm.* Journal of Endovascular Therapy, 2009. 16(1): p. 93-104.

149. Elkouri, S., et al., *Computed tomography and ultrasound in follow-up of patients after endovascular repair of abdominal aortic aneurysm.* Annals of Vascular Surgery, 2004. 18(3): p. 271-9.

150. Radiology, E.S.o., *Does type 1 endoleak always need to be treated?* 2010.

151. Fenster, A., D.B. Downey, and H.N. Cardinal, *Three-dimensional ultrasound imaging.* Physics in Medicine and Biology, 2001. 46(5): p. R67.

152. Cosgrove, D., et al., *Quantification of blood flow.* European Radiology, 2001. 11(8): p. 1338-1344.

153. Wolf, Y.G., et al., *Duplex ultrasound scanning versus computed tomographic angiography for postoperative*

evaluation of endovascular abdominal aortic aneurysm repair. **Journal of Vascular Surgery, 2000. 32(6): p. 1142-1148.**

154. d'Audiffret, A., et al., *Follow-up evaluation of endoluminally treated abdominal aortic aneurysms with duplex ultrasonography: Validation with computed tomography.* Journal of Vascular Surgery, 2001. 33(1): p. 42-50.

155. Raman, K.G., et al., *Color-flow duplex ultrasound scan versus computed tomographic scan in the surveillance of endovascular aneurysm repair.* Journal of Vascular Surgery, 2003. 38(4): p. 645-651.

156. Sprouse Ii, L.R., et al., *Is Ultrasound More Accurate than Axial Computed Tomography for Determination of Maximal Abdominal Aortic Aneurysm Diameter?* European Journal of Vascular and Endovascular Surgery, 2004. 28(1): p. 28-35.

157. White, G.H., W. Yu, and J. May, *"Endoleak"—A Proposed New Terminology to Describe Incomplete Aneurysm Exclusion by an Endoluminal Graft.* Journal of Endovascular Surgery, 1996. 3(1): p. 124-125.

158. AbuRahma, A.F., et al., *Computed tomography versus color duplex ultrasound for surveillance of abdominal*

aortic stent-grafts. **J Endovasc Ther, 2005. 12(5): p. 568-73.**

159. Nordon, I.M., et al., *Secondary interventions following endovascular aneurysm repair (EVAR) and the enduring value of graft surveillance.* European Journal of Vascular & Endovascular Surgery. 39(5): p. 547-54.

160. Radiology, E.S.o., *Type 1a endoleak*. 2012.

161. Chabbert, V., et al., *Midterm Outcomes of Thoracic Aortic Stent-Grafts: Complications and Imaging Techniques.* Journal of Endovascular Therapy, 2003. 10(3): p. 494-504.

162. Cantisani, V., et al., *Prospective Comparative Analysis of Colour-Doppler Ultrasound, Contrast-enhanced Ultrasound, Computed Tomography and Magnetic Resonance in Detecting Endoleak after Endovascular Abdominal Aortic Aneurysm Repair.* European Journal of Vascular and Endovascular Surgery, 2011. 41(2): p. 186-192.

163. Binkert, C.A., et al., *Translumbar Type II Endoleak Repair Using Angiographic CT.* Journal of Vascular and Interventional Radiology, 2006. 17(8): p. 1349-1353.

164. Bushberg, J., *Essential Physics of Medical Imaging*.

165. Alerci, M., et al., *Prospective, intraindividual comparison of MRI versus MDCT for endoleak detection after endovascular repair of abdominal aortic aneurysms.* European Radiology, 2009. 19(5): p. 1223-1231.

166. Cornelissen, S.A.P., et al., *Detection of Occult Endoleaks After Endovascular Treatment of Abdominal Aortic Aneurysm Using Magnetic Resonance Imaging With a Blood Pool Contrast Agent: Preliminary Observations.* Investigative Radiology, 2010. 45(9): p. 548-553 10.1097/RLI.0b013e3181e992ac.

167. Ersoy, H., et al., *Blood Pool MR Angiography of Aortic Stent-Graft Endoleak.* American Journal of Roentgenology, 2004. 182(5): p. 1181-1186.

168. Cornelissen, S.A., et al., *Visualizing type IV endoleak using magnetic resonance imaging with a blood pool contrast agent.* Journal of Vascular Surgery, 2008. 47(4): p. 861-864.

169. Haulon, S., et al., *Diagnosis and Treatment of Type II Endoleak after Stent Placement for Exclusion of an Abdominal Aortic Aneurysm.* Annals of Vascular Surgery, 2001. 15(2): p. 148-154.

170. Cejna, M., et al., *MR angiography vs CT angiography in the follow-up of nitinol stent grafts in endoluminally treated aortic aneurysms.* European Radiology, 2002. 12(10): p. 2443-2450.

171. Insko, E.K., et al., *MR Imaging for the Detection of Endoleaks in Recipients of Abdominal Aortic Stent-Grafts with Low Magnetic Susceptibility.* Academic Radiology, 2003. 10(5): p. 509-513.

172. Ayuso, J.R., et al., *MRA is useful as a follow-up technique after endovascular repair of aortic aneurysms with nitinol endoprostheses.* Journal of Magnetic Resonance Imaging, 2004. 20(5): p. 803-810.

173. Pitton, M.B., et al., *MRI Versus Helical CT for Endoleak Detection After Endovascular Aneurysm Repair.* American Journal of Roentgenology, 2005. 185(5): p. 1275-1281.

174. van der Laan, M.J., et al., *Computed Tomography versus Magnetic Resonance Imaging of Endoleaks after EVAR.* European Journal of Vascular and Endovascular Surgery, 2006. 32(4): p. 361-365.

175. van der Steen, A.F.W., C.L. de Korte, and E.I. Céspedes, *Intravascular Ultrasound Elastography.* Ultraschall in Med, 1998. 19(05): p. 196-201.

176. Hoskins, P.R., *Principles of ultrasound elastography.* Ultrasound, 2012. 20(1): p. 8-15.

177. Doyley, M.M. and K.J. Parker, *Elastography: General Principles and Clinical Applications.* Ultrasound Clinics, 2014. 9(1): p. 1-11.

178. *Young's Modulus*.

179. Ophir, J., et al., *Elastography: Ultrasonic imaging of tissue strain and elastic modulus in vivo.* European Journal of Ultrasound, 1996. 3(1): p. 49-70.

180. Ophir, J., et al., *Elastography: A quantitative method for imaging the elasticity of biological tissues.* Ultrasonic Imaging, 1991. 13(2): p. 111-134.

181. Skovoroda, A.R., S.Y. Emelianov, and M. O'Donnell, *Tissue elasticity reconstruction based on ultrasonic displacement and strain images.* Ultrasonics, Ferroelectrics and Frequency Control, IEEE Transactions on, 1995. 42(4): p. 747-765.

182. Maurice, R.L. and M. Bertrand, *Lagrangian speckle model and tissue-motion estimation-theory [ultrasonography].* Medical Imaging, IEEE Transactions on, 1999. 18(7): p. 593-603.

183. Maurice, R.L. and M. Bertrand, *Tissue Strain Estimation Using a Lagrangian Speckle Model*, in *Acoustical Imaging*, S. Lees and L. Ferrari, Editors. 1997, Springer US. p. 113-117.

184. Maurice, R.L., et al., *Non-invasive high-frequency vascular ultrasound elastography.* Physics in Medicine and Biology, 2005. 50(7): p. 1611.

185. *Noninvasive Vascular Elastography: Theoretical Framework.* IEEE Transactions on Medical Imaging, 2004. 23(2): p. 164.

186. Mercure, E., et al., *Performance evaluation of different implementations of the Lagrangian speckle model estimator for non-invasive vascular ultrasound elastography.* Medical Physics, 2008. 35(7): p. 3116-3126.

187. Carrell, T.W.G., A. Smith, and K.G. Burnand, *Experimental techniques and models in the study of the development and treatment of abdominal aortic aneurysm.* British Journal of Surgery, 1999. 86(3): p. 305-312.

188. Lerouge, S., et al., *Endovascular Aortic Aneurysm Repair with Stent-Grafts: Experimental Models Can*

Reproduce Endoleaks. **Journal of Vascular and Interventional Radiology, 2004. 15(9): p. 971-979.**

189. Blankensteijn, J.D., et al., *Two-Year Outcomes after Conventional or Endovascular Repair of Abdominal Aortic Aneurysms.* New England Journal of Medicine, 2005. 352(23): p. 2398-2405.

190. Tadros, R.O., et al., *The impact of stent graft evolution on the results of endovascular abdominal aortic aneurysm repair.* Journal of Vascular Surgery, (0).

191. Sun, Z., *Diagnostic value of color duplex ultrasonography in the follow-up of endovascular repair of abdominal aortic aneurysm.* J Vasc Interv Radiol, 2006. 17(5): p. 759-64.

192. Beeman, B.R., et al., *Duplex ultrasound imaging alone is sufficient for midterm endovascular aneurysm repair surveillance: a cost analysis study and prospective comparison with computed tomography scan.* Journal of Vascular Surgery, 2009. 50(5): p. 1019-24.

193. Go, M.R., et al., *What is the clinical utility of a 6-month computed tomography in the follow-up of endovascular aneurysm repair patients?* 2008: Journal of Vascular Surgery. 47 (6) (pp 1181-1187), 2008. Date of Publication: June 2008.

194. Sternbergh, I.W.C., et al., *Redefining postoperative surveillance after endovascular aneurysm repair: Recommendations based on 5-year follow-up in the US Zenith multicenter trial*. 2008: Journal of Vascular Surgery. 48 (2) (pp 278-285), 2008. Date of Publication: August 2008.

195. Maurice, R.L., et al., *Noninvasive vascular elastography: theoretical framework.* IEEE Trans Med Imaging, 2004. 23(2): p. 164-80.

196. Maurice, R.L., et al., *Noninvasive vascular elastography for carotid artery characterization on subjects without previous history of atherosclerosis*. Medical Physics. 35 (8) (pp 3436-3443), 2008. Date of Publication: 2008.

197. Schmitt, C., et al., *Noninvasive vascular elastography: toward a complementary characterization tool of atherosclerosis in carotid arteries.* Ultrasound Med Biol, 2007. 33(12): p. 1841-58.

198. Destrempes, F., et al., *Segmentation method of intravascular ultrasound images of human coronary arteries.* Computerized Medical Imaging and Graphics, 2014. 38(2): p. 91-103.

199. Fromageau, J., et al., *Noninvasive vascular ultrasound elastography applied to the characterization of experimental aneurysms and follow-up after endovascular repair.* Phys Med Biol, 2008. 53(22): p. 6475-90.

200. Stavropoulos, S.W. and S.R. Charagundla, *Imaging techniques for detection and management of endoleaks after endovascular aortic aneurysm repair*. 2007: Radiology. 243(3). JUN 2007. 641-655.

201. Destrempes, F., *Segmentation of plaques in sequences of ultrasonic B - mode images of carotid arteries based on motion estimation and a bayesian model.(Technical report).* IEEE Transactions on Biomedical Engineering, 2011. 58(8): p. 2202.

202. Mercure, E., et al., *A local angle compensation method based on kinematics constraints for non-invasive vascular axial strain computations on human carotid arteries.* Computerized Medical Imaging and Graphics, 2014. 38(2): p. 123-136.

203. Kulcsár, Z., et al., *Intra-Aneurysmal Thrombosis as a Possible Cause of Delayed Aneurysm Rupture after Flow-Diversion Treatment.* American Journal of Neuroradiology, 2011. 32(1): p. 20-25.

204. Ashton, J.H., et al., *Compressive mechanical properties of the intraluminal thrombus in abdominal aortic aneurysms and fibrin-based thrombus mimics.* Journal of Biomechanics, 2009. 42(3): p. 197-201.

205. Gasser, T.C., et al., *Failure properties of intraluminal thrombus in abdominal aortic aneurysm under static and pulsating mechanical loads.* Journal of Vascular Surgery, 2008. 48(1): p. 179-188.

206. Cornelissen, S.A., et al., *Use of Multispectral MRI to Monitor Aneurysm Sac Contents After Endovascular Abdominal Aortic Aneurysm Repair.* Journal of Endovascular Therapy, 2011. 18(3): p. 274-279.

207. Engellau, L., et al., *Magnetic resonance imaging and MR angiography of endoluminally treated abdominal aortic aneurysms.* European Journal of Vascular and Endovascular Surgery, 1998. 15(3): p. 212-219.

208. Dayal, R., et al., *Characterization of retrograde collateral (type II) endoleak using a new canine model.* Journal of vascular surgery, 2004. 40(5): p. 985-994.

209. Dias, N.V., et al., *Intra-aneurysm sac pressure measurements after endovascular aneurysm repair: Differences between shrinking, unchanged, and expanding aneurysms with and without endoleaks.*

Journal of Vascular Surgery. 39 (6) (pp 1229-1235), 2004. Date of Publication: June 2004.

210. Dias, N.V., et al., *Endoleaks after endovascular aneurysm repair lead to nonuniform intra-aneurysm sac pressure*. Journal of Vascular Surgery. 46 (2) (pp 197-203), 2007. Date of Publication: August 2007.

211. Ellozy, S.H., et al., *Abdominal aortic aneurysm sac shrinkage after endovascular aneurysm repair: correlation with chronic sac pressure measurement.* J Vasc Surg, 2006. 43(1): p. 2-7.

212. (CHUM), C.h.d.l.U.d.M. *Abdominal Aortic Aneurysm Follow-up After Endovascular Repair by Non-invasive Vascular Elastography* 2013; Available from: http://clinicaltrials.gov/ct2/show/NCT01907386?term=abdominal+aortic+aneurysm&recr=Not+yet+recruiting&rslt=Without&type=Intr&titles=abdominal+aortic+aneurysm+follow-up+after+endovascular+repair+by+non-invasive+vascular+elastography&cntry1=NA%3ACA&state1=NA%3ACA%3AQC&locn=Montreal&rank=1.

213. Cespedes, I., et al., *Elastography: Elasticity Imaging Using Ultrasound with Application to Muscle and*

Breast In Vivo. **Ultrasonic Imaging, 1993. 15(2): p. 73-88.**

214. Emelianov, S.Y., et al. *Reconstructive ultrasound elasticity imaging for renal pathology detection*. in *Ultrasonics Symposium, 1997. Proceedings., 1997 IEEE*. 1997.

215. Education, I.f.A.M., *Breast Elastography*. 2014.

216. *Correlation of Cognitive Function with Ultrasound Strain Indices in Carotid Plaque.* Ultrasound in Medicine & Biology, 2014. 40(1): p. 78.

217. de Korte, C.L. and A.F.W. van der Steen, *Intravascular ultrasound elastography: an overview.* Ultrasonics, 2002. 40(1–8): p. 859-865.

218. de Korte, C.L., et al., *Identification of Atherosclerotic Plaque Components With Intravascular Ultrasound Elastography In Vivo: A Yucatan Pig Study.* Circulation, 2002. 105(14): p. 1627-1630.

219. Schaar, J.A., et al., *Characterizing Vulnerable Plaque Features With Intravascular Elastography.* Circulation, 2003. 108(21): p. 2636-2641.

220. Floc'h, S.L., et al., *On the potential of a new IVUS elasticity modulus imaging approach for detecting*

vulnerable atherosclerotic coronary plaques: in vitro vessel phantom study. **Physics in Medicine and Biology, 2010. 55(19): p. 5701.**

221. Nishimura, R.A., et al., *Intravascular ultrasound imaging: In vitro validation and pathologic correlation.* Journal of the American College of Cardiology, 1990. 16(1): p. 145-154.

222. Pearce, B.J. and W.D. Jordan Jr, *Using IVUS during EVAR and TEVAR: Improving Patient Outcomes.* Seminars in Vascular Surgery, 2009. 22(3): p. 172-180.

223. Hoshina, K., et al., *A Retrospective Study of Intravascular Ultrasound use in Patients Undergoing Endovascular Aneurysm Repair: Its Usefulness and a Description of the Procedure.* European Journal of Vascular and Endovascular Surgery, 2010. 40(5): p. 559-563.

224. Larzon, T., R. Lindgren, and L. Norgren, *Endovascular Treatment of Ruptured Abdominal Aortic Aneurysms: A Shift of the Paradigm?* Journal of Endovascular Therapy, 2005. 12(5): p. 548-555.

225. Maurice, R.L., et al., *Noninvasive vascular elastography: theoretical framework.* Medical Imaging, IEEE Transactions on, 2004. 23(2): p. 164-180.